CHEMICAL AND ISOTOPIC STUDIES IN COASTAL AREAS OF THE ARABIAN SEA AND SALINE LAKES OF RAJASTHAN (INDIA)

Thesis submitted to

The Maharaja Sayajirao University of Baroda

for the Degree of

Doctor of Philosophy

in

Geology

by

Dinanath Yadav

June 1995

Physical Research Laboratory
Navrangpura
Ahmedabad 380 009
Gujarat (INDIA)

CERTIFICATE

I hereby declare that the work presented in this thesis is original and has not formed the basis for the award of any Degree or Diploma by any University or Institution.

Dinanath Yadav

Dinanath Yadav

(Candidate)

Certified by :

Prof. S. Krishnaswami,

(Guide),

Physical Research Laboratory,

Ahmedabad 380 009, India

Prof. S. J. Desai,

(Co-Guide),

M. S. University of Baroda,

Baroda 390 002, India

Head, Deptt. of Geology,

M. S. University of Baroda,

Baroda 390 002, India.

Contents

Part–B

List of Tables

Part-A

Part–B

List of Figures

Part-A

Part–B

Acknowledgements

I thank Dr. M.M. Sarin for his sincere, time valued suggestions and guidance throughout my study period. I am indebted to Prof. S. Krishnaswami for his remarkable and critical advices without which this thesis would not have taken the present shape. I am grateful to Prof. B.L.K. Somayajulu who introduced me to the study of the marine geochemistry of the Arabian sea coastal sediments. Without his initiative and constant effort this thesis would have been incomplete. I am thankful to Prof. S.J. Desai, M.S. University, Baroda for his valuable suggestions and help in completing the thesis.

I thank Dr. R. Ramesh for his help in the measurement of oxygen isotope of water samples and guidance to model the experimental results. I also thank Mr. R.A. Jani and Mr. J.T. Padia for demonstrating the mass-spectrometric operations and their help in the analysis of water samples.

During my research at PRL I had discussions with a number of earth science group members on various occasions which were very encouraging and thoughtful. For this, thanks are due to Drs. S.K. Gupta, A.K. Singhvi, S.K. Bhattacharya, R.K. Pant, P.N. Shukla, K. Pande and Mr. Navin Juyal.

I feel fortunate for having friends like Santhanam, Prahalad, Sivakumaran, Patra, Ramachandran, Raju, Poulose, Himadri, Bans, Debabrato, Supriyo, Sam and many others who shared my views and also helped me at many instances. I am especially thankful to Varun and Arul for their help during computational calculations.

I enjoyed the company of Mr. R. Rengarajan, Mr. Ravi Bhushan, Mr. Sunil K. Singh, Mr. J. P. Bhavsar, Mr. A. R. S. Pandian and Ms. Pauline Joseph of the Chemistry Lab who provided me some sort of homely environment during the study period. Also, the help and co-operation of the staff members of the PRL library, Computer Centre and the draughtsman Mr. S.C Bhavsar is thankfully acknowledged.

This study was funded in part by grant–in–aids received from the Dept. of Ocean Development (New Delhi) and the ISRO/DOS Global Change programme (I/DGBP).

During the Sambhar field trips I was helped by many staff members of the Sambhar Salt Limited (SSL), in particular, Mr. A. K. Johiri, Mr. Dayanand Sharma and Mr. B. K. Taneja. The hospitality provided by the SSL is gratefully acknowledged.

Finally I would like to thank my father for his patient observations and blessings all through my study at PRL.

Abstract

This thesis presents a systematic geochemical study of the Western Continental Margin of India and the Sambhar salt lake in Rajasthan. The first study (Part-A) is aimed at understanding the biogeochemical processes occurring in the margin sediments and their role as a sink or source for trace elements to the open ocean. Part-B focusses on the evolution of chemical and isotopic composition of the Sambhar lake during the annual wetting and drying cycles and attempts to place contraints on the source of salt to the lake basin.

Part–A: Geochemical study of sediments from the Western Continental Margin of India (WCMI)

Six sediment cores of about 20–25 cm length have been analyzed for selected U-Th series radionuclides (^{238,234}U, ^{232,230}Th, ^{226}Ra and ^{210}Pb) and major and trace elements. These sediment cores are from the upper slope (water depth $\sim$ 300 m) and lower slope (water depth $\sim$ 2500 m) regions which transect through the sub-oxic and oxic environmental conditions across the WCMI. The objective of this study is to understand the spatial and temporal variations (on a century time scale) of $CaCO_3$, organic matter (OM), particle reactive (^{210}Pb, ^{232,230}Th) and redox sensisitive (U, Mn and Fe) elements.

The chronology of the sediments has been determined based on the $^{210}Pb_{excess}$ method which provides a good handle to describe the temporal variations in the deposition of lithogenic and biogenic components of the sediment. The sediment accumulation rates range from 0.25–1.83 mm/y which corresponds to a time span of about 100–800 years BP for the core lengths. In one of the cores, the depth profile of ^{137}Cs concentration is also measured which yields a sediment accumulation rate consistent with that derived from the $^{210}Pb_{excess}$ method. The contents of $CaCO_3$ and OM are relatively higher in the upper slope region. $CaCO_3$, though biogenic in nature, its abundance in most of the cores is dominated by relict calcareous materials as evidenced by "older" ^{14}C ages in both surface and deeper sections. Such an observation limits the use of $CaCO_3$ in the cores to obtain information on the temporal changes in the water column productivity. The relatively high abundance of organic matter in upper slope sediments results from a combination of high biological productivity and high sedimentation rate. A uniform distribution of $CaCO_3$ over the length of core sampled in upper slope region indicates that

environmental conditions have remained unchanged during the time span represented by the core length. However, in the lower slope sediments, $CaCO_3$ increases by as much as 60% in the deeper sections indicating its relatively higher deposition in the past which may be due to increased contribution of the relict calcareous materials.

The ^{210}Pb inventory shows a positive correlation with the rate of sediment accumulation. This implies that ^{210}Pb (and other similar particle reactive nuclides) gets focussed and deposited in regions of high sediment accumulation. For this reason, the depositional flux of $^{210}Pb_{excess}$ shows spatial variation along the WCMI sediments with values in some cores considerably in excess to that expected from atmospheric fallout and water column production.

The Mn concentration (on a $CaCO_3$ free basis) and the Mn/Al ratio in upper slope sediments (averaged over entire core length) is low by a factor of about three compared to that transported by Narbada/Tapti river suspended particles ($\sim$ 1000 ppm). This has been interpreted in terms of its mobilization in reducing conditions. The amount of manganese mobilized from the upper slope sediments from an area bounded by the four cores analyzed is about $\sim 5.0 \times 10^{10}$ g/y, nearly same order of magnitude as the supply of dissolved Mn by world rivers to the ocean. In contrast, some of the upper slope sediments show uranium enrichment by a factor of five compared to open ocean sediments. These sediment cores are characterized by the $^{234}U/^{238}U$ activity ratio typical of seawater, suggesting that the dominant source of U to these sediments is seawater. The removal flux of uranium suggests that nearly 3% of its dissolved supply by the world rivers is sequestered in the WCMI region. Furthermore, the depth profiles of Mn concentration and U/Th ratio in these sediments do not show any significant variations indicating that the redox conditions prevailing over the region have not changed during the last few centuries. Thus, it can be concluded that the upper slope sediments of WCMI act as a "sink" for oceanic uranium and "source" for dissolved manganese to seawater.

The distribution of Mn in the lower slope sediments shows definite structure with high concentration near the sediment-water interface. This high concentration could result from (i) the diagenesis occurring in sedimentary column which mobilizes the Mn from the bottom sections to the surface where it is reprecipitated, (ii) transport of soluble Mn from upper slope region. The profile of U/Th weight ratio in the lower slope sediments

shows a continuous increase with depth indicating U removal deeper in the sediments from seawater due to reducing/sub-oxic conditions prevailing in the sub-surface layer.

The metal/Al ratios in WCMI sediments have been found to be in the same range as that reported in the Narbada/Tapti river particles. Also, there is no significant increase in Cu/Al, Zn/Al, Pb/Al and Ni/Al ratios at the core tops relative to the bottom sections. These results reflect metal abundances in margin sediments to be dominated by fluvial sources and there is no significant anthropogenic inputs of these elements during the last century.

Part–B: Geochemical and isotopic study of the Sambhar lake, Rajasthan (India)

The oxygen isotopic composition, major ions and selected U-Th series radionuclides ($^{238,234}U$, $^{226,228}Ra$, ^{210}Po and ^{210}Pb) have been studied in various reservoirs of the Sambhar lake viz. groundwaters, river waters, lake brines and sub-surface brines to characterize them in terms of their chemical and isotopic composition. In addition, attempt has been made to identify the source water composition of the brine, possible source of salt to the lake basin and mixing of water bodies in the region.

The oxygen isotopic composition ($\delta^{18}O$) of lake and river waters during monsoon and the groundwaters in most of the seasons is in the range of meteoric precipitation (−6.4 to −3.2 $^{o}/_{oo}$) indicating that oxygen isotopic composition of these reservoirs is dominated by atmospheric precipitation. A good correlation between $\delta^{18}O$ and salt content (TDS) in groundwaters from the region collected during monsoon and winter seasons reflects a two component mixing between low TDS, low $\delta^{18}O$ and high TDS, high $\delta^{18}O$ endmembers. The lowest $\delta^{18}O$ (−5.5 $^{o}/_{oo}$) observed in the lake during July 92 indicates that the lake is recharged by atmospheric precipitation and surface run-off. The effect of recharge is also seen in the $\delta^{18}O$ content in some of the sub-surface brines which decreases from ∼+5 $^{o}/_{oo}$ to −1 $^{o}/_{oo}$ in some of the wells immediately after the monsoon, caused by recharge either from atmospheric precipitation or from the lake waters during the monsoon season. The $\delta^{18}O$ of the lake water increases from ∼ −5$^{o}/_{oo}$ immediately after the monsoon to ∼+21$^{o}/_{oo}$ during summer and remains steady at this value. The isotopic evolution trend in the lake is broadly of Rayleigh fractionation type, however, the saturation in $\delta^{18}O$ during the late stage of evaporation is explained by the Craig-Gordon model whi

enrichment and preferential retention in the aqueous phase. Compared to groundwaters and river waters, the U/TDS ratio in the lake water is low during most of the seasons. Such an observation indicates that the uranium input from surface run-off is diluted by the salt present in the lake bed. The amount of recycling of salt from the lake bed during the recharge period based on the result of U/TDS ratio in river and lake water is calculated to be 95% of the total salt which is also consistent with an estimate from the Na/Cl ratio.

The NaCl content of rain water from the location is about 2 mg/l. An upper limit on estimate of NaCl depositing over whole catchment area of the lake based on the measured NaCl content in rain water is calculated to be ~5000 tons which is less than $\leq$3% of the current salt production from the lake basin. The inventory of salt in the Sambhar lake after monsoon (Oct 92) is about 10^6 tons. The annual supply of salt via rains is <1% of the inventory. These estimates, therefore, suggest that rains are not a major source of salt to the lake at present. An estimate of the input of salt to the lake basin from river and groundwaters collected during recharge period (based on the geometric mean of Cl concentration and assuming 50% of water in lake derived from them) is about 6% of the salt inventory in the lake. These estimates, therefore, suggest that rains and surface/sub-surface run-off are not major source of salt to the lake in present day condition. Another hypothesis of the source of salt to this area is via aeolian transport of marine aerosol particles from the Gulf of Kutch. The study of uranium and its isotopic ratio places some constraints on the importance of the source of salt to the basin. As mentioned earlier, uranium shows a strong positive correlation with TDS and has a uniform $^{234}U/^{238}U$ ratio 1.65±0.03 during the annual evaporation cycle. If there is significant contribution of marine aerosols with associated uranium then the U/TDS and the $^{234}U/^{238}U$ activity ratio are expected to decrease since seawater is characterized by U/TDS and uranium activity ratios ~0.1 μg/g and 1.14±0.02 respectively. As this is not observed, importance of aeolian transport of marine aerosol particles as a source of salt to the lake appears to be negligible.

A very low Ra/TDS ratio (lower by two to three orders of magnitudes) in the brines compared to the groundwaters and river waters suggests that Ra isotopes have been removed from these waters. Such an observation consistent with low concentrations of Ca and Mg ions in the lake brines. The radium isotopes also show saturation in their

activities during evaporation in salinity range of 100–370 g/l. These results, therefore, suggest that Ra isotopes have been removed during early stages of evaporation by co-precipitation with Ca-Mg minerals and in the later stages the concentration saturates because of equilibration with the clay minerals. The distribution of ^{210}Po and ^{210}Pb nuclides in various water reservoirs has indicated their difference in particle reactivity. The groundwaters show ^{210}Po/^{210}Pb activity ratio far less than unity indicating preferential removal of ^{210}Po onto particulates. However, in lake and pan waters, the ^{210}Po/^{210}Pb activity ratio is greater than one which is rarely observed in natural waters. This has been explained by the preferential complexation of ^{210}Po relative to ^{210}Pb by the algal material present in these waters. On the other hand, the ^{210}Po/^{210}Pb activity ratio is nearly one in most of the sub-surface brines suggesting that particle reactivity of both the nuclides in these waters is identical.

The chemical and isotopic composition of the Sambhar lake and its source waters analyzed in this study, as stated above, place constraints on the source of salt to the lake basin. The present annual amount of salt contributed by surface/sub-surface inflow waters and atmospheric precipitation is 1–2 orders of magnitude lower than the inventory of salt in the lake. Also, contribution of salt from atmospheric transport of marine aerosol particles does not seem to be a significant source to the lake. The important processes occurring currently in the lake are recycling of the salt from the lake bed during recharge period followed by evaporation and precipitation of Ca-Mg minerals which result an alkaline Na–Cl type of brine.

PART – A

Geochemical study of sediments from the Western Continental Margin of India

Chapter 1

Introduction

The role of continental margins in regulating the marine geochemical cycles of elements and as a repository of high resolution records of climate and environmental history is getting increasingly recognized. The primary components of margin sediments are weathering products delivered by rivers and biogenic materials settling from the overlying water-column. Some of the recent studies (Martin and Windom, 1991; Milliman,1991) indicate that bulk of the suspended sediments delivered by the rivers to the ocean are deposited in the ocean margins and only less than one fourth of this supply escapes to the open ocean. The biological productivity along the margins is generally high due to higher rates of nutrient input via rivers and coastal upwelling processes. This biological productivity contributes significantly to the organic matter, $CaCO_3$ and opal content of the sediments. Thus, margins sites, in general, have high rates of sediment accumulation (typically a few mm/y) of terrigenous and biogenic materials. These sedimentation rates are orders of magnitude higher than those observed in typical open ocean areas (Goldberg and Koide,1962; Rosholt et al,1961). Therefore, it is possible to retrieve high resolution records of climatic and environmental conditions during the past few centuries from the study of margin sediments.

The sediments in margin areas are usually rich in organic matter resulting from the high biological productivity in the overlying water column. Recent estimates of the primary production suggests that about 18–30 % of world ocean productivity occurs in the shelf regions (Wollast,1991; Martin and Thomas,1994). These values are very significant since the margins occupy only 7% of the total ocean surface. It has been inferred that

about 80% of primary production in margin regions is sustained by recycling of nutrients (Martin and Thomas,1994); the remaining being "new production" resulting from supply of nutrients either from riverine, atmospheric or upwelled deep waters. Spitzy and Ittekkot (1991) have estimated that the global organic carbon input by rivers is lower by a factor of two compared to this new production. Likewise, based on the global nitrogen budget, it has been suggested that upwelling of deep waters is the major source of nutrients for the new production in the margin areas (Wollast,1993; Walsh,1991). Furthermore, the global geochemical mass-balance study of dissolved Cu, Cd, Ni and Zn in margin areas indicates that their inputs from upwelled waters exceed the combined inputs of the riverine and atmospheric sources (Martin and Thomas, 1994). These results, therefore, suggest that there is continuous exchange of the biogenic materials and trace metals between continental margins and the open ocean. These exchange processes and the associated magnitude and direction of fluxes of biogenic elements have been a subject of current interest in the Global Change Studies.

A significant fraction of organic matter depositing in the margin sediments undergoes diagenesis making the margins an active site of benthic sedimentary processes which affect the marine biogeochemical cycle of elements. Biodegradation of organic matter also results in sub-oxic/anoxic conditions in the overhead water-column as well as near the sediment-water interface. Such conditions influence to a great extent the mobility of redox sensitive elements, notably manganese and uranium within a sediment column. Similarly some of the particle reactive elements such as Pa, Po and Pb are sequestered in the margin sediments due to enhanced boundary scavenging processes (Bacon et al,1976; Anderson et al,1983). Thus, the study of margin sediments is useful in understanding the weathering history of adjacent land-mass, biological productivity in the water-column, recent anthropogenic inputs of materials, and exchange of various elements between the coastal margins and the open ocean.

In this context, sediments from the Western Continental Margin of India (WCMI) are important as they underlie a unique marine geochemical province of the eastern Arabian sea. The two Indian monsoons, southwest (SW) and northeast (NE), result in reversal of surface ocean currents both in magnitude and direction. The SW monsoon being far more intense causes extensive upwelling in many regions of the Arabian sea. The upwelling

induces high biological productivity in water-column which, in turn, causes significant rain of organic matter to the sediments. The combustion of organic matter during its transit through the water-column and also in sediments dictates the profiles of dissolved oxygen, nitrate, nitrite, sulphate and other chemical constituents both in seawater and in sediment pore water. A unique feature of the Arabian sea is the presence of a sub-oxic layer in the intermediate depths associated with intense denitrification (Naqvi,1994). It is expected that the distribution of particle-reactive and redox sensitive elements in the water column and sediments would be significantly influenced by these conditions. In addition, three west flowing rivers of the Indian sub-continent, the Indus, Narbada and the Tapti supply large amount of sediments and nutrients to the Arabian sea. The annual discharge of suspended load by the Indus river to the Arabian sea is about 1×10^8 tons (Milliman and Meade,1983) whereas the Narbada and Tapti together account for 0.6×10^8 tons (Borole et al,1982a). The fluvial material derived from these rivers is by and large deposited along the continental margin of the eastern part of the Arabian sea due to clockwise surface circulation during peak discharge periods (Ramswamy et al,1991). In addition to the river discharge, there is also significant input of aeolian dust into the Arabian sea (Goldberg and Griffin,1970; Kolla et al,1981; Sirocko and Sarnthein,1989).

A number of studies on the surface-sediments from the Western Continental Margin of India have been reported. These studies focus primarily on the chemical and mineralogical composition of the sediments (Nair,1969; Rao,1978; Nair and Hashimi,1980,1981; Nair et al,1982; Borole et al,1982a; Gupta and Hashimi,1985; Paropkari et al,1992); particularly the spatial variations in the abundances of $CaCO_3$, Mg, Mn, organic carbon, clay-minerals and some trace elements. Broadly, these variations have been ascribed to weathering of adjacent land-mass, mixing of relict calcareous materials with those depositing from the water-column, spatial variations in the water-column productivity and influence of external forcings such as the tides and monsoonal winds. Rao (1978) has reported variations in $CaCO_3$ content of the inner shelf (water depth < 50 m) and the outer shelf sediments (water depth 50–100 m) where it ranges from 5–25% and 50–94%, respectively. Such variations have been interpreted in terms of relative contributions from recent terrigenous and relict calcareous materials in the outer shelf region (Nair and Hashimi,1980). In the same region, Nair and Hashimi (1981) have observed that aragonite is the dominant

mineral followed by low and high magnesium calcites in sediments and oolitic limestone samples. Earlier studies have reported enrichment of U (Borole et al,1982b) in anoxic shelf and slope sediments indicating its authigenic removal from seawater whereas Mn diffuses out under reducing conditions (Borole et al,1982a). Such studies point out the importance of these margin sediments as both source and sink for trace elements. Although, the distribution of organic carbon in sediments of the Arabian sea shows a broad correlation with surface productivity, the two do not appear to be directly coupled (Paropkari et al, 1992). High organic carbon (> 4%) is generally found in the upper slope sediments whereas moderate carbon content (1–4%) is observed in the lower slope regions. Lower organic carbon (< 1%) is reported in deep Arabian sea sediments beyond the lower slope. Critical evaluation of the spatial variability in the organic carbon content reveals that its high abundance coincides with the oxygen minimum zone in the overlying water-column suggesting its better preservation (Paropkari et al, 1992).

Although the riverine contribution of sediments to the eastern Arabian sea, spatial variability in mineralogic composition and elemental abundances of surface sediments are well documented and understood, there are major gaps in the understanding and interpretation of the temporal variability of redox sensitive elements (e.g. U, Mn, Fe). Also, the spatial variability of some of the particle reactive nuclides (e.g. ^{232}Th, ^{230}Th, ^{210}Pb) in the margin regions of western India and the processes controlling their distribution need to be understood.

Goals of the present study

In this study, an attempt has been made to determine the depositional fluxes of selected sedimentary constituents during the past few centuries and their relation to chemical properties, and biogeochemical processes occurring along the WCMI. This has been accomplished through geochronological and geochemical studies of sediment cores collected from this region. The specific objectives are:

(i) to determine the spatial and temporal variations in the abundances and depositional fluxes of selected sedimentary components and elements along the WCMI;

(ii) to assess the role of these sediments in sequestering and/or supplying elements to the Arabian sea interior;

(iii) to infer environmental changes, if any, that have occurred along the margin during the past few centuries.

With these objectives sediment cores were collected from the WCMI and analyzed for a suite of elements and natural radioactive isotopes belonging to U–Th series. This study is presented in the following chapters: Chapter 2 describes the experimental details and analytical procedures that were adopted. Chapter 3 deals with results and discussion followed by a summary in Chapter 4.

Chapter 2

Experimental Techniques

In order to evaluate the role of sediments from the WCMI in sequestering and/or releasing natural radionuclides and selected transition metals to the eastern Arabian sea, several short cores were collected and analyzed for various chemical constituents. The Arabian sea is strongly influenced by atmospheric forcing driven by the SW and NE Indian monsoon winds which cause seasonal oscillations in upwelling and primary productivity regimes. Recent study of Shetye et al (1990) has shown that the coastal circulation pattern during SW and NE monsoons is driven by local forcings such as the wind stress and hydrodynamic pressure gradients. The circulation pattern in the eastern Arabian sea as inferred from the hydrographic data (temp., salinity, and density) collected during the SW monsoon (1987) is similar to that of eastern boundary currents in which surface current flows along the longshore component of the wind stress (Shetye et al,1990). However, during the NE monsoon the coastal current flows against the longshore component of the wind stress (Shetye et al,1991).

A typical characteristic of the eastern boundary current is that surface ocean waters experience high photosynthetic activities and deep waters are anoxic or sub-oxic. The supply of nutrients e.g. PO_4–P and NO_3–N to upper layer of ocean is largely controlled by upwelling besides regenerative supply by local bacterial activity. The average annual column productivity (100 m water depth) between 20–25^{0}N and 60–70^{0}E ranges from 0.5 to 1 gC/m^2·d (Quasim,1977). The intermediate waters of the Arabian sea are characterized by sub-oxic/denitrification layer. Paradoxically, the most intense denitrification is reported to occur not beneath the areas of high productivity but below regions of rela-

tively weaker productivity along the continental margin (Naqvi,1994). Such features are distinctly different from other oceanic regions such as the eastern tropical Pacific ocean which is characterized by biologically productive surface waters and denitrifying zone in deeper layers.

2.1 Sampling

The above mentioned features of the eastern Arabian sea make it pertinent to study the spatial and temporal variations in the biogenic and trace elemental composition of the margin sediments. In this context, five sediment cores viz. L-8, J-7, I-5, K-11 and M-12 (Fig. 2.1), each of ~25 cm length, were raised in Dec 1988 during the 47th cruise of ORV Sagar Kanya. All these cores were collected using a spade corer (size 50×30× 20 cm) to minimize mixing of surface sections during coring. Another core 2502 (Fig. 2.1) of ~1 m length was collected using a gravity corer during Feb 1992. This core was studied upto a length of ~30 cm from the surface. The four cores, (L-8, J-7, I-5 and 2502) are from the upper slope region with water depth ranging from 280 to 350 m, where the core of denitrification layer (centered at ~300 m depth, Naqvi et al., 1990) meets the sediment-water interface. The remaining two cores, viz. K-11 and M-12 are from the lower slope where water depth is ~2500 m (Table 2.1). Immediately after collection, sub-cores of ~5 cm diameter and ~25 cm in length were sampled and subsequently the cores were cut into 1−2 cm sections for the top 10 cm length and remaining part into 2 cm sections.

The physical texture of the cores indicates that they are composed of calcareous mud. In few cores, the presence of anoxic conditions just below the sediment-water interface was evident from the smell of H_2S during sampling (Table 2.1). Such sediments, because of their anoxic nature are unlikely to be influenced by bioturbation and hence are better suited for obtaining chronological information of the margin geochemical processes.

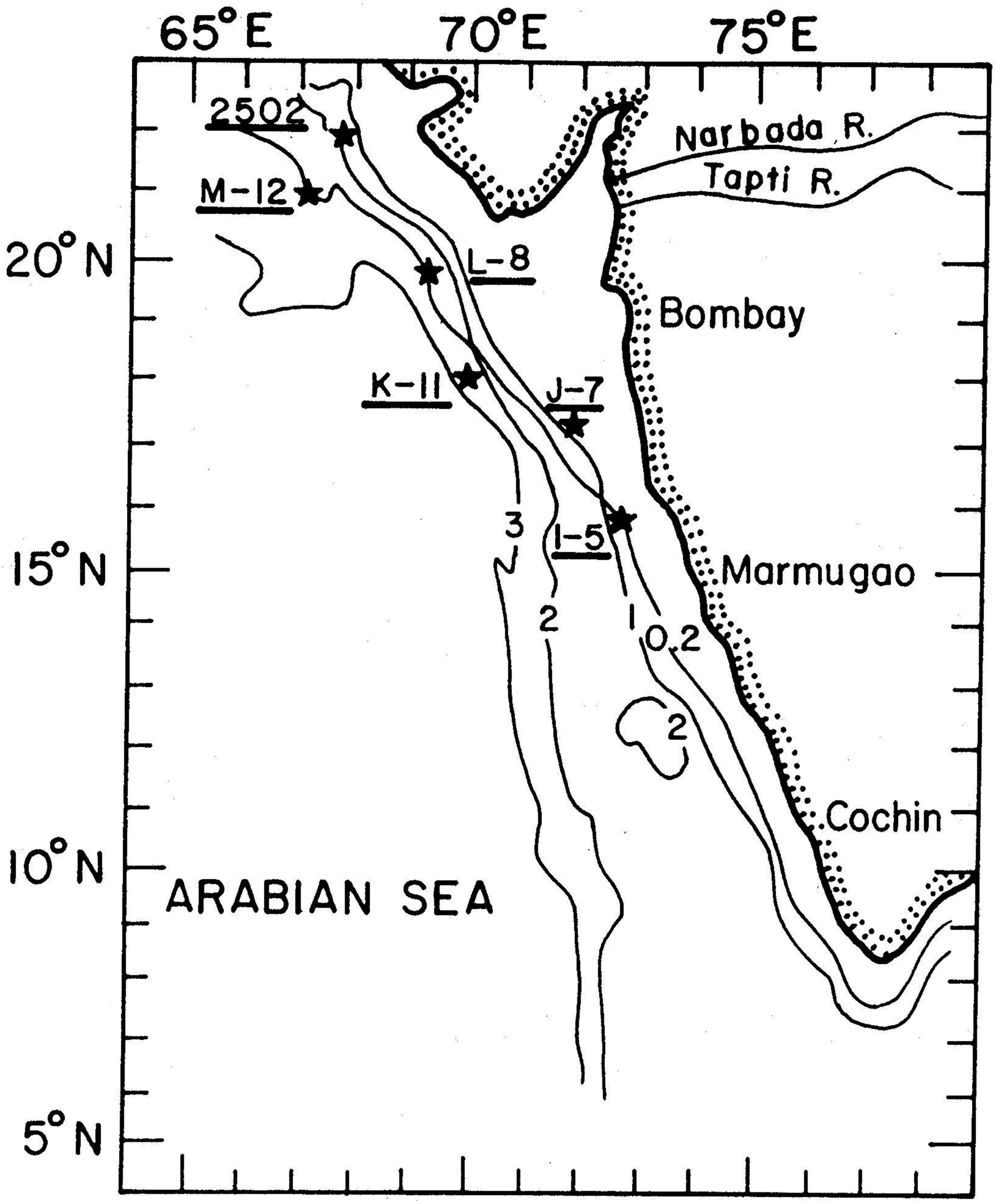

Fig. 2.1 Map showing core locations (⋆) along the WCMI with water-depth contours in km.

Table 2.1: Relevant details of sediment cores studied from the WCMI

Core	Location	Water depth (m)	Shipboard description
Upper slope			
L-8	$19^0 54' N, 69^0 24' E$	340 m	Light and green-grey clayey material H_2S smell below ~5 cm depth
J-7	$17^0 16' N, 71^0 47' E$	350 m	Coarse grained sediment with calcareous ooze and H_2S smell below ~5 cm depth
I-5	$15^0 23' N, 72^0 50' E$	350 m	Dark brown sand/silt with calcareous ooze
2502	$21^0 52' N, 68^0 E$	280 m	Brownish clayey material
Lower slope			
K-11	$18^0 01' N, 70^0 E$	2640 m	Light to dark brown clay material
M-12	$21^0 N, 67^0 E$	2300 m	Coarse grained brownish sediment

2.2 Chemical and isotopic measurements

In the laboratory, samples were dried at 110°C for 10–12 h and were analyzed for $CaCO_3$, LOI (loss on ignition, an index for organic matter), radionuclides (^{238}U, ^{232}Th, ^{230}Th, ^{226}Ra, ^{210}Pb), major and trace elements (Fe, Al, Mn, Cu, Ni, Zn and Pb). A brief description of the analytical procedures employed for these measurements is given below.

(i) $CaCO_3$ and LOI measurements:

About 100 mg of the powdered sediment sample was repeatedly leached with 10 ml of 2% acetic acid (v/v). After each leaching, the slurry was centrifuged and supernate solution was collected and made to 50 ml. An aliquot of this solution was analyzed for Ca by the EDTA titration method using solochrome blackT as the indicator (Bassett et al,1978). Along with the samples, a number of standard solutions made

from anhydrous $CaCO_3$ were also analyzed. Based on these analyses, $CaCO_3$ content of the samples was calculated. Samples in duplicate were also analyzed to check the reproducibility of the measurements. The weight loss on ignition (LOI) has been used as an index of organic matter. This was ascertained from the weight loss by heating ~1.0 g of dry, powdered sediment sample in air at 400^0C for 6–8 h.

(ii) Radionuclide measurements:

A number of nuclides belonging to the U–Th series (^{238}U, ^{234}U, ^{232}Th, ^{230}Th, ^{226}Ra and ^{210}Pb) were measured in the various sections of the sediment cores. Their distribution provides information on sediment accumulation rates, prevailing redox conditions and deposition of detrital and authigenic phases. These measurements were made following the standard radiochemical procedures (Krishnaswami and Sarin, 1976; Sarin et al 1979,1992). Briefly, ~ 2–3 g powdered sample was brought into solution by HF–$HClO_4$–HNO_3–HCl treatment in presence of ^{209}Po and ^{232}U–^{228}Th yield tracers.

The sample solution was finally converted in 0.5–0.6N HCl (~100 ml), to which ~50 mg of ascorbic acid was added in order to complex Fe^{3+}. From this solution, the Po isotopes (^{209}Po,^{210}Po) were autoplated onto a silver disc suspended in solution at a constant temperature of ~ 70^0C for 3h (Yadav et al,1992). The activities of the Po isotopes on the Ag disc were assayed by α-counting using a Si surface-barrier detector coupled to a pulse-height analyzer. The specific activity of ^{210}Pb in sediments was calculated from the measured activity of ^{210}Po.

After the Po plating, the solution was dried, residue digested with HNO_3 and dissolved in 9N HCl medium for further radiochemical separation (Fig.2.2). Uranium and thorium isotopes were separated from the solution and purified on an anion exchange column (AG1×8 Resin 100–200 mesh, Cl- form). The purified U and Th separates were then electroplated onto platinum planchets and assayed by α-spectrometry (Krishnaswami and Sarin,1976; Sarin et al,1992).

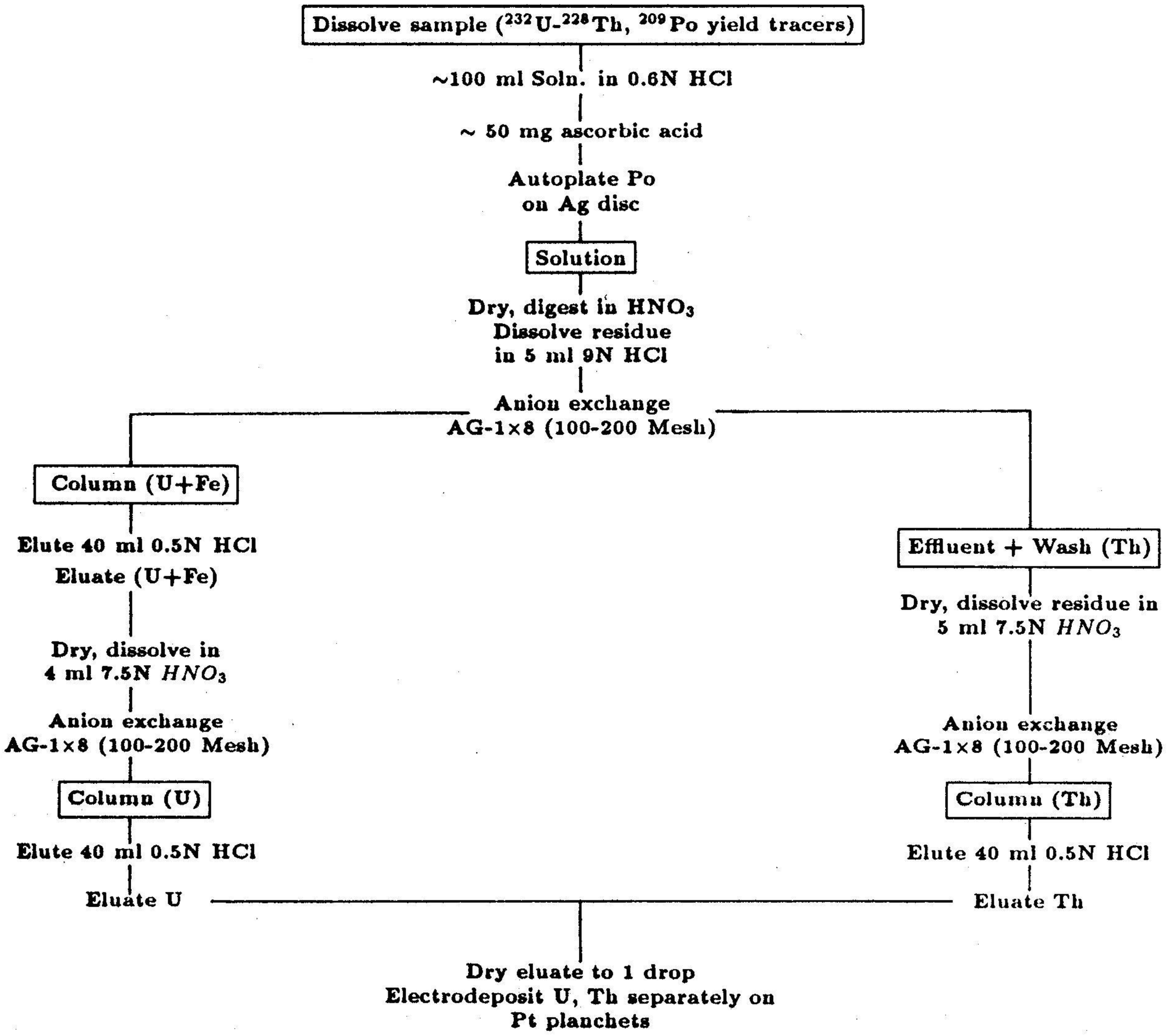

Fig. 2.2 Flow chart of the analytical procedure for separation of U, Th and Po isotopes from sediment samples (Sarin et al,1992).

For calculating the ^{232}Th and ^{230}Th concentrations, it was assumed that ^{232}Th and ^{228}Th are in radioactive equilibrium in the samples. This assumption may not be strictly valid in surface section of the cores, as there could be diffusional loss of ^{228}Ra and scavenging of ^{228}Th from bottom waters. However, as the activity of ^{228}Th tracer added as a yield monitor is 5–10 times the inherent ^{228}Th concentration, small departure from radioactive equilibrium ($\pm$ 25%) between ^{228}Th and ^{232}Th would not significantly alter the ^{232}Th and ^{230}Th concentrations calculated assuming ^{232}Th $\equiv$ ^{228}Th. To check on this two sediment samples [J-7(2–4 cm) and L-8(2–4 cm)] from upper slope region were processed for Th isotopes with and without spike. The

calculated ratio of $^{228}Th/^{232}Th$ based on these analyses (Table 2.2) show that small departures in $^{228}Th/^{232}Th$ equilibrium do not affect the measured ^{230}Th and ^{232}Th concentrations. The replicate measurements of the U–Th nuclides in the samples indicate reproducibility of the results better than ±2 %.

Table 2.2 : Thorium measurements to check validity of assumption, $^{228}Th \equiv ^{232}Th$.

Section	$^{228}Th/^{232}Th$	
	(a)	(b)
J-7 (2–4)	1.29±.04	10.29±.31
L-8 (2–4)	1.04±0.04	6.08±.21

(a) based on measurement in unspiked sample
(b) based on measurement in spiked sample

A separate aliquot of ~0.5 g dry powdered sediment sample was brought into solution by the HF–$HClO_4$–HNO_3–HCl treatment. The solution was transferred to a Rn measuring flask and purged with He gas and stored for the growth of ^{222}Rn. After about 2–3 weeks, the ^{222}Rn grown in from ^{226}Ra was milked and its activity assayed using scintillation counters (Mathieu,1988). The efficiency of extraction and counting was determined using ^{226}Ra standards. The standards and blanks were run periodically to check on the extraction efficiency and system characteristics.

The errors given in radionuclide concentrations are $\pm 1\sigma$ uncertainties calculated by appropriately summing the errors from counting statistics, blank corrections, and tracer calibrations. Blank runs for U ($^{238,234}U$) and Th ($^{232,230}Th$) showed activity levels < 1% of the signal values.

(iii) Major and Trace elements:

~0.5 g dry powdered sediment sample was brought into solution by digesting with HF–$HClO_4$–HNO_3–HCl treatment and made to 50 ml. The concentrations of Al, Ca, Fe, Mn, Ni, Cu, Zn and Pb were measured by Atomic Absorption Spectrophotometry (AAS) (Sarin et al,1979). The accuracy of measurements was checked by measuring these

elements in USGS rock standards W-1 and G-2. The results are listed in Table 2.3 which show that the agreement between reported values (Flanagan,1973) and those measured in this study is reasonably good, except for Ni and Pb for which our values are significantly higher. The higher values result from molecular absorption which were not corrected using the deuterium background corrector. However, these values are not expected to affect the relative distribution of metal abundances in various sediment sections.

Table 2.3 : Results of analysis of USGS rock standards W-1 and G-2

Elements	Flanagan (1973)	Present work*
<u>USGS-W1</u>		
Na (%)	1.57	1.56±0.07
K (%)	0.5–0.55	0.50±0.03
Ca (%)	7.81–8.10	7.96±0.13
Mg (%)	4.0–4.05	3.82±0.14
Fe (%)	7.60–7.77	7.72±0.14
Al (%)	7.86	7.90±0.06
Cu (ppm)	112–121.5	119±0.2
Zn (ppm)	69–80	87.5±3
Ni (ppm)	70–90	91.0±2
Mn (ppm)	1254–1394	1372±23
<u>USGS-G2</u>		
Ca (%)	1.39–1.54	1.43
Pb (ppm)	31.2	53.1

* Errors given are ± 1σ based on repeat analyses. For Ca and Pb, in USGS-G2 no errors are given as they are based on a single measurement.

Another approach to obtain precision of the various parameters measured in this study is made through the calculation of the coefficient of variation using the following formula

(Brewer et al,1976).

$$C.V. = \sqrt{\frac{\Sigma(d_i/x_i)^2}{2n}} \times 100 \qquad (2.1)$$

where d_i is the difference in concentration between duplicates with their mean x_i and n is the total sets of duplicate samples covering a wide range of concentrations. The repeat measurements showed reproducibility better than ±5% for $CaCO_3$ content in the range of 32 to 71%. The C.V. for different elements for the measured range of their concentrations are: Al 2%, Fe 4%, Ca 2%, Mn 2%, Ni 6%, Cu 5%, Zn 2% and Pb 7%.

The application of the radionuclide measurements and those of the major and trace elements to address the goals of the thesis are discussed in the next chapter.

Chapter 3

Results and Discussion

The spatial and temporal variations in the depositional fluxes of redox sensitive and particle reactive elements viz. U, Mn, ^{210}Pb and ^{230}Th have been studied along the WCMI. These data have been used for delineating the role of margin sediments in regulating their marine geochemical balance. In addition, temporal variations in the depositional fluxes of various elements will provide information on the environmental history of the region. To achieve some of these goals, the chronology of the sediments is very essential. This has been established by the ^{210}Pb method. For the lower slope cores an attempt has also been made to determine the sediment accumulation rate based on the ^{230}Th measurement in surface sections. Results on the chemical and isotopic analyses have been compared between the upper and lower slope sediments to evaluate the differences in the depositional patterns of various elements and their causative factors.

3.1 Geochronology of sediments

Chemical scavenging of particle reactive nuclides such as ^{210}Pb from the water-column and its subsequent delivery to sediments provides a means for evaluating the chronology of sediments. Towards this, it is necessary to ascertain the concentration of ^{210}Pb in sediments derived from the water-column, commonly termed as $^{210}Pb_{excess}$ or unsupported ^{210}Pb. In ^{210}Pb geochronology, the total ^{210}Pb content of sediments is considered to be made up of two components, ^{210}Pb derived from the water-column and ^{210}Pb continually being produced in the sediments from the decay of ^{226}Ra. The activity of $^{210}Pb_{excess}$ in

sediment section is estimated from the relation:

$$^{210}Pb_{excess} = ^{210}Pb_{total} - ^{210}Pb_{supported} \tag{3.1}$$

where $^{210}Pb_{total}$ is the total ^{210}Pb activity measured in the sample and $^{210}Pb_{supported}$ is the ^{210}Pb activity in radioactive equilibrium with ^{226}Ra. The two basic assumptions involved in the ^{210}Pb based geochronology are: (a) the flux of ^{210}Pb to the sediment has remained unchanged and (b) no migration of this radionuclide has taken place over the dating interval. If these assumptions hold good, then for steady state, the ^{210}Pb concentration at any depth in the sedimentary column would be governed by particle mixing, sedimentation, radioactive decay, and its production from ^{226}Ra. The equation governing ^{210}Pb distribution (Goldberg and Koide, 1962; Nozaki et al,1977; Krishnaswami and Lal,1978) is:

$$\frac{\partial}{\partial z}\left(D\frac{\partial(\rho A)}{\partial z}\right) - S\frac{\partial(\rho A)}{\partial z} + \lambda P\rho - \lambda(\rho A) = \frac{\partial(\rho A)}{\partial t} \tag{3.2}$$

Where D is the particle mixing coefficient (cm^2/time), S is the sediment accumulation rate (cm/time), A is the specific activity of ^{210}Pb (dpm/g) and ρ is the in-situ density of sediment (g/cm^3). Eqn. (3.2) is a generalized form and allows for variation in mixing coefficient and density with depth. However, more commonly, D and ρ are assumed constant and system is considered to be in steady state, $\frac{\partial(\rho A)}{\partial t} = 0$. In shelf and margin sediments estimates of D can be derived by measuring ^{234}Th (Aller and Cochran,1976; Aller et al, 1980; Aller and DeMaster,1984) and/or fall-out nuclides e.g. ^{137}Cs and $^{239,240}Pu$ (Guinasso and Schink,1975). In the present study, attempts to derive information on particle mixing through measurement of ^{234}Th (Aller and Cochran,1976; Aller and DeMaster,1984) were not successful because of the long time delay between sampling and laboratory measurements. Since the upper slope sediments are from regions of anoxic or sub-oxic environments, biological activities leading to particle mixing is expected to be insignificant. Under these conditions, it has been assumed that D=0, i.e. no particle mixing occurs in the upper slope sediments. However, the importance of sediment mixing resulting from physical processes is difficult to assess.

With D=0, constant ρ and $\frac{\partial(\rho A)}{\partial t} = 0$, eqn. (3.2) reduces to:

$$\rho\left[-S\frac{\partial A}{\partial z}+\lambda P-\lambda A\right]=0 \tag{3.3}$$

Setting boundary condition, $A = A_0$ at z = 0, the solution of eqn. (3.3) is,

$$(A-P)=(A_0-P)_o\cdot e^{(-\frac{\lambda}{S})\cdot z}$$

$$or,\quad (A_{210}-A_{226})=(A_{210}-A_{226})_o\cdot e^{(-\frac{\lambda}{S})\cdot z} \tag{3.4}$$

$$or,\quad {}^{210}Pb_{excess}=({}^{210}Pb_{excess})_o\cdot e^{(-\frac{\lambda}{S})\cdot z} \tag{3.5}$$

Where A_{210} and A_{226} are the activities (dpm/g) of ^{210}Pb and ^{226}Ra nuclides respectively and $(A_{210}-A_{226})_0$ is the $^{210}Pb_{excess}$ activity at surface z=0.

The assumption of constant ρ is supported by the observation that it does not show significant downcore variations (except the core M-12) as calculated from the $CaCO_3$–density relationship (Lyle and Dymond,1976). In the upper slope region, for the core J-7, uniform density of 0.58 g/cm^3 has been found throughout the core length, for L-8 it ranges from 0.42 to 0.51 g/cm^3 (mean = 0.44), for I-5 it ranges from 0.57 to 0.64 g/cm^3 (mean = 0.61) and for 2502 it ranges from 0.39 to 0.51 g/cm^3 (mean = 0.43). Similarly in lower slope region, the density of K-11 ranges from 0.42 to 0.51 g/cm^3 (mean = 0.47) and for the core M-12 it ranges from 0.29 to 0.43 g/cm^3 (mean = 0.33). The geometric mean of column averaged density of all the cores is 0.47. In all elemental flux calculations a value of 0.5 g/cm^3 for ρ has been used in this study.

To assess the validity of assumption that there is no particle mixing (i.e. D=0) in the upper slope sediments, ^{137}Cs ($t_{1/2}$=30.2 y) was measured in one of the cores, J-7, by non-destructive γ-ray spectrometry. The results are given in Table 3.1 and relative downcore variation of ^{137}Cs is presented in Fig. 3.1. The activity of ^{137}Cs could be detected to a depth of $\sim$ 6 cm from the surface, with its peak in 4–5 cm depth section. The sediment accumulation rate for this core was calculated from the peak ^{137}Cs concentration which corresponds to 1963, the year of its maximum fallout (Pierson,1971; Pennington et al,1973; Delaune et al,1978; Hermanson,1990), and 1988, the year of sample collection. The calculated sediment accumulation rate of $\sim$ 1.8 mm/y based on ^{137}Cs profile is same

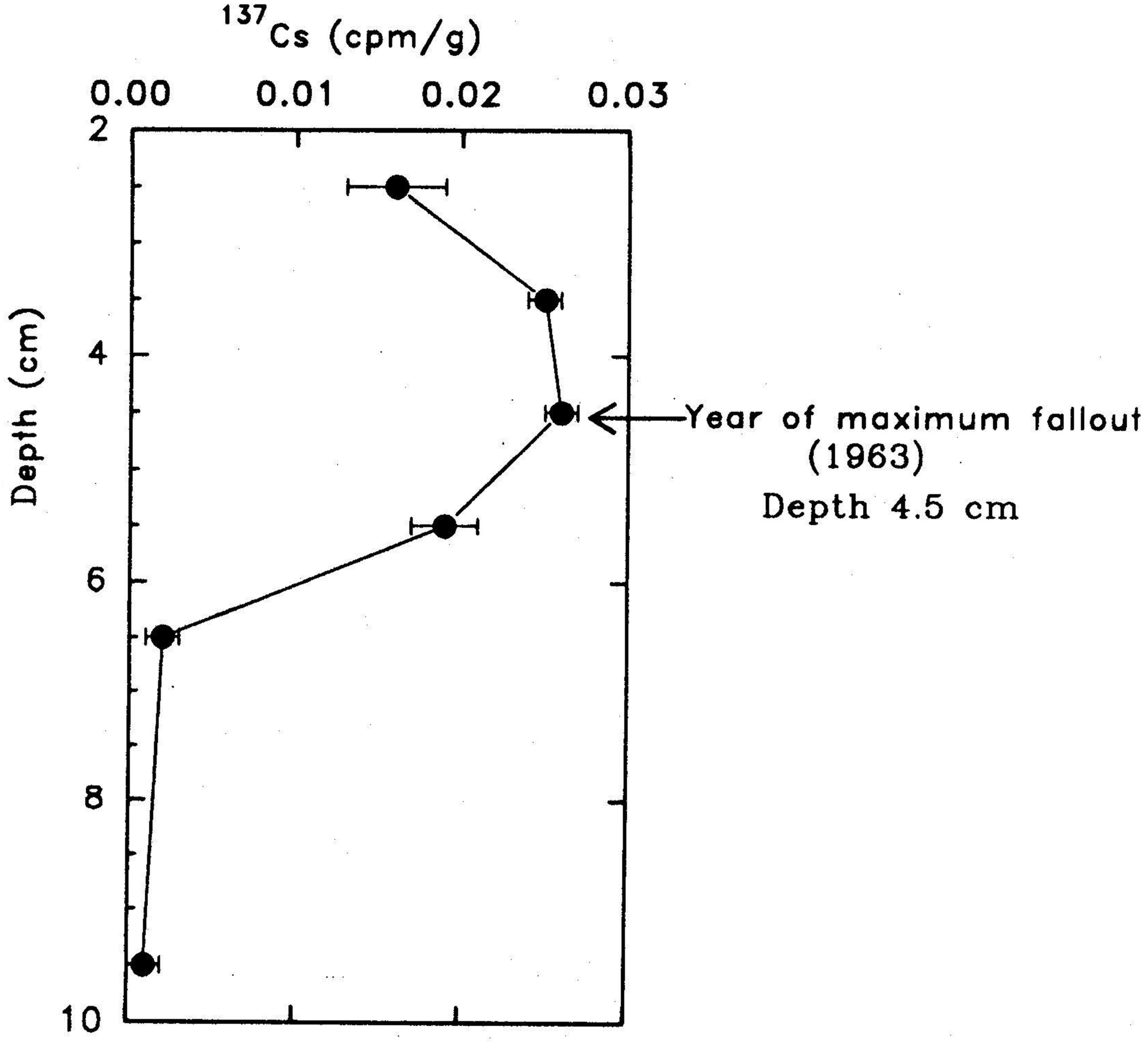

Figure 3.1: ^{137}Cs depth profile for the sediment core J-7

as that derived from the ^{210}Pb chronology as mentioned below. If the bioturbation effects are significant, then the activity of ^{137}Cs is expected further deep in the sediments, and hence the rate of sediment accumulation would be higher. As this is not observed in the core J-7, particle mixing due to bioturbation is ruled out. Therefore, assumption of D=0 (i.e no particle mixing) for these sediments in the upper slope which show smooth exponential decay of $^{210}Pb_{excess}$ is valid and hence eqn. (3.5) can be used for sediment chronology with a better degree of confidence.

Table 3.1: Distribution of ^{137}Cs in the sediment core J-7

Depth section (cm)	^{137}Cs (cpm/g)
(2–3)	0.016±0.003
(3–4)	0.025±0.001
(4–5)	0.026±0.001
(5–6)	0.019±0.002
(6–7)	0.002±0.001
(9–10)	0.001±0.001

Eqn. (3.5) predicts exponential decay of $^{210}Pb_{excess}$ with depth. The $^{210}Pb_{excess}$ vs. depth profiles for the upper slope sediments are given in Fig. 3.2. The depth profiles of all cores except 2502 show smooth exponential decay with depth which has been interpreted in terms of sediment accumulation and radioactive decay. The ^{210}Pb derived sediment accumulation rates range from 0.25 to 1.83 mm/y (Fig. 3.2) for the various cores. The activity of unsupported ^{210}Pb ($^{210}Pb_{excess}$) in the surface (0–2 cm) section of the bulk sediments from upper slope region ranges from 10.6 to 31 dpm/g (Table 3.2), while the radium supported ^{210}Pb is ~0.7 dpm/g.

In core I-5, the $^{210}Pb_{excess}$ activity decreases to very low values in the (4–6 cm) section itself. This makes it difficult to obtain an estimate of sediment accumulation in the core. However, the best fit line drawn through three data points (Fig. 3.2) yields a sediment accumulation rate of 0.39 mm/y for this core. The core 2502 shows an evidence of particle mixing in the surface as reflected by the near uniform activity of $^{210}Pb_{excess}$ in the (0–7) cm interval from the surface (Fig.3.2). In this core, therefore, the sediment accumulation rate has been determined from the $^{210}Pb_{excess}$ data in the depth interval (7–30cm) (Fig. 3.2). Assuming that the sediment accumulation rates based on $^{210}Pb_{excess}$ in the cores to be same throughout the core length; the time span covered by the upper slope cores is estimated to be in the range of 100–800 years (J-7: 120 y; L-8: 800 y and I-5: 360 y).

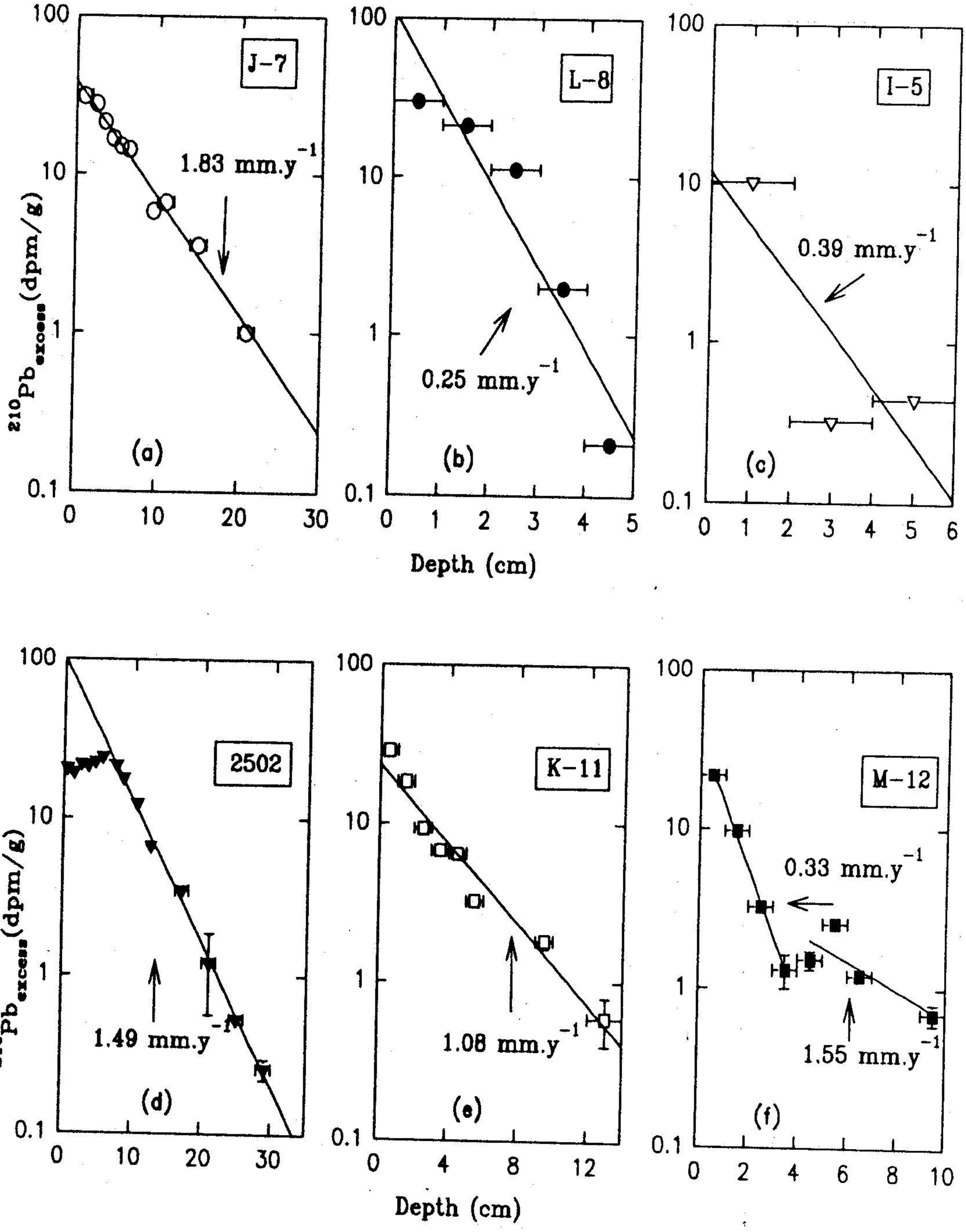

Figure 3.2: Concentration—depth profiles of $^{210}Pb_{excess}$ in sediment cores from the WCMI. The $^{210}Pb_{excess}$ distribution shows evidence of particle mixing in core 2502. In core M-12 there is a break in the slope at about 5 cm from the surface. The sediment accumulation rates of the cores, derived from the slope of the regression line are also given [eqn. (3.5)].

Table 3.2: $CaCO_3$ Concentration and Radionuclide Data† for the upper slope sediments

Sample Depth (cm)	$CaCO_3$ (%)	^{226}Ra (dpm.g^{-1})	$^{210}Pb_{excess}$ (dpm.g^{-1})	^{238}U (dpm.g^{-1})	$^{234}U/^{238}U$	^{232}Th (dpm.g^{-1})	^{230}Th (dpm.g^{-1})
J-7							
(0-2)	67.4	0.71 ± 0.03	30.9 ± 0.8	4.45 ± 0.12	1.10 ± 0.02	0.34 ± 0.01	0.62 ± 0.02
(2-3)	65.3	0.57 ± 0.03	27.6 ± 0.5	4.98 ± 0.12	1.12 ± 0.01	0.34 ± 0.01	0.62 ± 0.02
(2-3)R	65.3	-	-	4.76 ± 0.17	1.15 ± 0.03	0.34 ± 0.02	0.63 ± 0.02
(3-4)	65.3	-	21.3 ± 0.6	5.19 ± 0.13	1.16 ± 0.01	0.42 ± 0.02	0.79 ± 0.03
(4-5)	71.4	-	16.7 ± 0.4	5.13 ± 0.13	1.11 ± 0.01	0.37 ± 0.01	0.71 ± 0.02
(5-6)	71.5	-	15.0 ± 0.3	4.97 ± 0.14	1.18 ± 0.02	0.39 ± 0.02	0.65 ± 0.03
(6-7)	67.3	0.67 ± 0.04	14.2 ± 0.3	5.10 ± 0.13	1.14 ± 0.02	0.39 ± 0.02	0.71 ± 0.02
(9-10)	72.1	0.67 ± 0.05	5.9 ± 0.2	-	-	-	-
(10-12)	67.9	-	6.7 ± 0.2	5.34 ± 0.13	1.13 ± 0.02	0.45 ± 0.02	0.76 ± 0.03
(14-16)	64.9	0.72 ± 0.04	3.6 ± 0.1	5.96 ± 0.15	1.12 ± 0.01	0.44 ± 0.02	0.69 ± 0.02
(18-20)	68.8	-	-	5.92 ± 0.14	1.12 ± 0.01	0.38 ± 0.01	0.70 ± 0.02
(20-22)	68.6	-	1.0 ± 0.05	5.94 ± 0.16	1.18 ± 0.02	0.40 ± 0.02	0.74 ± 0.04
L-8							
(0-1)	43.2	0.75 ± 0.03	29.9 ± 0.6	4.25 ± 0.11	1.09 ± 0.02	0.75 ± 0.04	0.96 ± 0.05
(1-2)	43.2	0.75 ± 0.03	21.2 ± 0.5	4.25 ± 0.11	1.11 ± 0.02	0.83 ± 0.03	0.94 ± 0.03
(2-3)	46.2	0.66 ± 0.03	11.2 ± 0.2	3.99 ± 0.09	1.13 ± 0.02	-	-
(3-4)	46.2	0.66 ± 0.03	2.0 ± 0.1	5.29 ± 0.14	1.13 ± 0.01	-	-
(2-4)	46.2	0.66 ± 0.03	-	5.88 ± 0.18	1.15 ± 0.02	0.72 ± 0.03	0.92 ± 0.04
(4-5)	46.7	-	0.21 ± 0.01	6.07 ± 0.19	1.13 ± 0.02	0.75 ± 0.03	0.99 ± 0.04
(5-6)	46.7	-	⋆	7.14 ± 0.19	1.10 ± 0.02	0.65 ± 0.02	0.82 ± 0.03
(6-7)	46.5	-	⋆	7.29 ± 0.17	1.14 ± 0.01	0.81 ± 0.02	1.04 ± 0.03
(18-20)	58.5	-	-	5.73 ± 0.18	1.13 ± 0.02	0.54 ± 0.02	0.77 ± 0.03

† concentration expressed on bulk sediment basis
R denotes repeat measurement
- indicates that measurements were not made
⋆ No measurable $^{210}Pb_{excess}$ observed.

Table 3.2 $CaCO_3$ Concentration and Radionuclide Data† for the upper slope sediments (CONTINUED)

Sample Depth (cm)	$CaCO_3$ (%)	^{226}Ra (dpm.g^{-1})	$^{210}Pb_{excess}$ (dpm.g^{-1})	^{238}U (dpm.g^{-1})	$^{234}U/^{238}U$	^{232}Th (dpm.g^{-1})	^{230}Th (dpm.g^{-1})
I-5							
(0-2)	75.2	-	10.2 ± 0.2	1.03 ± 0.03	1.18 ± 0.02	0.26 ± 0.01	0.49 ± 0.02
(2-4)	74.0	-	0.32 ± 0.03	1.15 ± 0.03	1.13 ± 0.02	0.26 ± 0.01	0.52 ± 0.02
(4-6)	73.4	-	0.44 ±0.02	1.29 ± 0.03	1.14 ± 0.02	0.37 ± 0.02	0.66 ± 0.02
(6-8)	73.4	-	⋆	1.29 ± 0.03	1.14 ± 0.02	0.36 ± 0.02	0.68 ± 0.02
(8-10)	70.0	-	⋆	1.52 ± 0.04	1.10 ± 0.02	0.42 ± 0.02	0.79 ± 0.02
(10-12)	66.7	-	⋆	1.57 ± 0.04	1.11 ± 0.02	0.49 ± 0.02	0.82 ± 0.02
(12-14)	68.7	-	⋆	1.88 ± 0.05	1.12 ± 0.02	0.49 ± 0.02	0.84 ± 0.03
2502							
(0-1)	37.6	0.79 ± 0.04	20.31 ± 0.47	-	-	-	-
(1-2)	37.6	-	19.22 ± 0.56	-	-	-	-
(2-3)	40.5	-	21.71 ± 0.57	-	-	-	-
(3-4)	40.5	0.76 ± 0.04	21.23 ± 0.50	-	-	-	-
(4-5)	38.2	-	22.41± 0.63	-	-	-	-
(5-6)	38.2	-	24.07± 0.62	-	-	-	-
(7-8)	46.4	-	21.32± 0.52	-	-	-	-
(8-9)	40.5	-	17.61± 0.47	-	-	-	-
(10-11)	40.6	-	12.29± 0.35	-	-	-	-
(12-13)	49.0	-	6.66± 0.18	-	-	-	-
(16-18)	47.8	0.94±0.05	3.43±0.11	2.90±0.01	1.13±0.03	1.66±0.06	1.40±0.05
(20-22)	-	0.88±0.05	1.20±0.06	2.80±0.01	1.19±0.03	1.68±0.06	1.39±0.05
(24-26)	50.0	0.86±0.05	0.54±0.04	2.30±0.01	1.13±0.03	1.53±0.05	1.27±0.05
(28-30)	59.3	0.81±0.04	0.26±0.04	2.90±0.02	1.13±0.02	1.46±0.05	1.20±0.04

†concentration expressed on bulk sediment basis

⋆ No measurable $^{210}Pb_{excess}$ observed.

- indicates that measurements were not made

Table 3.3 $CaCO_3$ concentration and Radionuclide Data† for the lower slope sediments

Depth (cm)	$CaCO_3$ (%)	^{226}Ra (dpm.g^{-1})	$^{210}Pb_{excess}$ (dpm.g^{-1})	^{238}U (dpm.g^{-1})	$^{234}U/^{238}U$	^{232}Th (dpm.g^{-1})	^{230}Th (dpm.g^{-1})
K-11							
(0-1)	43.9	3.86 ± 0.16	28.5 ± 0.6	0.78 ± 0.03	1.07 ± 0.04	0.88 ± 0.03	4.58 ± 0.12
(1-2)	49.2	-	18.1 ± 0.5	0.81 ± 0.03	1.04 ± 0.03	0.88 ± 0.03	4.53 ± 0.13
(2-3)	50.9	-	9.3 ± 0.3	0.81 ± 0.03	1.12 ± 0.04	0.87 ± 0.04	4.63 ± 0.14
(3-4)	51.2	-	6.7 ± 0.3	1.02 ± 0.03	0.99 ± 0.03	1.13 ± 0.04	4.84 ± 0.14
(4-5)	53.2	-	6.4 ± 0.3	0.92 ± 0.03	1.06 ± 0.03	1.00 ± 0.04	4.51 ± 0.14
(5-6)	51.6	6.0 ± 0.20	3.2 ± 0.3	1.04 ± 0.03	0.99 ± 0.02	1.05 ± 0.04	4.52 ± 0.14
(9-10)	54.6	-	1.8 ± 0.2	0.86 ± 0.03	1.05 ± 0.03	0.96 ± 0.03	4.18 ± 0.12
(12-14)	52.3	-	0.6 ± 0.2	0.92 ± 0.03	1.11 ± 0.03	0.87 ± 0.03	4.28 ± 0.11
(16-18)	56.3	2.60 ± 0.20	⋆	1.33 ± 0.05	1.09 ± 0.04	0.92 ± 0.03	3.63 ± 0.09
(18-20)	56.3	-	⋆	1.59 ± 0.04	1.08 ± 0.02	0.79 ± 0.03	2.99± 0.08
(22-24)	59.7	2.30±0.10	⋆	2.85 ± 0.08	1.09 ± 0.02	0.82 ± 0.03	3.01 ± 0.08
M-12							
(0-1)	18.2	5.80 ± 0.20	21.5 ± 0.6	1.26 ± 0.04	1.03 ± 0.03	2.78 ± 0.08	2.88 ± 0.08
(1-2)	18.2	6.50 ± 0.10	9.7 ± 0.4	1.25 ± 0.04	1.02 ± 0.03	2.58 ± 0.08	2.49 ± 0.08
(2-3)	23.2	3.30 ± 0.20	3.2 ± 0.3	1.25 ± 0.04	1.09 ± 0.03	2.29 ± 0.08	2.24 ± 0.08
(3-4)	23.2	3.10 ± 0.10	1.3 ± 0.3	1.47 ± 0.05	1.03 ± 0.03	2.10 ± 0.07	2.24 ± 0.07
(4-5)	27.4	3.20 ± 0.20	1.5 ± 0.2	1.44 ± 0.05	1.09 ± 0.03	2.19 ± 0.07	2.34 ± 0.08
(5-6)	-	3.70 ±0.10	2.5 ± 0.2	-	-	-	-
(6-7)	31.6	4.00 ±0.10	1.2 ±0.1	1.36 ± 0.04	1.06 ± 0.03	1.65 ± 0.05	2.95 ± 0.08
(9-10)	-	4.00 ± 0.10	0.7 ± 0.1	-	-	-	-
(12-14)	36.9	-	⋆	1.37 ± 0.04	1.08 ± 0.03	1.44 ± 0.04	3.02 ± 0.08
(20-25)	45.0	-	⋆	2.25 ± 0.06	1.08 ± 0.02	1.26 ± 0.04	2.98 ± 0.08

† concentration expressed on bulk sediment basis

- indicates that measurements were not made

⋆ No measurable $^{210}Pb_{excess}$ observed

For the two lower slope sediments cores (K-11 & M-12), because of the oxic conditions at the sediment-water interface, bioturbation cannot be ruled out. Therefore, for these two cores the sediment accumulation rates based on $^{210}Pb_{excess}$ decay (1.08 and 0.33 mm/y respectively for K-11 and M-12, Fig. 3.2) could be an upper limit. The $^{210}Pb_{excess}$ activity in surface section of K-11 and M-12 sediment cores (Table 3.3) is, 28.5 and 21.5 dpm/g respectively. The $^{210}Pb_{excess}$ versus depth profile for M-12 (Fig. 3.2) shows two distinct slopes indicating a change in sediment accumulation rate. The deeper sections (> 5 cm from surface) of the core have higher rate of sediment accumulation (1.55 mm/y) than that in the surface ~ 5 cm (0.33 mm/y).

An independent approach to determine the rate of sediment accumulation for the cores from the lower slope region is based on the measured concentration of $^{230}Th_{excess}$ activity (dpm/g) in their surface sections and comparing it with the ^{230}Th production rate from the overlying water-column. Analogous to ^{210}Pb, ^{230}Th content of sediments is also made of two components; one scavenged from seawater and the other continentally derived. The total activity of ^{230}Th in a sediment section, as measured by totally dissolving the sample, can be expressed as:

$$^{230}Th_{total} = ^{230}Th_{excess} + ^{230}Th_{detrital} \tag{3.6}$$

where $^{230}Th_{detrital}$ is the continentally derived component. One approach to obtain $^{230}Th_{detrital}$ component of sediments would be to assume that ^{238}U and ^{230}Th are in radioactive equilibrium. This may not be a quantitative approach as in the river suspended phases ^{230}Th is generally in excess of uranium (Scott,1982; Sarin et al,1990). Therefore, a better approach to assess the detrital contribution is from a knowledge of the $^{230}Th/^{232}Th$ ratios in river sediments draining into the margin. The Narbada, Tapi and the Indus are the rivers supplying sediments to the eastern Arabian sea, however, there is no data on the $^{230}Th/^{232}Th$ ratios of these sediments. In the absence of such data the activity of $^{230}Th_{detrital}$ was estimated using the relation:

$$^{230}Th_{detrital} = \left(\frac{^{230}Th}{^{232}Th}\right)_{upper\ slope} \cdot {}^{232}Th_{lower\ slope} \tag{3.7}$$

This approach assumes that the $^{230}Th/^{232}Th$ of upper slope sediments is representative of the detrital component. This assumption should be valid as these cores are from very

shallow water depths and hence the deposition of ^{230}Th from the overlying water column would be insignificant unless there is boundary scavenging and focusing of ^{230}Th.

Using the average ^{230}Th/^{232}Th activity ratio of (1.64 ±0.24) for L-8, J-7 and I-5 cores and ^{232}Th (0.88±0.03 dpm/g) measured in the upper section of the core K-11, $^{230}Th_{detrital}$ is calculated to be 1.44±0.39 dpm/g. From the $^{230}Th_{total}$ (4.58±0.12 dpm/g), $^{230}Th_{excess}$ activity of 3.14±0.41 dpm/g is estimated for the core K-11. The $^{230}Th_{excess}$ activity in surface section is related to the ^{230}Th depositional flux and sediment accumulation rate (Krishnaswami,1976) as:

$$A_0^{230} = \frac{F}{S \cdot \rho} \tag{3.8}$$

where $A_0{}^{230}$ is the $^{230}Th_{excess}$ activity at the core top (dpm/g), F is the depositional flux of ^{230}Th, i.e. equivalent to its production rate from ^{234}U in the water column, S the sediment accumulation rate and ρ is the density of sediment. The value of F for K-11 (water depth 2600 m) is 6.8 dpm/cm^2 $\cdot 10^3$ y. Using ρ = 0.5 g/cm^3 and A_0^{230} = 3.14±0.41 dpm/g, the sediment accumulation rate for the core is calculated to be 0.04 mm/y. This rate is about an order of magnitude lower than that derived from the $^{210}Pb_{excess}$ profile. If the $^{230}Th_{excess}$ based sediment accumulation rate is indeed valid then it would imply that the $^{210}Pb_{excess}$ distribution in this core is considerably influenced by particle mixing. Alternately, the high $^{230}Th_{excess}$ in the surface sediments could result from focussing and boundary scavenging effects (Anderson et al, 1983). Therefore, the above mentioned $^{230}Th_{excess}$ method of dating the sediments can be questionable. Attempt to use similar approach for deriving sediment accumulation rate in the core M-12 was not successful, as the (^{230}Th/^{232}Th) activity ratio in its surface section is comparable to or less than the mean ratio (1.64 ±0.24) in the upper slope sediments.

^{14}C chronology

In addition to ^{210}Pb and ^{230}Th nuclides, attempts were also made to determine the ages of these sediments using ^{14}C as these sediments are calcareous (18–75% $CaCO_3$). The ^{14}C measurements were made at the PRL (Chemistry) Radiocarbon laboratory (Bhushan et al,1994). The ^{14}C ages of various sections in core J-7 center around 7200 years; whereas in the core M-12, the ^{14}C ages show a reversal with the oldest age at the surface compared

to that for the deeper sections (Table 3.4). For the core K-11, the ^{14}C age increases from 3780±70 y in the (5−10) cm section to 7640±70 y in the (20−22.5) cm section (R. Bhushan, Personal communication). Prior to this work, ^{14}C ages for surficial sediments and limestone formations along the western shelf of India have been reported to be ranging from 11000 to 9000 years B.P. (Nair,1975; Nair et al,1979; Rao et al,1994).

The ^{14}C data obtained in this study can be explained based on the occurrence of relict calcareous materials such as oolitic and algal limestones and calcareous sand stones along the WCMI (Rao,1978; Nair and Hashimi,1980; Rao et al, 1994). Also, there is possibility of dead calcareous material from the milliolite deposits which are abundantly present in Saurashtra coast (Baskaran,1985). The mixing of these relict carbonates with nascent carbonate shells settling from the water column can yield older ages measured in this work. Unless the effect of mixing of various carbonates is ascertained it is not possible to obtain reliable ages based on ^{14}C. Therefore, the ^{14}C data have not been used to derive sediment accumulation rates.

Table 3.4: ^{14}C ages of WCMI sediments

Depth (cm)	Age B.P. (y)
J-7	
(0-4)	7100±85
(6-10)	7485±64
(24-29)	7093±62
M-12	
(0-4)	6323±106
(14-16)	4308±71
(20-25)	4623±76
K-11	
(5-10)	3786±70
(15-20)	7000±67
(20-22.5)	7641±72

3.2 $CaCO_3$ and Organic matter

The occurrence of both $CaCO_3$ and organic matter in sediments is biogenic in nature, their abundances are in some way related to the overhead water-column productivity. The abundance of $CaCO_3$ in upper slope sediments, along 350 m bathymetry over 5^0 latitudinal distance (20–15^0N), shows significant spatial variation. In cores J-7, L-8, I-5 and 2502, $CaCO_3$ content ranges from 37 to 75% (Table 3.2, Fig. 3.3). Within each of these cores there is no significant downcore variations. The calculated mean $CaCO_3$ abundance, along with the standard deviation in each core is: J-7 (68.6±2.7%), L-8 (47.7±4.3%), I-5 (73.9±0.8%) and 2502 (43.5±6.5%).

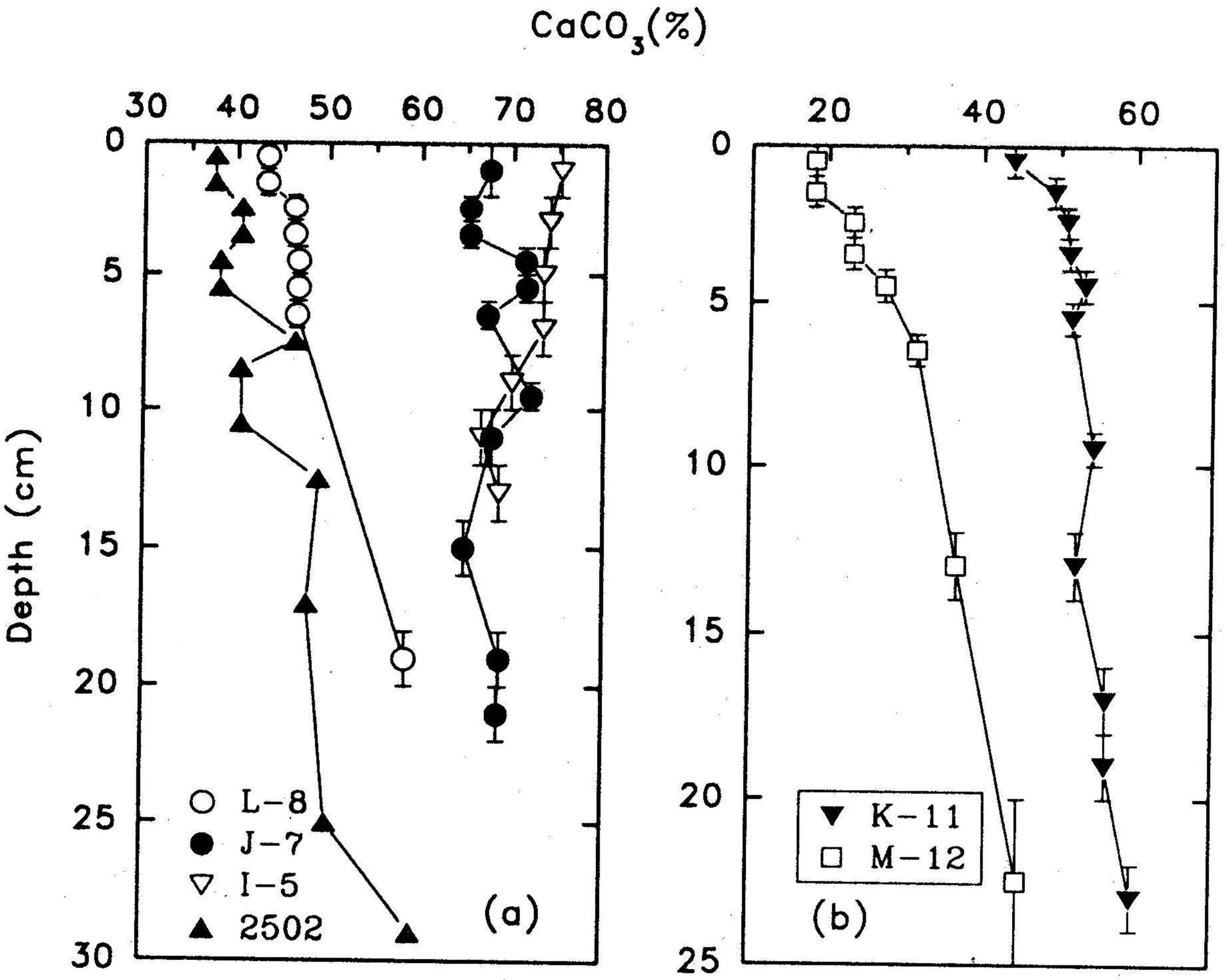

Figure 3.3: Variation in $CaCO_3$ content with depth for (a) upper and (b) lower slope sediments respectively.

The observed range in $CaCO_3$ abundances agrees well with the values reported in earlier studies (Rao,1978; Kolla et al,1981; Borole et al,1982a) for this region. Use of $CaCO_3$ content in sediments as a measure of paleoproductivity requires that the $CaCO_3$

in the sediments is solely derived from the biological productivity in the water column and that they are well preserved after deposition. This condition is, however, may not strictly valid for the WCMI sediments as they may have relict carbonates; as evidenced from the "older" ^{14}C ages of these carbonate sediments. Because of this, the $CaCO_3$ content of these sediments has not been used as a proxy for productivity. It is also noteworthy that $CaCO_3$ increases southward from 20^0N latitude, which has been attributed to enhanced biological production based on foraminiferal analysis (Naidu et al, 1992).

The content of organic matter (as inferred from loss in weight on ignition) decreases from 15% to 3% between 20 to 17^0N along the same 350 m bathymetry. The highest organic matter in surface sediments has been found in the core L-8 (15%) followed by that in the core J-7 (7.7%). These cores are essentially from anoxic regions (as evidenced by H_2S smell during sampling) where better preservation of organic matter is expected. Earlier study (Paropkari et al,1992) has shown that the organic matter in upper slope region is primarily of marine origin and is derived from productivity of overlying waters which varies from 0.25 to 0.75 $gC/m^2 \cdot d$. This range of productivity is nearly three times lower than that from other coastal regions of the Arabian sea. Also, moderate to high concentrations of organic carbon (2–4 and 4–16%) are reported over the entire upper slope region (Kolla et al,1981; Paropkari et al,1992). High organic carbon observed in this region is generally interpreted in terms of its efficient preservation under anoxic conditions (Kolla et al,1981; Paropkari et al,1992) which depends primarily on the high rate of sediment accumulation.

The calcium carbonate content in the sediment cores, K-11 and M-12, from the lower slope region ranges from 18 to 60% respectively. M-12 shows the lowest calcium carbonate concentration compared to all other cores analyzed in the present study. These values of $CaCO_3$ are again consistent with the previous studies (Kolla et al,1981). In both the lower slope cores, a systematic increase in $CaCO_3$ content with depth is observed (Fig. 3.3). Maximum $CaCO_3$ variation, to an extent of 60% relative to the surface, is seen in the core M-12. Such a change can result from temporal variation in depositional environment. An alternative interpretation for the downcore increase in $CaCO_3$ in these cores can be sought as due to the deposition of $CaCO_3$ (relative to detrital silicate) being higher in the past compared to that at the present. Nair and Hashimi (1981) have reported an increased

deposition of relict calcareous materilas during the Holocene period along the western continental shelf which might have also influenced the deeper section of the lower slope cores. The contribution of relict carbonates to various depth needs to be ascertained to use the $CaCO_3$ depositional flux as an index of paleoproductivity. The content of organic matter in both the lower slope cores is about 3% in their surface sections. A marked difference in organic matter contents between upper and lower slope sediments could be attributed to their combustion through the water column.

3.3 ^{210}Pb depositional flux

The $^{210}Pb_{excess}$ inventory and depositional flux provide information about the importance of overhead vs. boundary scavenging processes at the core sites (Bacon et al,1976; Spencer et al,1981; Cochran et al, 1983; Thomson et al,1993).

Inventories of $^{210}Pb_{excess}$ in the margin sediments can be calculated using the relation:

$$\mathbf{I} = \rho \cdot \int_0^\infty \mathbf{A(z)dz} \tag{3.9}$$

$$\mathbf{or,\ I} = \rho \cdot \Sigma(\mathbf{A_i}.\mathbf{z_i}) \tag{3.10}$$

and is related to the mean ^{210}Pb depositional flux by:

$$\mathbf{J} = \lambda_{210}.\mathbf{I} \tag{3.11}$$

where **I** is the $^{210}Pb_{excess}$ inventory in dpm/cm^2; ρ is the *in-situ* density of sediments (0.5 g/cm^3), z_i is the thickness of sample in cm at depth interval i; **J** is the mean $^{210}Pb_{excess}$ depositional flux at the core site in dpm/cm^2·y and λ_{210} is the ^{210}Pb decay constant(0.0311 y^{-1}). For the cores analyzed in this study, the calculated *in-situ* density ρ based on Lyle and Dymond (1976), ranges between 0.29 to 0.64 g/cm^3 and is fairly constant with depth with an exception of the core M-12. The assumption of constant density of 0.5 g/cm^3 is not strictly valid for the core M-12 where it increases with depth from 0.29 to 0.43 g/cm^3. The average density ($\overline{\rho}$) calculated for each core is given in Table 3.5, however, a value of 0.5 g/cm^3 is used for the calculation of I. The calculated values of the $^{210}Pb_{excess}$ inventory for the different cores are given Table 3.5 along with the sediment accumulation rates and

extrapolated $^{210}Pb_{excess}$ activities (i.e. A_o) at sediment-water interface. The value based on eqn. (3.10) is a better estimation of $^{210}Pb_{excess}$ inventory, as this represents the sum of measured $^{210}Pb_{excess}$ activities in the sediment column. Also in cores such as M-12, this method of finding the $^{210}Pb_{excess}$ inventory is logical as the sediment accumulation has changed with depth.

Table 3.5: Rates of sediment accumulation and $^{210}Pb_{excess}$ inventory in WCMI sediments

Core	$\overline{\rho}$ (g/cm^3)	S (mm/y)	A_0 (dpm/g)	I* (dpm/cm^2)	$J_{obs.}$ (dpm/cm^2·y)	$J_{exp.}$ (dpm/cm^2·y)
J-7	0.58	1.83	38.5	108.7	3.38	1.1
L-8	0.44	0.25	107.2	31.8	0.99	1.1
I-5	0.61	0.39	11.9	10.9	0.34	1.1
2502	0.43	1.49	100.0	133.1	4.14	1.1
K-11	0.47	1.08	28.4	41.5	1.29	1.85
M-12	0.33	0.33, 1.55	36.5	20.6	0.64	1.85

* based on eqn. (3.10)

Using eqn.(3.10), the calculated mean depositional flux of $^{210}Pb_{excess}$ in sediments from upper slope region (J-7, L-8, I-5 and 2502) ranges between 0.34 to 4.14 dpm/cm^2·y (Table 3.5). Since these sediment cores are from the region of water depth ranging between 280 to 350 m, the $^{210}Pb_{excess}$ flux derived from its *in-situ* production (from ^{226}Ra, typically 0.1 dpm/l; Sarin et al,1994) in the water column would be $\sim$ 0.1 dpm/cm^2·y, which is, around 10% of atmospheric fallout ($\sim$ 1 dpm/cm^2·y; Lal et al,1979). Therefore, $J_{exp.}$ flux would be 1.1 dpm/cm^2·y (Table 3.5) of which the dominant component is from the atmospheric fallout. For the two cores from the lower slope region (K-11 and M-12), in addition to atmospheric supply, the ^{210}Pb flux of 0.85 dpm/cm^2·y (Sarin et al,1992) from overlying water-column (based on ^{210}Pb–^{226}Ra disequilibrium) also contributes to the total ^{210}Pb inventory. Therefore, the ^{210}Pb flux in lower slope sediments is expected to be 1.85 dpm/cm^2·y (Table 3.5). The values of J_{obs} in these cores (K-11 and M-12) are 1.29 and 0.64 dpm/cm^2·y respectively.

The observed flux of $^{210}Pb_{excess}$ is, therefore, both low and high relative to the expected value (Table 3.5). Similar results have been reported in an earlier study (Borole,1988). However, in the upper slope region at some selected sites, the $^{210}Pb_{excess}$ flux far exceeds the expected depositional flux. For example, at the core locations J-7 and 2502, the $^{210}Pb_{excess}$ flux is higher by a factor of three and four respectively. The ratio of observed to expected $^{210}Pb_{excess}$ fluxes in these cores is much lower than that reported in other

margin regions such as Washington continental shelf and slope sediments (Carpenter et al,1981). Such higher supply of $^{210}Pb_{excess}$ flux to the Washington margin sediments has been explained through advection of seawater containing dissolved ^{210}Pb produced *in situ* from ^{226}Ra followed by enhanced scavenging (Carpenter et al,1981). A distinct difference in $^{210}Pb_{excess}$ flux in WCMI margin sediments and that in Washington shelf and slope regions is that at some sites along the WCMI, the observed values are significantly lower than the expected supply. This indicates that ^{210}Pb does not deposit at some sites due to high energy environment but gets focussed onto sediments at other sites. A significant positive correlation (r=0.89) has been observed between sediment accumulation rates and $^{210}Pb_{excess}$ inventory (I) in these sediments (Fig. 3.4).

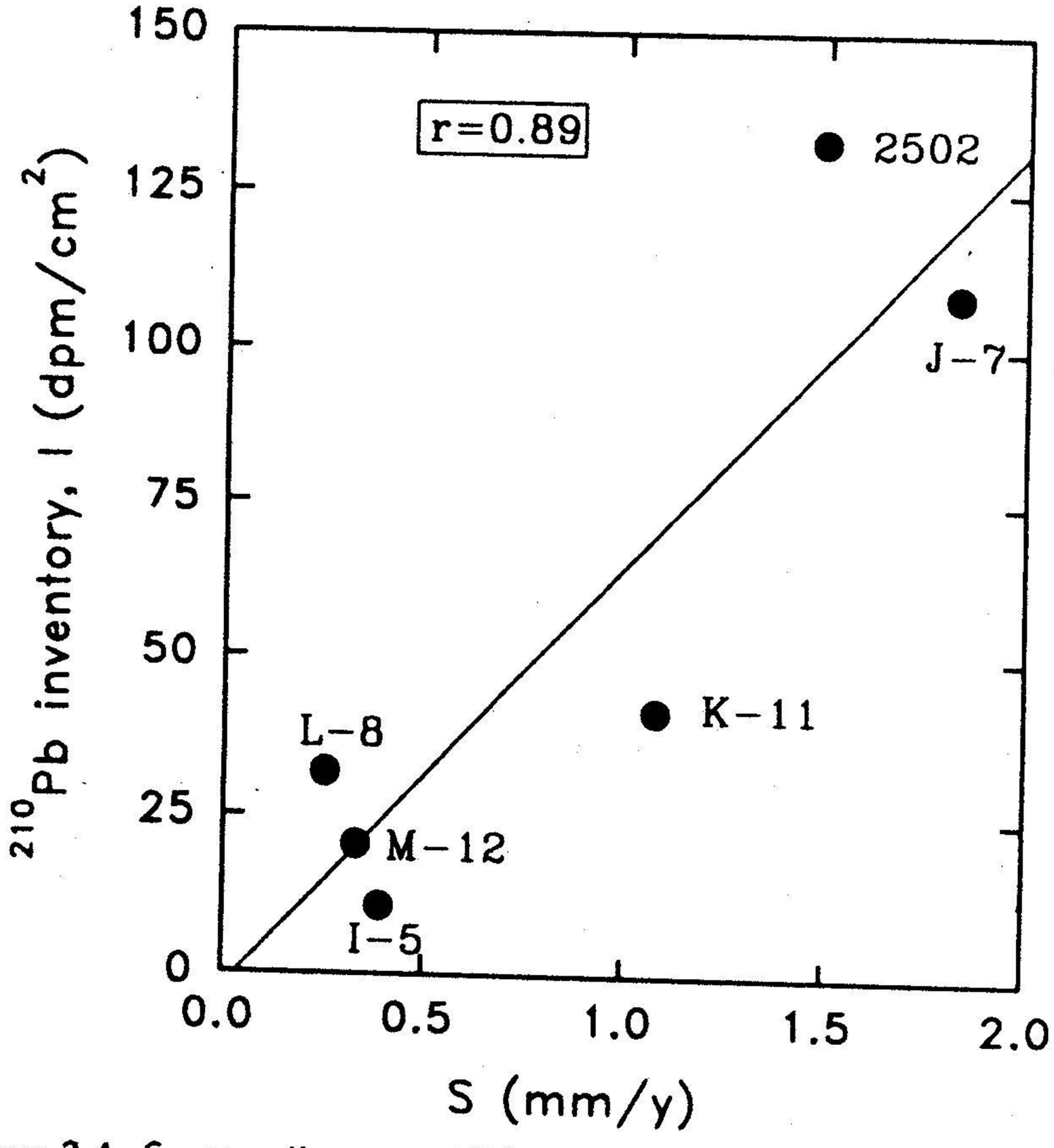

Figure 3.4: Scatter diagram of $^{210}Pb_{excess}$ derived sediment accumulation rates and $^{210}Pb_{excess}$ inventory in the sediment cores. The increasing $^{210}Pb_{excess}$ inventory with the sediment accumulation suggests focussing of ^{210}Pb along the margin sediments.

This enhanced $^{210}Pb_{excess}$ inventory is due to sediment focussing. These results point out that the source of ^{210}Pb to WCMI sediments is atmospheric but its deposition pattern is dependent on the accumulation rates of sediments.

3.4 Distribution of Mn in the WCMI sediments

It has been well documented that in anoxic marine sediments, where sediment accumulation is relatively high, manganese is mobilized as Mn(II) from the solid phase to solution (Lynn and Bonatti,1965; Holdren et al,1975; Jones and Murray,1985). In margin areas, the primary source of Mn to sediments is land-derived. Hence, one of the approaches to obtain information of Mn mobilization is to compare the abundances of Mn in margin sediments with that in the silicate matrix of the river-borne particles. The manganese concentration in sediments of the upper slope region of WCMI averaged over core length on a $CaCO_3$ basis (Table 3.6) varies from 285 to 350 ppm. This range of manganese concentration is similar to those reported earlier on surficial sediments of WCMI (Murty et al, 1978; Borole et al,1982a).

Table 3.6 : Mn concentration in the upper slope sediments on a $CaCO_3$ free basis.

Core: L-8		Core: J-7		Core: I-5	
Depth (cm)	Mn (ppm)	Depth (cm)	Mn (ppm)	Depth (cm)	Mn (ppm)
(0-1)	349	(0-2)	330	(0-2)	287
(1-2)	316	(2-3)	339	(2-4)	253
(2-3)	303	(3-4)	286	(4-6)	291
(3-4)	308	(4-5)	360	(4-6)R	273
(3-4)R	314	(5-6)	357	(6-8)	310
(4-5)	333	(6-7)	349		
(5-6)	343	(9-10)	362		
(6-7)	323	(10-12)	406		
(8-10)	328	(14-16)	354		
(10-14)	321	(18-20)	340		
(18-20)	359	(20-22)	390		
$\overline{Mn}$ =	327*	$\overline{Mn}$ =	352*	$\overline{Mn}$ =	283*

* concentration averaged over entire core length
R denotes replicate analysis

The mean Mn concentration on a $CaCO_3$ free basis for the three cores studied is $\sim$ 320 ppm, a factor of three lower compared to that reported in the river suspended particles ($\sim$1000 ppm) transported by the Narbada/Tapti rivers to this shelf region (Borole et al,1982a). The lower Mn concentration in these upper slope sediments could result from

its preferential mobilization or due to dilution by biogenic and detrital components such as opal, organic matter, quartz etc. To determine if the low Mn concentration in the shelf sediments is due to dilution effects, the Mn/Al weight ratios in these cores have been compared with the Mn/Al ratios of the Narbada/Tapti river particles. As the Mn/Al ratios in these cores do not vary significantly with depth, the mean values taken over entire core lengths are compared with the Mn/Al weight ratio in the river-borne particles. The average Mn/Al ratios for these cores are: J-7 $(64\pm2)\times10^{-4}$, L-8 $(58\pm3)\times10^{-4}$, I-5 $(60\pm7)\times10^{-4}$ compared to values of 116×10^{-4} and 174×10^{-4} for the Narbada and Tapti particles (Borole et al,1982a). The Mn/Al weight ratio in river particles is higher by a factor of two to three compared to that of the upper slope sediments. Such a large difference in Mn/Al ratio can arise only due to the process other than dilution. The most likely mechanism for the low Mn content in the upper slope sediments is its reductive mobilization.

The mobilization of Mn from solid phase to solution in reducing sediments has been well documented (Lynn and Bonatti,1965; Trefrey and Presley,1982; Heggie et al,1987). Such mobilization influences the distribution of Mn in sediments and in seawater (Martin and Knauer,1984; Johnson et al,1992). Considering that the upper slope sediments are from reducing region and that dilution by biogenic and detrital components is not the cause of the low Mn abundance in them, it can be suggested that mobilization of Mn from solid phase to seawater under sub-oxic/anoxic conditions results in its low concentration. Also uniform distribution of Mn (Fig. 3.3) over the core length sampled for the upper slope sediments indicates that the sub-oxic/anoxic environment has remained unchanged over ~100–800 years BP.

For a typical sediment accumulation rate of 1 mm/y (typically observed in upper slope region, Table 3.5), a rough estimate of flux of Mn mobilized from these sediments can be obtained from the relation:

$$F_{Mn} = S \cdot \rho(C_r - C_s) \tag{3.12}$$

where F_{Mn} is the flux of Mn mobilized ($\mu g/cm^2 \cdot y$), S is the sediment accumulation rate, ρ *in-situ* density, C_r and C_s are the Mn concentration in river particles ($\sim$ 1000 ppm) and in the upper slope sediments on $CaCO_3$ free basis ($\sim$ 350 ppm). The value of F_{Mn} is

calculated to be 35 μg/cm^2·y. If the flux of Mn, as estimated above, is representative of an area 5^{0}lat×3^{0}long bounded by these cores, F_{Mn} is calculated to be ~5.0 × 10^{10} g/y which is nearly 15% of the dissolved Mn (~ 3 × 10^{11} g/y) transported by world rivers to ocean (Martin and Meybeck,1979). The estimated release of Mn from WCMI re-emphasizes the importance of the margin sediments in regulating the marine geochemical cycle of redox sensitive elements such as Mn. Furthermore, manganese mobilized from the upper slope region can be a potential source for the dissolved manganese maxima observed in the Arabian sea intermediate waters (Saager et al, 1989; Saager, 1994). However, it may also be possible that mobilization of Mn is occurring in the sub-oxic/denitrification layers from the sinking fluvial material or in the sediments. To understand and quantify the Mn mobilization from settling river particles through water column, it would be necessary to collect these particles using sediment traps and analyze them for Mn.

Table 3.7: The benthic manganese flux from margin sediments

Margin sites	Mn flux (μg/cm^2·y)	Reference
WCMI (upper slope)	~ 35	This study
Central California coast line	~ 10	Johnson et al, 1992
Gulf of St. Lawrence	~ 140−180	Sundby and Silverberg,1985
Mississippi Delta	~ 30−850	Trefry and Presley, 1982
Eastern Berring shelf	~ 1	Heggie et al, 1987

The flux of manganese solublized due to either of these proposed mechanisms vary from place to place (Heggie et al,1987; Johnson et al,1992). It is generally related to rates of sedimentation, biological productivity and also to the particle mixing by bioturbation (Aller, 1980). Johnson et al (1992) have reported that the average benthic flux (μg/cm^2·y) of Mn, (measured by using benthic chambers) from continental margin of Central California is supported predominantly by sinking particulate organic carbon and to a lesser extent by $CaCO_3$ dissolution. They have hypothesized that remineralization of organically bound Mn occurs primarily in a thin fluff layer (< 1 mm) at the sediment surface. Sundby and Silverberg (1985) have studied manganese cycling in Laurentian

trough (water depth, 300–400 m) and applied a diagenetic modelling and mass–balance calculations to derive the Mn flux. They observed that only 13–29% of total manganese escaped from the sediment surface amounting to a net flux of 140–180 $\mu g/cm^2 \cdot y$ (Table 3.7). The magnitude of particle mixing by bioturbation was considered to be a deciding factor for increasing rate of Mn cycling both in the sediment core (internal cycling) and the fraction escaping to overlying waters.

Trefry and Presley (1982) have interpreted the deficiency of Mn in the Mississippi delta sediments, compared to that in the river particulates, as due to its mobilization under reducing conditions. Using the concentration gradient of Mn in sediment pore waters they calculated the outgoing diffusive manganese flux from sediments (water depth < 100 m) in the range of 30–850 $\mu g/cm^2 \cdot y$ (Table 3.7).

The low manganese concentration in the upper slope sediments by a factor of 3–4 compared to that transported through Narbada/Tapti river particles shows a clear indication of Mn mobilization from them to seawater. The pathways of Mn cycling and associated flux in upper slope sediments has been depicted in a schematic diagram, Fig. 3.5. The present study reemphasizes the importance of Mn cycling from anoxic shelf and slope sediments of the margin areas that can probably explain the source for the dissolved Mn maxima occurring in Arabian sea intermediate waters as mentioned earlier. This may also contribute to the high Mn concentration in the surface section of the lower slope sediments.

The manganese distribution in the two cores, K-11 and M-12, from the lower slope region shows features, which are distinctly different from those observed in the upper slope sediment cores, with high Mn values (1900 and 10160 ppm on $CaCO_3$ free basis) occurring in surface sections (Fig. 3.6, Table 3.8). In core M-12 the Mn concentration decreases with depth and attains a value of 900 ppm, for K-11 the Mn concentration shows a shallow depth (4–5 cm) maximum and then decreases to a value of $\sim$ 700 ppm below 10 cm depth. Such a distribution of Mn is typical of the slope sediments where Mn released at depths in sedimentary column by diagenetic processes is sequestered at the oxic sediment-water interface (Yeats et al,1979; Sundby and Silverberg,1985; Aller,1990). In contrast to the upper slope sediments, the concentration of Mn averaged over the entire core length for K-11 and M-12, is $\sim$1400 and $\sim$1700 ppm, respectively on a $CaCO_3$ free

basis. These values of Mn are relatively higher than that in fluvial sediments transported by the Narbada/Tapti rivers and average crustal rock.

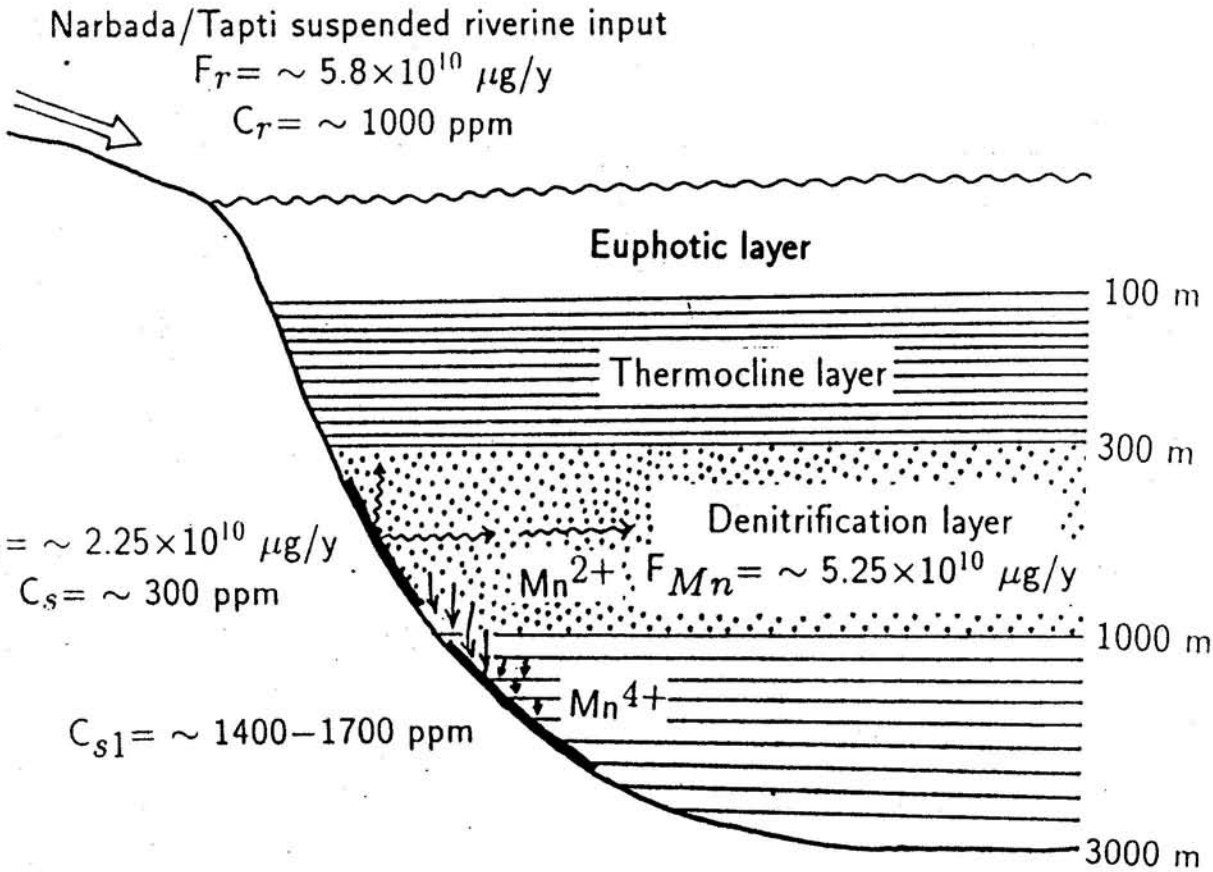

Figure 3.5: Schematic diagram showing Mn cycling between solid and aqueous phases in WCMI representing 5°Lat×3°Long area where : C_r is concentration and F_r the flux of Mn transported by riverine suspended matters. C_s and F_s refer to concentration and flux of Mn mobilized from reducing upper slope sediments to the denitrification layer. Further, C_{s1} is the average concentration of Mn observed in lower slope sediments. Although dissolved riverine Mn input and its atmospheric transport are neglected, a reasonable degree of balance is observed between F_r and $(F_s + F_{Mn})$. In the lower slope sediments, the mechanism for excess Mn depositing at the sediment-water interface due to upward migration from reducing sub-surface layers as well as its authigenic removal from overlying waters is also shown.

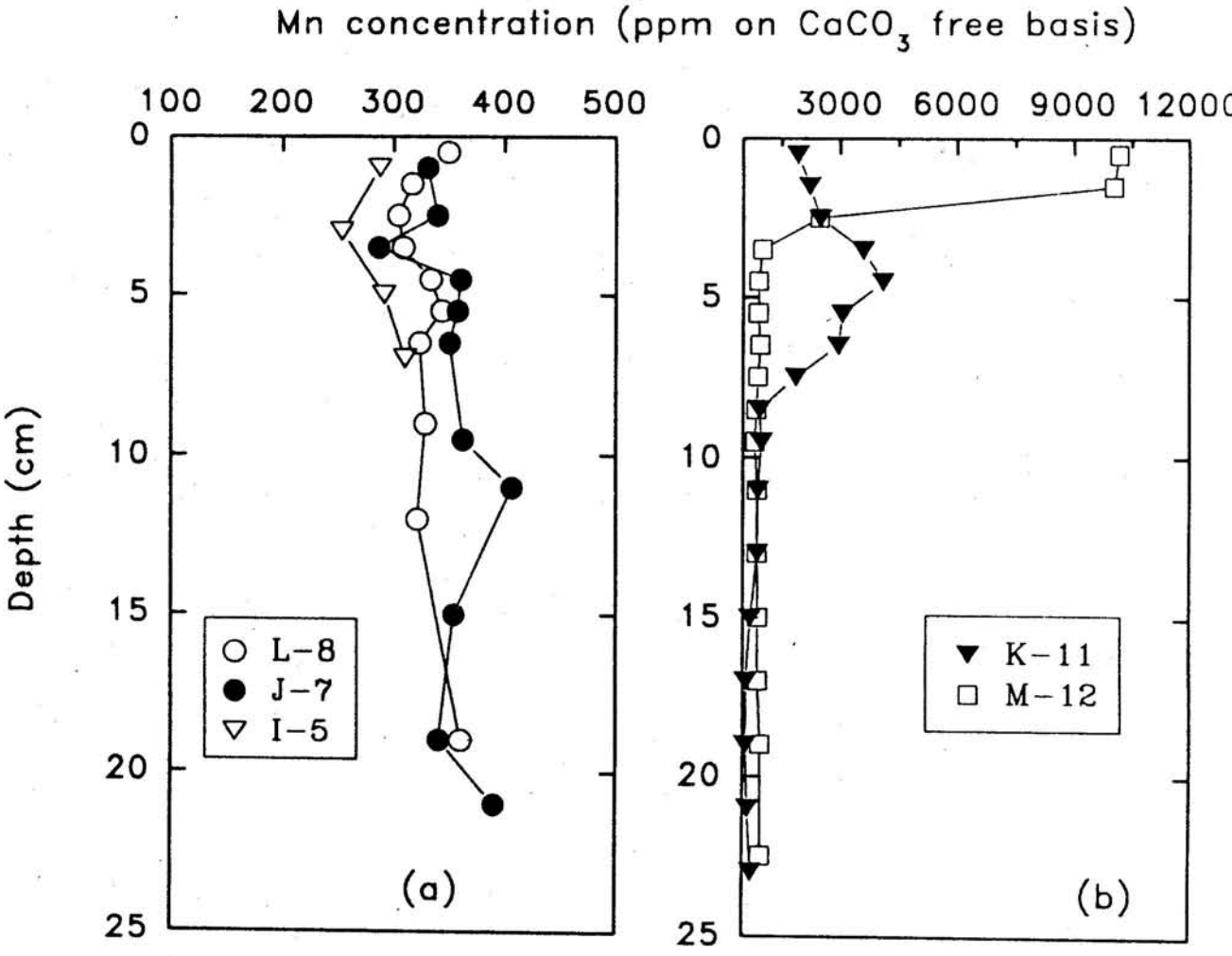

Figure 3.6: Downcore variation of Mn abundance in (a) the upper and (b) lower slope sediments. The Mn concentration in the upper slope sediments are much lower than that in the Narbada/Tapti river particles and show no discernible trend with depth. In contrast, the Mn distribution in the lower slope sediments show a distinct structure with high values near the sediment-water interface.

The bathymetric map of the study area (Fig. 2.1) indicates that the lower slope region follows closely the upper slope, and hence, it is reasonable to speculate that part of the manganese mobilized from the upper slope region is reprecipitated at the oxidising sediment-water interface in addition to that mobilized from the sub-surface layer. In fact, such a phenomenon has been reported to occur in other oceanic regions viz. the Gulf of

Mexico and Mississippi Delta (Trefry and Presley,1982; Heggie et al,1987).

3.4.1 Oxidation of Org. C and Mn reduction

The manganese reduction in nearshore sediments is represented by the following relation,(Aller,1990):

$$C_{org} + 2MnO_2 + 3CO_2 + 2H_2O = 4HCO_3 + 2Mn^{2+} \tag{3.13}$$

This shows that two moles of Mn^{+2} is generated during the oxidation of one mole of C_{org}. Therefore, it is possible to estimate the amount of C_{org} oxidized from the Mn^{2+} released based on this stoichiometry. The rough estimate of Mn flux mobilized from the upper slope, as discussed earlier, is $\sim$0.6 μM/cm^2·y. This Mn, if attributed to C_{org} oxidation, would suggest that the oxidation rate for C_{org} in the upper slope region is $\sim$ 0.3μM/cm^2·y. The primary production in upper slope region is about 0.5 gC/m^2·d $\equiv$ 1.5 mM/cm^2·y (Paropkari et al,1992). Comparing this with the C_{org} oxidation flux based on Mn reduction, it implies that reduction of Mn contributes to $< 1\%$ oxidation of C_{org} fixed by the photosynthetic activity.

In the lower slope sediments, the depth profile of "excess" Mn concentration can be represented by particle mixing and Mn reduction rate similar to that proposed by Aller,1980. This is represented by

$$\frac{\partial C_s^*}{\partial t} = D \cdot \frac{\partial^2 C_s^*}{\partial z^2} - R = 0 \tag{3.14}$$

Where D is the mixing coefficient, C_s^* is the solid-phase "excess" Mn concentration and R is the Mn reduction rate. It is assumed that D is constant over the depth interval used in the model calculation. The "excess" manganese (i.e. total solid-phase Mn minus the average background [1] value in μg/g) in top (0–4 cm) of the core M-12 is converted in units of mass/volume (μM/cm^3) by using in-situ sediment density of 0.5 g/cm^3 and its depth profile is fitted with an exponential function (Aller,1980):

[1] Background Mn concentration refers to unreactive Mn which remains almost constant after a certain depth from the surface

Table 3.8: Mn concentration in the lower slope sediments on $CaCO_3$ free basis.

Core: K-11		Core: M-12	
Depth (cm)	Mn (ppm)	Depth (cm)	Mn (ppm)
(0-1)	1903	(0-1)	10161
(1-2)	2211	(1-2)	10017
(2-3)	2479	(2-3)	2470
(3-4)	3581	(3-4)	997
(4-5)	4092	(4-5)	908
(5-6)	3052	(4-5)R	930
(6-7)	2952	(5-6)	897
(7-8)	1862	(6-7)	947
(7-8)R	1841	(7-8)	889
(8-9)	922	(8-9)	847
(9-10)	975	(9-10)	810
(10-12)	881	(10-12)	865
(12-14)	865	(12-14)	864
(12-14)R	839	(14-16)	884
(14-16)	692	(16-18)	887
(16-18)	574	(18-20)	944
(18-20)	564	(20-25)	958
(20-22)	631		
(22-24)	711		
$\overline{Mn}$ =	1410*	$\overline{Mn}$ =	1705*

* concentration averaged over entire core length
R denotes replicate analysis

$$C_s^* = C_{so}^* \cdot e^{-\beta.z} \tag{3.15}$$

where C_s^* and C_{so}^* are the solid phase Mn concentration at any depth and at the sediment surface and β is the attenuation coefficient. The only unknown in eqn. (3.14) is D for determining (R), the Mn reduction rate. Assuming the exponential depth profile of $^{210}Pb_{excess}$ in top 10 cms of M-12 as solely due to particle mixing, the mixing coefficient D (Krishnaswami and Lal,1978), is calculated to be 0.18 cm^2/y. Using this value of D and exponential function for "excess" Mn concentration in eqn. (3.14) which results R, the Mn reduction rate. Integral of R over the depth interval for which "excess" Mn is observed, yields average Mn reduction flux of 0.45 $\mu M/cm^2 \cdot y$, and hence the flux of organic carbon oxidized from the sediment pile is $\sim$ 0.22 $\mu M/cm^2 \cdot y$.

Table 3.8: Mn concentration in the lower slope sediments on $CaCO_3$ free basis.

Core: K-11		Core: M-12	
Depth (cm)	Mn (ppm)	Depth (cm)	Mn (ppm)
(0-1)	1903	(0-1)	10161
(1-2)	2211	(1-2)	10017
(2-3)	2479	(2-3)	2470
(3-4)	3581	(3-4)	997
(4-5)	4092	(4-5)	908
(5-6)	3052	(4-5)R	930
(6-7)	2952	(5-6)	897
(7-8)	1862	(6-7)	947
(7-8)R	1841	(7-8)	889
(8-9)	922	(8-9)	847
(9-10)	975	(9-10)	810
(10-12)	881	(10-12)	865
(12-14)	865	(12-14)	864
(12-14)R	839	(14-16)	884
(14-16)	692	(16-18)	887
(16-18)	574	(18-20)	944
(18-20)	564	(20-25)	958
(20-22)	631		
(22-24)	711		
$\overline{Mn}$ =	1410*	$\overline{Mn}$ =	1705*

* concentration averaged over entire core length
R denotes replicate analysis

$$C_s^* = C_{so}^* \cdot e^{-\beta.z} \tag{3.15}$$

where C_s^* and C_{so}^* are the solid phase Mn concentration at any depth and at the sediment surface and β is the attenuation coefficient. The only unknown in eqn. (3.14) is D for determining (R), the Mn reduction rate. Assuming the exponential depth profile of $^{210}Pb_{excess}$ in top 10 cms of M-12 as solely due to particle mixing, the mixing coefficient D (Krishnaswami and Lal,1978), is calculated to be 0.18 cm^2/y. Using this value of D and exponential function for "excess" Mn concentration in eqn. (3.14) which results R, the Mn reduction rate. Integral of R over the depth interval for which "excess" Mn is observed, yields average Mn reduction flux of 0.45 $\mu M/cm^2 \cdot y$, and hence the flux of organic carbon oxidized from the sediment pile is $\sim$ 0.22 $\mu M/cm^2 \cdot y$.

As discussed above, a clear distinction exists for Mn distribution in sediments from the upper and lower slope regions mainly because of change in redox conditions. The depth profile of solid phase Mn in lower slope core M-12 was modelled with the particle mixing model (Aller,1980,1990), the result of which yielded carbon oxidation flux of 0.22 $\mu M/cm^2 \cdot y$. This estimated oxidative flux of organic carbon is nearly same compared to that of the upper slope anoxic sediments. The total carbon flux being oxidized from the WCMI sediments, $\sim$ 0.52 $\mu M/cm^2 \cdot y$, is less than 1% of the primary productivity.

3.5 Distribution of uranium in slope sediments

In reducing marine environments, contrary to the mobilization of manganese, uranium is sequestered from seawater. As a result, the concentration of uranium is generally high in anoxic sediments (Veeh et al, 1967; Mo et al,1973; Cochran et al,1986 Anderson et al,1989; Barnes and Cochran,1990; Klinkhammer and Palmer,1991). The importance of such anoxic region as a potential sink for oceanic uranium has been a topic of discussion since long.

The abundance of uranium (^{238}U) in surface sediments of upper slope region ranges from 1.0 to 5.0 dpm/g on bulk basis (Table 3.2). The lowest concentration of uranium ($\sim$1 dpm/g) is observed in the I-5 core followed by that in 2502 ($\sim$3.0 dpm/g) and maximum concentration of $\sim$ 5 dpm/g in L-8 and J-7 cores. The $^{234}U/^{238}U$ activity ratio in these sediments closely resembles that of seawater,1.14$\pm$0.02 (Koide and Goldberg,1965; Ku et al,1977; Chen et al,1986). Similar to this study, the concentration of uranium and its activity ratio ($^{234}U/^{238}U$) in surficial sediments from this region (ARB-46, ARB-52, ARB-54 and ARB-65H) have been reported earlier by Borole et al (1982b). They observed uranium concentration ranging from 3.9 to 7.5 ppm and its activity ratio identical to that of seawater value. The reported uranium concentration is higher than that in the Narbada/Tapti river particles by a factor of 3 to 6 and its maximum concentration is confined in the upper slope sediments. All these results strongly suggest that bulk of uranium in upper slope sediments is derived from seawater and hence this region acts as a potential sink for the dissolved uranium. The mechanism of high uranium content in the upper slope sediments is still not clear. The good correlation between ^{238}U con-

centration and LOI (organic matter) is suggestive of an association between these two constituents (Somayajulu et al,1994). However, from the present data it is difficult to discern if the association is genetic or due to the formation of sub-oxic/anoxic conditions in the sediments which help sequester uranium from seawater or it could be due to better preservation of C_{org} in high sedimentation region. It is also possible that part of the uranium in these sediments is derived from relict calcareous materials (e.g. oolites, corals, algal limestones and milliolites) present in the WCMI sediments (Rao,1978; Nair and Hashimi,1980). Some of these calcareous materials may have uranium concentrations ranging from 1 to 3 dpm/g (Sackett et al,1973; Baskaran,1985), similar to that has been found in this study in cores I-5 and 2502. The role of these upper slope sediments as a sink for authigenic uranium, however, is further discernible from the high $^{238}U/^{232}Th$ weight ratios (1 to 5, Fig. 3.7) in them compared to the average value for crustal rock, 0.25 (Gascoyne, 1982). Furthermore, Fig.3.7 shows almost uniform U/Th weight ratio (except L-8) throughout the core length, which attests to the earlier contention, based on solid phase Mn data, that reducing conditions in the upper slope region have remained fairly unchanged during the past ~100–800 years.

Based on uranium concentration in surface sediments and rate of sediment accumulation for upper slope sediments, the flux of uranium sequestered from seawater ranges between 30–550 $\mu g/cm^2 \cdot ka$. Since anoxic sediments are a potential sink for dissolved uranium supplied to ocean by world rivers, role of upper slope sediments from the WCMI could be significant in global perspective. The total dissolved uranium supply to ocean is 1.14×10^{10} g/y (Borole et al,1982b; Barnes and Cochran,1990; Sarin et al,1990). Considering typical U concentration of 5 ppm (usually found in upper slope sediments) depositing at a rate of 1 mm/y, the depositional flux of uranium is calculated to be 250 $\mu g/cm^2 \cdot ka$. Therefore, an upper limit for the amount of uranium depositing over an area of 5^0 lat $\times$ 3^0 long, 3.75×10^8 g/y, is about 3% of the total dissolved uranium supply to the ocean. Such an observation reemphasizes the importance of organic carbon rich margin sediments in balancing the input of dissolved uranium through world rivers. Klinkhammer and Palmer (1991) have estimated that nearly 75% of the dissolved uranium input to ocean is balanced by such margin sites and rest by the hydrothermal systems.

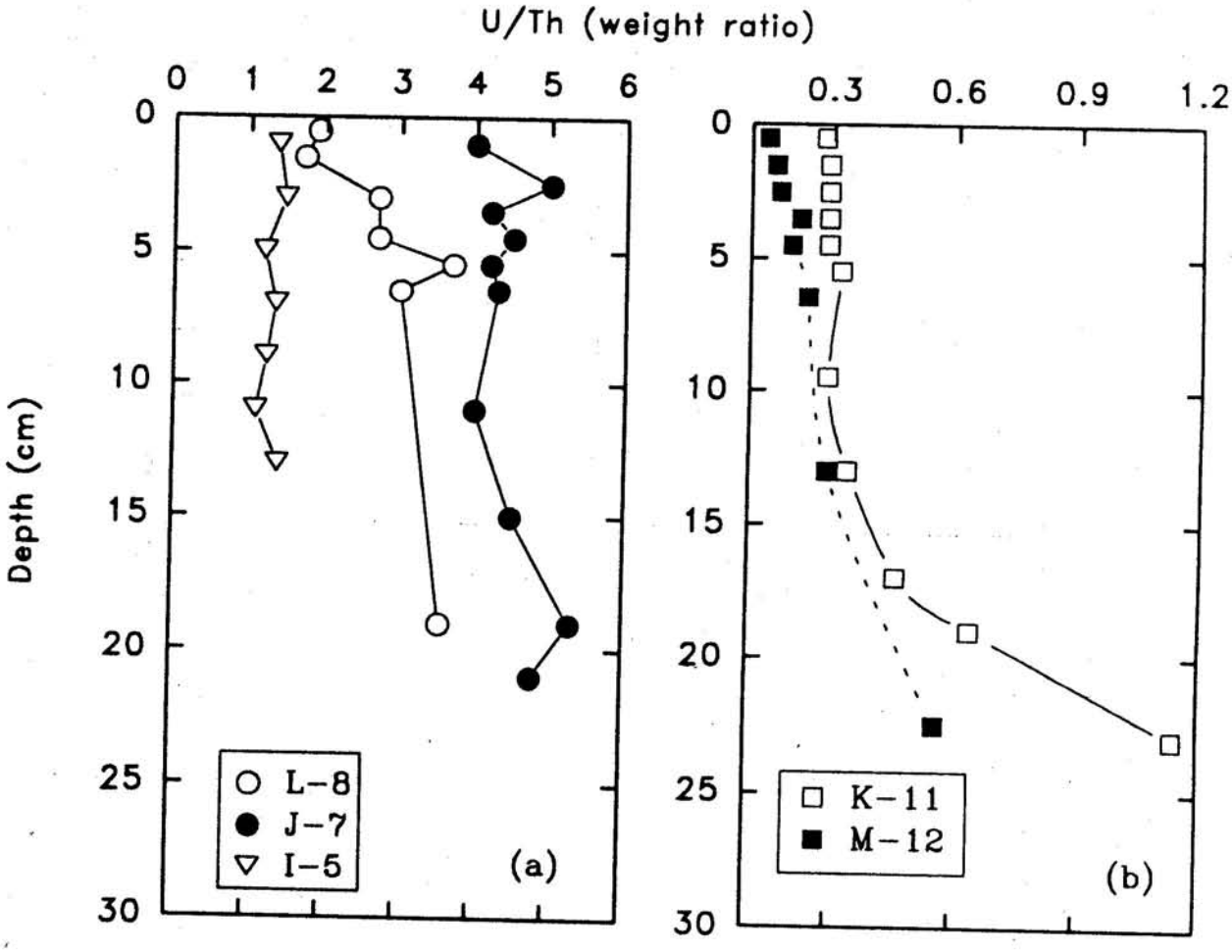

Figure 3.7: Downcore variation of U/Th weight ratio in (a) upper and (b) lower slope sediments. The upper slope sediments show that U/Th weight ratio remains almost constant with depth whereas the ratio increases with depth in the lower slope sediments.

In the lower slope region, the uranium concentration in surface sediments (K-11 and M-12) is about 1.0 dpm/g with activity ratio typically of 1.07±0.03 (Table 3.3). The low uranium abundance and its activity ratio in lower slope sediments (K-11 and M-12) present a distinction relative to the upper slope region which is most likely due to the oxidising conditions prevailing at the sediment-water interface. Such conditions are not favourable for authigenic deposition of uranium from seawater to the sediments. However, oxidation of organic matter may consume considerable amount of available oxygen resulting in sub-oxic condition deeper in the sediment pile. This may help in sequestering U from seawater to deeper depths of the sediment section. The reducing condition in deeper sediment

section is evident from the solid phase Mn profile which shows low Mn concentration relative to the surface (Fig. 3.6). Therefore, increase in U/Th weight ratios (Fig. 3.7) with depth in these sediments is suggestive of U pumping from seawater to deeper depths. Such post depositional enrichment of U is also reported from other oceanic regions such as the Berring sea (Yamada and Tsunogai, 1983/1984). The exact mechanism of high U concentration at deeper depths can be understood if U is analyzed in sediment pore waters at various depths. It is to be noted that within the sediment pile, uranium shows a two component mixture as evidenced from activity ratio of uranium (1.07±0.03, Table 3.3) which is intermediate between detrital component and that of seawater.

3.6 Geochemistry of major and trace elements

Study on the distribution patterns of various major and trace elements in the sedimentary column provides useful information on the biogeochemical processes occurring in the sediments. Also, it is important to assess the role of recent anthropogenic inputs in modifying the natural input of various elements to margin areas via fluvial sediments. The various pathways of the pollutants (viz. anthropogenic heavy metals along with organic/inorganic materials) to the coastal regions are through direct dumping of sweage, river run-off and atmospheric contribution. The influence of anthropogenic activities is reflected through enrichment of heavy metals above a certain baseline value in surficial sediments of the coastal environment (Chow et al,1973; Bruland et al,1974; Goldberg et al, 1978,1979; Lyons et al,1983). It has been recognized that burning of fossil fuels has increased the concentration levels of Cu, Zn, Pb in certain coastal regions (Bruland et al,1974; Erlenkeuser et al,1974; Goldberg et al,1977; 1978).

A suite of elements viz: Fe, Al, Cu, Zn, Pb, and Ni were measured in the WCMI sediments (Tables 1A and 2A given in Appendix−A). Assuming Al as an index for silicates the abundances of various metals have been normalized with respect to Al in order to eliminate the diluent effects of $CaCO_3$ and OrgC. In the upper slope sediments, Cu/Al, Zn/Al and Fe/Al weight ratios range from $(11-22) \times 10^{-4}$, $(19-30) \times 10^{-4}$ and (0.64−0.76) respectively (Table 3.9). These metal to aluminum ratios are well within those reported for the Narbada/Tapti river suspended sediments (Borole et al,1982) thus indicating the

dominance of fluvial source. The core I-5 shows exceptionally high Fe/Al (1.88), Ni/Al (56×10^{-4}) and Zn/Al (40×10^{-4}) ratios which could be attributed to relatively low abundance of clays. Borole et al,1982a have reported almost identical composition of Fe, Mn, Cu and Zn both in suspended bulk sediments and $< 4\mu$m fractions of the riverine suspended particles. These results suggest that the physico-chemical processes such as flocculation of particles, adsorption/desorption of metals on particulates do not modify significantly the elemental abundances of river borne particles during their transit through the estuarine regions of Narbada/Tapti rivers.

The association of various elements in margin sediments is understood by studying their inter-elemental correlations. For example, Mn, Ni, Cu, Zn and Pb in upper slope sediments show high positive correlations with Al (r: 0.72–0.99) suggesting that these elements get deposited along with the detrital clays. However, Ca shows strong negative correlation with Al (r=–0.97) indicating that its distribution is not controlled by the detrital clays and hence its source could be biogenic.

Table 3.9 Metal/Al ratios in WCMI sediments

metal/Al ratio	L-8	J-7	I-5	K-11	M-12
Fe/Al	0.64–0.76	0.69–0.75	1.60–1.88	0.67–0.78	0.66–0.72
Cu/Al	$(11-22)\times10^{-4}$	$(16-21)\times10^{-4}$	$(22-27)\times10^{-4}$	$(16-19)\times10^{-4}$	$(8-14)\times10^{-4}$
Zn/Al	$(19-30)\times10^{-4}$	$(20-23)\times10^{-4}$	$(32-40)\times10^{-4}$	$(19-22)\times10^{-4}$	$(14-19)\times10^{-4}$
Ni/Al	$(25-34)\times10^{-4}$	$(30-38)\times10^{-4}$	$(44-56)\times10^{-4}$	$(19-25)\times10^{-4}$	$(10-18)\times10^{-4}$
Pb/Al	$(18-22)\times10^{-4}$	$(19-28)\times10^{-4}$	$(30-42)\times10^{-4}$	–	–

The anthropogenic influence of heavy metals is generally inferred from their increasing concentrations towards the near surface sections by a factor of more than two with respect to bottom sections. Since the ^{210}Pb chronology established for the upper and lower slope sediment cores has yielded ages ranging between 100–800 years BP, therefore, these sediments can provide the pollution history during the last few centuries. For the upper slope region, Cu/Al, Zn/Al and Pb/Al ratios do not show any systematic increasing trend (Fig. 1A, given in Appendix–A). Such observations are contrary to the observed profiles of heavy metals in sediments from other coastal/estuarine regions viz. Chesapeake Bay, Baltic sea and Loch Etive (Scotland) (Erlenkeuser et al,1974; Goldberg

et al,1978,1979; Ridgway and Price,1987), which have been reported to be affected by intense anthropogenic activities. In lower slope region, for the two cores (K-11 & M-12), the metal/Al ratios (Table 3.9) viz. Fe/Al: ~0.70; Cu/Al: (10–15) $\times 10^{-4}$; Zn/Al: (18–20) $\times 10^{-4}$ and Ni/Al: (17–20) $\times 10^{-4}$ also agree very well with that of river borne particles (Borole et al,1982) and the upper slope sediments (this study). Also, similar to the upper slope region, there are no discernible increasing trend of metal/Al ratios with respect to bottom sections of the core (see Appendix–A, Fig. A2), thus indicating that anthropogenic inputs are relatively insignificant.

The depth profiles of Cu/Al and Pb/Al ratios in core L-8 show an increasing gradient and then decreases to baseline value at the surface (Appendix–A, Fig. A1). Such observation indicates that low Cu concentration at the core top is not due to the dilution effects caused by organic carbon and $CaCO_3$. The decreasing trend in either concentration of Cu or Cu/Al ratio near the sediment surface is probably related to the sub-oxic diagenetic mobilization of Cu, along with the manganese oxides, to overlying seawater (Klinkhammer,1980; Sawlan and Murray,1983).

It has been suggested that copper undergoes oxidative mobilization due to destruction or 'burning' of the organic copper carrier phase at the sediment-water interface (Klinkhammer,1980; Chester et al,1988). This mobilization of Cu gives rise to the high concentration of dissolved copper as reported by Heggie et al (1986) and Saager (1994) in seawater near the seafloor. The mobilization of copper from the lower slope region (core M-12) is quite evident from the low concentration of Cu or low value of Cu/Al ratio at the surface section of the core (see Appendix–A, Fig. 2A). The Zn/Al and Ni/Al ratios in K-11 have increased by about 25% at 5 cm depth with respect to the bottom sections. Such increase in Zn/Al and Ni/Al ratios coincide with increase in Mn concentration (Fig. 3.6) at that depth. It appears that Zn and Ni mobilized from deeper sections via pore waters are reprecipitated back in sediments along with Mn. The diagenetic geochemical behaviour of Ni and Mn is somewhat similar, as reported in an earlier study (Klinkhammer,1980). It can be inferred from the present study that Zn also probably undergoes diagenetic reactions similar to that of Mn and Ni.

Thus, the depth profiles of metal/Al ratios do not show a significant increase in the values at the core tops relative to the baseline in these margin sediments. These results

show that the upper slope sediments of the eastern Arabian sea presently under the influence of reducing environment, have not been significantly perturbed by the recent anthropogenic activities during the last few centuries.

Chapter 4

Summary and Conclusions

Study of short sediment cores collected from the Western Continental Margin of India has provided important information on the temporal and spatial variability of biogenic components and geochemical behaviour of selected elements. The important conclusions of the present study are:

1. In general, sediments from the upper slope region are charaterized by the high abundances of $CaCO_3$ and Org. matter. $CaCO_3$, though biogenic in nature, its abundance in most of the cores is dominated by relict calcareous materials as evidenced by "older" ^{14}C ages (7200–4000 years BP) observed in various sections. Thus, $CaCO_3$ abundance in the upper slope sediments cannot be directly used as an index of biological productivity. Organic matter content in the upper slope sediments ranges from 7 to 15%, reflecting high biological productivity resulting from the upwelling of nutrient rich bottom waters and higher rates of sedimentation. The sediments from the upper slope region do not show any significant temporal variability with respect to $CaCO_3$; whereas in the lower slope its content varies as a function of depth by as much as 60%. It appears that the environmental conditions have not changed over the upper slope region during the last few centuries. For the lower slope region, it is difficult to identify the process involved in $CaCO_3$ variation, however, it is likely that $CaCO_3$ supply to sediments was relatively higher in the past.

2. The geochronology of the cores has been established based on the $^{210}Pb_{excess}$ method which yielded rates of sediment accumulation ranging from 0.25 to 1.83 mm/y for

the upper and lower slope sediments. The rate of sediment accumulation obtained for one of the cores from the upper slope sediments based on the ^{137}Cs depth profile is consistent with the value obtained from the ^{210}Pb method which ensures the ^{210}Pb chronology for all the cores. The inventory of $^{210}Pb_{excess}$ (Σ dpm/cm^2) along the margin ranges from 11 to 130 and shows a positive correlation with the sediment accumulation rate. These results suggest that ^{210}Pb deposition along the WCMI sediments is heterogenous and is focussed in regions of high sedimentation.

3. Geochemically, upper and lower slope sediments behave differently; the latter acts as a "sink" for oceanic uranium and a "source" for dissolved manganese to seawater. Sequestering of uranium from seawater to sediments and manganese mobilization out of sediments in upper slope sediments is largely controlled by the prevalent reducing conditions at the sediment-water interface. The uranium concentration of these sediments is typically 5 ppm with $^{234}U/^{238}U$ activity ratio of 1.14 ± 0.02, identical to that of seawater. In addition, the U/Th weight ratio in these sediments is quite high (1–5) compared to the average crustal value of 0.25. All these data suggest that uranium in these sediments is derived from seawater. Also, a near constancy in U/Th weight ratio down to about 25 cm depth implies that reducing condition at the sediment-water interface has remained unchanged since the last few centuries. An estimate of U being sequestered from seawater in the upper slope sediments of WCMI is nearly 3% of the dissolved U supply to the ocean via world rivers.

4. The flux of manganese mobilized from the upper slope sediments is of the same order as its dissolved supply to the ocean (3.0×10^{11} g/y) by the world rivers. The high flux of Mn mobilized from reducing sediments can possibly explain dissolved Mn maxima reported in the Arabian sea intermediate waters. The flux of labile organic carbon being oxidized from the margin sediments resulting from Mn reduction is $\sim$ 0.52 μM/cm^2·y which is less than 1% of the primary productivity.

5. The metal/Al ratios (Fe/Al, Cu/Al and Zn/Al) in margin sediments are similar to that reported for Narbada-Tapti river particles. Furthermore, a strong positive correlation exists between Cu, Zn, Ni, Pb and Al indicating that the distribution of

the trace elements is dominated by the fluvial sources. With no significant increase in either metal or metal/Al ratios of Cu, Zn, Pb and Ni at the core tops in these margin sediments relative to the bottom sections indicates that these metal concentrations are not significantly influenced by recent anthropogenic activities.

References

Aller R C and Cochran J K (1976) $^{234}Th/^{238}U$ disequilibrium in near-shore sediment : particle reworking and diagenetic time scale, *Earth Planet. Sci. Lett.*, **29**, 37–50.

Aller R C (1980) Estuarine Physics and Chemistry:Studies in Long Island Sound, pp 351–410. In: *Advances in Geophysics*, Diagenetic processes near the sediment-water interface of Long Island Sound II. Fe and Mn, Academic Press, Bary Saltzman (ed), **22**, Academic Press.

Aller R C, Benninger L K and Cochran J K (1980) Tracking particle-associated processes in near-shore environments by use of $^{234}Th/^{238}U$ disequilibrium, *Earth Planet. Sci. Lett.*, **47**, 161–175.

Aller R C (1990) Bioturbation and manganese cycling in hemipelagic sediments, *Phil. Trans. R. Soc. Lond.*, **A331**, 51–68.

Aller R C and DeMaster D J (1984) Estimates of particle flux and reworking at the deep-sea floor using $^{234}Th/^{238}U$ disequilibrium, *Earth Planet. Sci. Lett.*, **67**, 308–318.

Anderson R F, Bacon M P and Brewer P G (1983) Removal of ^{230}Th and ^{231}Pa at ocean margins, *Earth Planet. Sci. Lett.*, **66**, 73–90.

Anderson R F, Lehuray A P, Fleisher M Q and Murray J W (1989) Uranium deposition *in Saanich Inlet* sediments, Vancouver Island, *Geochim. Cosmochim. Acta* **53**, 2205–2213.

Bacon M P, Spencer D W and Brewer P G (1976) $^{210}Pb/^{226}Ra$ and $^{210}Po/^{210}Pb$ disequilibria in seawater and suspended particulate matter, *Earth Planet Sci. Lett.*, **32**, 277–296.

Barnes C E and Cochran J K (1990) Uranium removal in oceanic sediments and the oceanic U balance, *Earth Planet. Sci. Lett.*, **97**, 94–101.

Baskaran M (1985) Radiometric, mineralogical and trace elemental studies of the Saurastra quaternary carbonate deposits: Implications to their ages and origin, *PhD thesis*, Guj. Univ. (India)

Baskaran M, Sarin M M and Somayajulu B L K (1984) Composition of mineral fractions of the Narbada and Tapti estuarine particles and the adjacent Arabian sea sediments off western India, *Chem. Geol.*, **45**, 33–51.

Bassett J, Denney R C, Jeffery G H and Mendham J (1978) Vogel's textbook of quantitative inorganic analysis including elementary instrumental analysis, pp 320–321, The English Language Book Society, London.

Bhushan R, Chakrabarty S and Krishnaswami S (1994) Physical Research Laboratory (Chemistry) Radiocarbon Date list I, *Radiocarbon*, **36**, No. 2, 251–256.

Bonatti E, Fisher D E, Joensuu D O and Rydell H S (1971) Post-depositional mobility of some transition elements, phosphorous, uranium and thorium in deep-sea sediments, *Geochim. Cosmochim. Acta*, **35**, 189–201

Borole D V (1988) Clay sediment accumulation rates on the monsoon-dominated western continental shelf and slope region of India, *Mar. Geol.*,**82**, 285–291.

Borole D V, Sarin M M, Somayajulu B L K (1982a) Composition of Narbada and Tapti estuarine particles and adjacent Arabian sea sediments, *Indian J. mar. Sci.*, **11**, 51–62.

Borole D V, Krishnaswami S and Somayajulu B L K (1982b) Uranium isotopes in rivers, estuaries and adjacent coastal sediments of western India : their weathering, transport and oceanic budget, *Geochim. Cosmochim. Acta*, **46**, 125–137.

Brewer P G, Spencer D W, Biscaye P E, Hanley A, Sachs P L, Smith C L, Kadar S and Fredericks J (1976) The distribution of particulate matter in the Atlantic Ocean, *Earth and Planet. Sci. Lett.*, **32**, 393–402.

Bruland K W, Bertine K, Koide M and Goldberg E D (1974) History of metal pollution in the Southern California coastal zone, *Environ. Sci. Tech.*, **8**, 425–432.

Carpenter R, Bennett J T and Peterson M L (1981) ^{210}Pb activities in and fluxes to sediments of the Washington continental slope and shelf, *Geochim. Cosmochim. Acta*, **45**, 1155–1172.

Chen J H, Edward R L and Wasserburg G J (1986) ^{238}U, ^{234}U and ^{232}Th in seawater, *Earth Planet. Sci. Lett.*, **1986**, 241–251.

Chester R, Thomas A, Lin F J, Basham A S and Jacinto G (1988) The solid state speciation of copper in surface water particulates and oceanic sediments, *Mar. Chem.*, **24**, 261–292.

Chow T J, Bruland K W, Bertine K, Soutar A, Koide M and Goldberg E D (1973) Lead pollution : Records in Southern california coastal sediments, *Science*, **181**, 551–552.

Cochran J K, Bacon M P, Krishnaswami S and Turekian K K (1983) ^{210}Po and ^{210}Pb distributions in the central and eastern Indian Ocean, *Earth Planet. Sci. Lett.*, **65**, 433–452.

Cochran J K, Carey A E, Sholkovitz E R and Surprenant L D (1986) The geochemistry of uranium and thorium in coastal marine sediments and sediment pore waters, *Geochim. Cosmochim. Acta*, **50**, 663–680.

Delaune R D, Patrick Jr W H and Buresh R J (1978) Sedimentation rates determined by ^{137}Cs dating in a rapidly accreting salt marsh, *Nature*, **275**, 532–533.

Erlenkeuser H, Suess E and Willkam H (1974) Industrialization affects heavy metal and carbon isotope concentrations in recent Baltic sea sediments, *Geochim. Cosmochim. Acta*, **38**, 823–842.

Flanagan F J (1973) 1972 values for international geochemical reference samples, *Geochim. Cosmochim. Acta*, **37**, 1189–1200.

Gascoyne M (1982) Geochemistry of the actinides and their daughters, pp 33–55. In: *Uranium Series Disequilibrium Applications to Environmental Problems*, Ivanovich M and Harmon R S (eds.), Calrendon Press, Oxford.

Guinasso N L and Schink D R (1975) Quantitative estimates of biological mixing rates in abyssal sediments, *J. Geophy. Res.*, **80**, 3032–3043.

Goldberg E D and Koide M (1962) Geochronological studies of deep sea sediments by the ionium/thorium method, *Geochim. Cosmochim. Acta*, **26**, 417–450.

Goldberg E D and Griffin J J (1970) The sediments of the northern Indian Ocean, *Deep-Sea Res.*, **7**, 513–517.

Goldberg E D, Gamble E, Griffin J J and Koide M (1977) Pollution history of Narragansett Bay as recorded in its sediments, *Estuarine Coastal Mar. Sci.*, **5**, 549–561.

Goldberg E D, Hodge V, Koide M, Griffin J J, Gamble E, Bricker O P, Matisoff G, Holdren Jr G R and Barun R (1978) A pollution history of Chesapeake Bay, *Geochim. Cosmochim. Acta*, **42**, 1413–1425.

Goldberg E D, Griffin J J, Hodge V, Koide M and Windom H (1979) Pollution history of the Savannah River Estuary, *Environ. Sci. Tech.*, **13**, 588–594.

Gupta M V S and Hashimi N H (1985) Fluctuation in glacial and interglacial sediment discharge of the river Indus as seen in a core from the Arabian sea, *Indian J. Mar. Sci.*, **18(1)**, 66–70

Hermanson M H (1990) ^{210}Pb and ^{137}Cs chronology of sediments from small, shallow Arctic lakes, *Geochim. Cosmochim. Acta*, **54**, 1443–1451.

Heggie D, Kahn D and Fischer K (1986) Trace metals in metalliferous sediments, MANOP site M: interfacial pore water profiles, *Earth Planet. Sci. Lett.*, **80** , 106–116.

Heggie D, Klinkhammer G and Cullen D (1987) Manganese and copper fluxes from continental margin sediments, *Geochim. Cosmochim. Acta*, **51**, 1059–1070.

Holdren G R Jr., Bricker O P III and Matsoff G (1975) A model for the control of dissolved manganese in interstitial waters of Chesapeake Bay, pp 364–381. In:

Marine chemistry in the coastal environment, T. M. Church (ed.), A C S symposium series no. **18**.

Johnson K S, Berelson W M, Coale K H, Coley T L, Elrod V A, Fairley W R, Lams H D, Kilgore T E, Nowicki J L (1992) Manganese flux from continental margin sediments in a transect through the oxygen minimum, *Science*, **257**, 1242–1245.

Jones C J and Murray J W (1985) The geochemistry of manganese in the northeast Pacific ocean off Washington, *Limnol. Oceanogr.*, 30(1), 81–92

Klinkhammer G P (1980) Early diagenesis in sediments from the eastern equatorial Pacific, II. Pore water metal results, *Earth Planet. Sci. Lett.*, **49**, 81–101.

Klinkhammer G P and Palmer M R (1991) Uranium in the oceans: Where it goes and why, *Geochim. Cosmochim. Acta*, **55**, 1799–1806

Koide M and Goldberg E D (1965) $^{234}U/^{238}U$ ratios in seawater. In: *Progress in Oceanography* (ed M Sears), **3**, 173–179

Kolla V, Ray P K and Kostecki J A (1981) Surficial sediments of the Arabian sea, *Mar. Geol.*, **41**, 183–204.

Krishnaswami S (1976) Authigenic transition elements in Pacific pelagic clays, *Geochim. Cosmochim. Acta*, **40**, 425–434

Krishnaswami S and Sarin M M (1976) The simultaneous determination of Th, Pu, Ra isotopes, ^{210}Pb, ^{55}Fe, ^{32}Si and ^{14}C in marine suspended phases, *Anal. Chim. Acta*, **83**, 143–156.

Krishnaswami S and Lal D (1978) Radionuclide Limnochronology, pp 153–177. In :*Lakes: Chemistry Geology Physics*, Lerman A (ed.), Springer-Verlag, New York.

Ku T L, Knauss K G and Mathieu G G (1977) Uranium in open oceans : concentration and isotopic composition, *Deep-Sea Res.*, **24**, 1005–1017.

Lal D, Nijampurkar V N, Rajagopalan G and Somayajulu B L K (1979) Annual fallout of ^{32}Si, ^{210}Pb, ^{22}Na, ^{35}S and ^{7}Be in rains in India, *Proc. Indian Acad. Sci.*, **88**, 29–40

Lyle M and Dymond J R (1976) Metal accumulation rates in the southeast Pacific - errors introduced from assigned bulk densities, *Earth Planet. Sci. Lett.*, **30**, 164–168

Lynn D C and Bonatti E (1965) Mobility of manganese in diagenesis of deep sea sediments, *Mar. Geol.*, **3**, 457–474

Lyons W B, Armstrong P B and Gaudette H E (1983) Trace metal concentrations and fluxes in Bermuda sediments, *Mar. Pollut. Bull.*, **14**, 65–68.

Martin J M and Meybeck M (1979) Elemental mass-balance of material carried by major world rivers, *Mar. Chem.*, **7**, 173–206.

Martin J H and Knauer G A (1984) VERTEX: manganese transport through oxygen minima, *Earth Planet. Sci. Lett.*, **67**, 35–47.

Martin J M and Windom H L (1991) Present and future role of ocean margins in regulating marine geochemical cycles of trace elements, pp 45–67. In: *Ocean Margin Processes in Global Change*, Mantoura R F C, Martin J M and Wollast R (eds.), Wiley, Chichester.

Martin J M and Thomas A J (1994) The global insignificance of telluric input of dissolved trace metals (Cd, Cu, Ni and Zn) to ocean margins, *Mar. Chem.*, **46**, 165–178.

Mathieu, G G (1988) Systems for measurement of ^{222}Rn at low levels in natural waters. *Health Phys.*, **55**, 989–992.

Milliman J D and Meade R H(1983) World-wide delivery of river sediment to the oceans, *J. Geol.*, **91**, 1–21.

Milliman J D (1991) Flux and fate of fluvial sediment and water in coastal seas, pp 69–89. In: *Ocean Margin Processes in Global Change*, Mantoura R F C, Martin J M and Wollast R (eds.), Wiley, Chichester.

Mo T, Suttle A D and Sackett W M (1973) Uranium concentrations in marine sediments, *Geochim. Cosmochim. Acta*, **37**, 35–51.

Murty P S N, Rao M Ch, Paropkari A L and Topgi R S (1978) Distribution patterns of aluminum, titanium, manganese, copper and nickel in sediments of the northern half of the western continental shelf of India, *Indian J. Mar. Sci.*, **7**, 67–71

Naidu P D, Babu C P and Rao Ch M (1992) The upwelling record in the sediments of the western continental margin of India, *Deep-Sea Res.*, **39**, 715–723.

Nair R R (1969) Phosphotized oolites on the western continental shelf of India, *Proc. Nat. Inst. Sci. India*, **35**, 858–863.

Nair R R (1975) On the nature and origin of small-scale topographic prominences on the western continental shelf of India, *Indian J. Mar. Sci.*, **4**, 25–29.

Nair R R, Hashimi N H and Gupta M V S (1979) Holocene limestones of part of the western continental shelf of India, *J. Geol. Soc. India*, **20**, 411–420.

Nair R R and Hashimi N H (1980) Holocene climate inferences from sediments of the western Indian continental shelf, *Proc. Indian Acad. of Sci. (Earth Planet. Sci.)*, **89**, 299–315

Nair R R and Hashimi N H (1981) Mineralogy of the carbonate sediments– Western Continental Shelf of India, *Mar. Geo.*, **41**, 309–319.

Nair R R, Hashimi N H and Rao Purnachandar V (1982) Distribution and dispersal of clay minerals on the western continental shelf of India, *Mar. Geo.*, **50**, M1-M9.

Naqvi S W A (1994) Denitrification processes in the Arabian sea, *Proc. Indian Acad. Sci. (Earth Planet. Sci.)*, **103**, No. 2, 279–300.

Naqvi S W A, Noronha R J, Somasundar K and Sengupta R (1990) Seasonal changes in the denitrification regime of the Arabian sea, *Deep-Sea Res.*, **37**, 593–611.

Noshkin V E and Bowen V T (1973) Concentrations and distributions of long-lived fallout radionuclides in open ocean sediments, pp 671–686. In: *Radioactive Contamination of the Marine environment*, IAEA, Vienna.

Nozaki Y, Cochran J K and Turekian K K (1977) Radiocarbon and ^{210}Pb distribution in sub-mersible taken deep sea cores from Project Famous, *Earth Planet. Sci. Lett.*, **34**, 167–173.

Paropkari A L, Babuprakash C, Mascarenhas A (1992) A critical evaluation of depositional parameters controlling the variability of organic carbon in Arabian sea sediments, *Mar. Geol.*, **107**, 213–226.

Peirson D H (1971) Worldwide deposition of longlived fission products from nuclear explosions, *Nature*, **234**, 79–80.

Pennington W, Cambray R S and Fisher E M (1973) Observation on lake sediments using fallout ^{137}Cs as a tracer, *Nature*, **242**, 324–326.

Quasim S Z (1977) Biological productivity of the Indian Ocean, *Indian J. Mar. Sci.*, **6**, 122–137.

Ramswamy V, Nair R R, Manganini S J, Ittekkot V and Haake B (1991) Lithogenic fluxes to the deep Arabian sea measured by sediment traps, *Deep-Sea Res.*, **38**, 169–184

Rao Ch M (1978) Distribution of CaCO3, Ca^{2+} and Mg^{2+} in sediments of the northern half of western continental shelf of India, *Indian J. Mar. Sci.*, **7**, 151–154

Rao V P, Veerayya M, Nair R R, Dupeuble P A and Lamboy M (1994) Late Quaternary *Halimeda* bioherms and aragonitic faecal pellet-dominated sediments on the carbonate platform of the western continental shelf of India, *Mar. Geol.*, **121**, 293–315.

Ridgway I M and Price N B (1987) Geochemical associations and post-depositional mobility of heavy metals in coastal sediments : Loch Etive, Scotland, *Mar. Chem.*, **21**, 229–248.

Rosholt J N, Emiliani C, Geiss J, Koczy F F and Wangersky P J (1961) Absolute dating of deep sea cores by the $^{231}Pa/^{230}Th$ method, *J. Geol.*, **69**, 162–185.

Saager P M (1994) The biogeochemical distribution of trace elements in the Indian ocean, *Proc. Indian Acad. Sci. (Earth Planet Sci.)*, 103, 237–278.

Saager P M, DeBaar H J W and Burkhill P H (1989) Manganese and iron in Indian ocean waters, *Geochim. Cosmochim. Acta*, **53**, 2259–2267.

Sackett W M, Mo T, Spalding R F and Exner M E (1973) A reevaluation of the marine geochemistry of uranium, pp 757–769. In: *Radioactive contamination of the marine environment*, IAEA Symp. Proc.

Sarin M M, Borole D V and Krishnaswami S (1979) Geochemistry and geochronology of sediments from the Bay of Bengal and the equatorial Indian Ocean, *Proc. Indian Acad. Sci.*, **88**, Part II, 131–154.

Sarin M M, Krishnaswami S, Somayajulu B L K and Moore W S (1990) Chemistry of uranium, thorium, and radium isotopes in the Ganga–Brahmaputra river system : Weathering processes and fluxes to the Bay of Bengal, *Geochim. Cosmochim. Acta*, **54**, 1387–1396.

Sarin M M, R Bhushan, R Rengarajan and Yadav D N (1992) The simultaneous determination of ^{238}U series nuclides in seawater: Results from Arabian sea and Bay of Bengal, *Indian J. of Mar. Sci.*, **21**, 121–127.

Sarin M M, Krishnaswami S, Ramesh R and Somayajulu B L K (1994) ^{238}U decay series nuclides in the north eastern Arabian sea: Scavenging rates and cycling processes, *Continental Shelf Res.*, **14**, 251–265.

Sawlan J J and Murray J W (1983) Trace metal mobilization in the interstitial waters of red clay and hemipelagic marine sediments, *Earth Planet. Sci. Lett.*, **64**, 213–230.

Scott M R (1982) The chemistry of U and Th-series nuclides in rivers, pp 181–201. In: *Uranium Series Disequilibrium Applications to Environmental Problems*, Ivanovich M and Harmon R S (eds.), Calrendon Press, Oxford.

Shetye S R, Gouveia A D, Shenoi S S C, Sundar D, Michael G S, Almeida A M and Santanam K (1990) Hydrography and circulation off the the west coast of India during the Southwest Monsoon 1987, *J. Mar. Res.*, **48**, 359–378.

Shetye S R, Gouveia A D, Shenoi S S C, Sundar D, Michael G S, Almeida A M and Santanam K (1991) The coastal current off western India during northeast monsoon, *Deep-Sea Res.*, **38**, 1517–1529.

Sirocko F and Sarnthein M (1989) Wind–borne deposits in the northwestern Indian Ocean: Record of Holocene sediments versus modern satellite data, pp 401–433. In: *Paleoclimatology and Paleometeorology, Modern and Past patterns of Global atmospheric transport*, Leinen M and Sarnthein M (eds.).

Spencer D W, Bacon M P and Brewe P G (1981) Models of the distribution of ^{210}Pb in a section across the North Equatorial Atlantic Ocean, J. Mar. Res., **39**, 119–138.

Spitzy A and Ittekkot V (1991) Dissolved and particulate organic matter in rivers, pp 5–17. In: *Ocean Margin Processes in Global Change*, Mantoura R F C, Martin J M and Wollast R (eds.), Wiley, New York, N Y.

Somayajulu B L K, Yadav D N and Sarin M M (1994) Recent sedimentary records from the Arabian sea, *Proc. Indian Acad. Sci. (Earth Planet Sci.)*, **103**, No. 2, 315–327.

Sundby B and Silverberg N (1985) Manganese fluxes in the benthic boundary layer, *Limnol. Oceanogr.*, **30(2)**, 372–381.

Thomson J, Colley S, Anderson R, Cook G T and MacKenzie A B (1993) ^{210}Pb in the sediments and water column of the northeast Atlantic from 47 to 59^{0}N along 20^{0}W, *Earth Planet. Sci. Lett.*, **115**, 75–87.

Trefry J H and Presley B J (1982) Manganese fluxes from Mississippi Delta sediments, *Geochim. Cosmochim. Acta*, **46**, 1715–1726.

Veeh H H (1967) Deposition of uranium from the ocean, *Earth Planet. Sci. Lett.*, **3**, 145–150.

Walsh J J (1991) Importance of continental margins in marine biogeochemical cycling of carbon and nitrogen, *Nature*, **350**, 53–55.

Wollast R (1991) The coastal organic carbon cycle: Fluxes, sources and sinks, pp 365–381. In: *Ocean Margin Processes in Global Change*, R F C Mantoura, J M Martin and R Wollast (eds.), Wiley, Chichester.

Wollast R (1993) Interaction of carbon and nitrogen cycles in the coastal zone, pp 195–210. In: Interaction of C, N, P and S biogeochemical Cycles and Global Change, R Wollast, F T Mackenzie and L Chou (eds.), NATO ASI Ser., **14**, Springer, Berlin.

Yadav D N, Sarin M M and Somayajulu B L K (1992) Western Continental Margins of India: Are they sink or source for trace elements in the Arabian sea ?, pp 359–367. In: *Oceanography of the Indian Ocean*, Desai B N (ed.), Oxford & IBH Pub. Co., New Delhi.

Yamada M and Tsunogai S (1983/1984) Post depositional enrichment of uranium in sediment from the Berring sea, *Mar. Geol.*, **54**, 263–276.

Yeats P A, Sundby B and Bewers J M (1979) Manganese recycling in coastal waters, *Mar. Chem.*, **8**, 43–55.

PART –B

Geochemical study of the Sambhar lake

Chapter 5

Introduction

Rajasthan state, in the Thar desert of India is endowed with a large number of saline lakes notably the Sambhar, Didwana, Kuchaman, Lunkaransar and the Pachbhadra. These lakes are shallow and ephemeral. Among these, the Sambhar lake, situated at $26^0 52' - 27^0 2'$N, $74^0 53' - 75^0 13'$E, is the largest with an area of $\sim$ 225 km^2 (Fig. 5.1). It is a closed sedimentary basin which is reported to have been formed by neotectonism (Deshmukh and Rai,1991) and aeolian activity as the lake boundary is bounded by wind-blown sand-dunes. About 2 $\times 10^5$ tons of NaCl is manufactured annually from the Sambhar lake waters and shallow sub-surface brines in its basin. The origin of salt in the lake basin has been a subject of scientific interest during the recent years. The various hypotheses proposed include: (i) dissolution of salt from halite beds (relict of Tethys sea) within the basin (Godbole,1952) (ii) weathering of country rocks followed by evaporation (Aggarwal,1951) and (iii) aeolian transport of salt laden aerosol particles from the Gulf of Kutch by SW monsoon winds (Holland & Christie,1909). Of these, the first two can be grouped under "internal" and the third as an "external" source of salt. A comprehensive review on the sources of salt in the Sambhar lake is given by Biswas et al (1982).

5.1 Geology, Hydrology and Climate of the Sambhar lake

For better understanding of the evolution of saline lakes and brines, relevant information on local climate, hydrology, sedimentation history and tectonics are very helpful.

Figure 5.1: Map showing the sample locations in and around the Sambhar lake. The groundwater wells are indicated by encircled point ◉ and sub-surface brine wells are shown by asterik symbol ($\star$). Shallow groundwater samples from the river bed are taken to be representative of river waters. In the figure, major village sites for location of groundwaters and some of the salt producing sites for sub-surface brine wells are also shown, however, additional samples were also collected at a distance of 50−100 m from those marked locations. The map also describes important geomorphic features of the lake area.

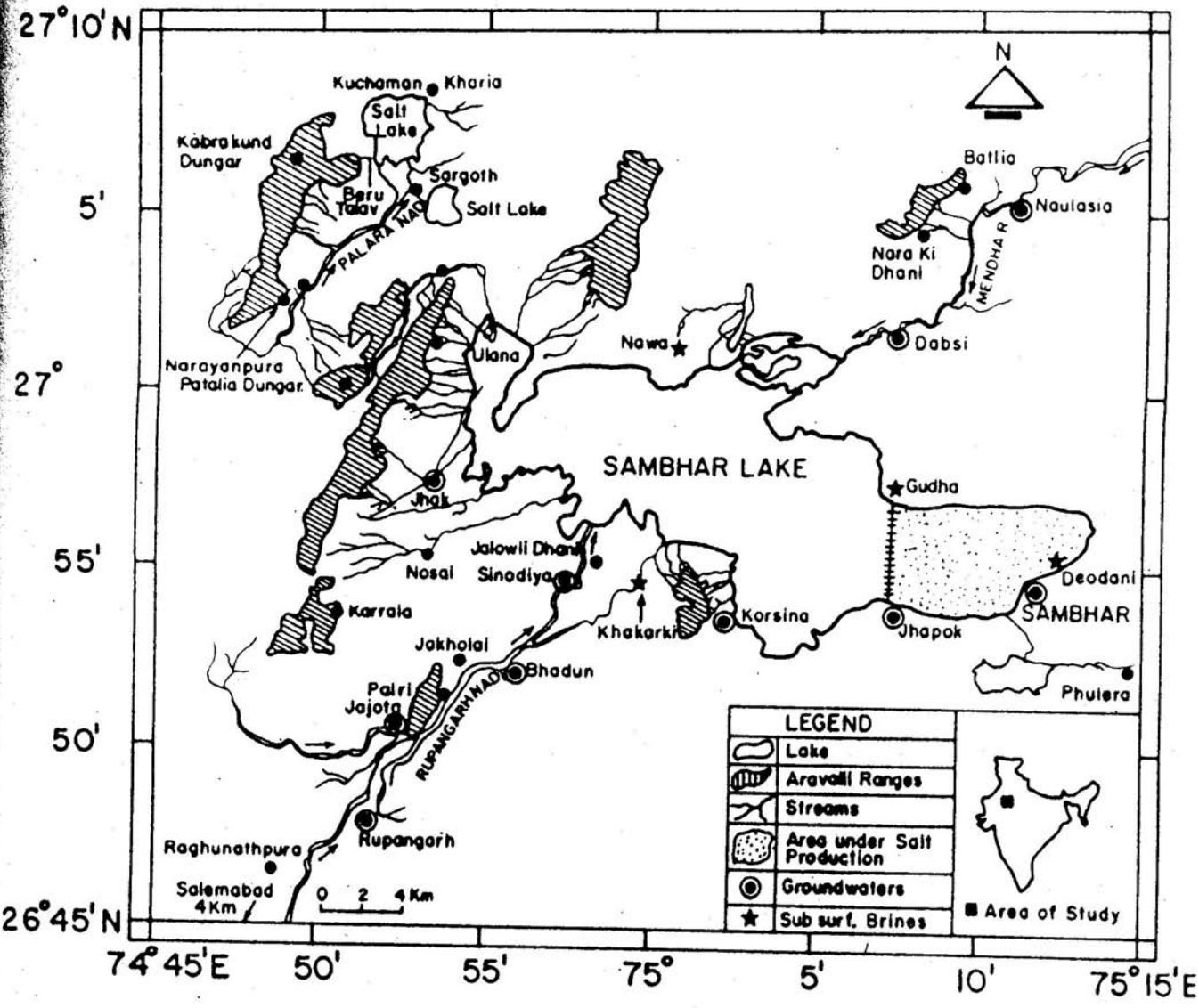
27°10'N
5'
27°
55'
50'
26°45'N
74°45'E
50'
55'
75°
5'
10'
75°15'E
N
Kuchaman
Kharia
Salt Lake
Kabrakund Dungar
Beru Talav
Sargoth
Salt Lake
PALARA NAG
Narayanpura Patalia Dungar
Ulana
Nawa
Batlia
Naulasia
Nara Ki Dhani
MENDHAR
Dabsi
SAMBHAR LAKE
Gudha
Jhak
Jalowli Dhani
Nosal
Sinodiya
Karrala
Khakarki
Korsina
Jhapok
Deodani
SAMBHAR
Jakholai
Bhadun
Pairi
Jajota
RUPANGARH NAG
Phulera
Raghunathpura
Rupangarh
Salemabad 4Km
0 2 4 Km
LEGEND
Lake
Aravalli Ranges
Streams
Area under Salt Production
Groundwaters
Sub surf. Brines
Area of Study

The Sambhar lake is located at an elevation of 360 m above the Mean Sea Level. The lake is underlain by Pre-Cambrian basement rocks, predominantly consisting of schiests, phyllites and quartzites. The crystalline basement is overlain by Quaternary clays and silts (Aggarwal, 1951). The base of the Quaternary sedimentary column is made of fluvial deposit of alluvial sand and clays indicating humid climatic condition in the past. The lake basin is surrounded by windblown high terraces of sand and clay. In the present-day geohydrologic set-up, the principal source of water to the lake is local precipitation and drainage from the catchment. The catchment area ($\sim$ 5600 km^2, Biswas et al,1982) of the lake has small and large streams e.g. Roopangarh, Mendha, Kharian and Khandel (Aggarwal,1951), however, their supply of water to the lake is limited because of aeolian activity in the region and man-made dams constructed for irrigation purposes. Of these rivers, currently only the Roopangarh and the Mendha seem to supply water to the lake (Fig. 5.1), and flow in these streams is highly seasonal and occurs only for a few days during the SW monsoon (June–September). These rivers drain mainly through Pre-Cambrian schists, phyllites and slates. From the field observation, it is evident that water table of the adjacent groundwaters is generally 5–10 m above the lake bed. However, at places within the river basin (for example near Roopangarh town), groundwaters are available at 20–30 m above the lake bed. This indicates a significant hydraulic gradient that favours the groundwaters flow towards the lake basin in addition to the surface run-off during the monsoon season. The groundwaters of this region show considerable variations in their salinity, among these the low salinity waters are used for irrigation and domestic purposes.

Climatic data from the three meteorological stations (Jaipur, Sikar and Ajmer) close to the Sambhar lake show that January is the coldest month with minimum temperature of about 6 – 8^{0}C and May is the hottest month with maximum temperature ranging between 39 – 41^{0}C. The maximum average relative humidity during the monsoon season is about 76% in the month of July and minimum of about 15–20% during summer months before the onset of monsoon. Information on wind regime indicates that the diurnal average speed varies from 4 to 12 kmph (Mar–July) and minimum being at 2–3 kmph during the winter (Dec–Feb). The lake receives an average annual rainfall of 50 cm and is characterized by evaporation almost balancing the inflow. As a result, Sambhar represents

a seasonal lake with water drying up almost completely during the hot and dry summer months and getting replenished during the monsoon.

Changes in climatic conditions during the recent past have also influenced the geomorphic evolution of the Thar desert and its associated features. The stratigraphic and radiocarbon chronologies of the three lake basins in the Thar desert namely the Sambhar, Didwana and Lunkaransar and the proxy records contained in them indicate similar climatic conditions over the region (Sareen,1952; Singh et al,1972; Wasson et al,1984). These studies show that prior to 13 ka BP the lake condition was hypersaline; around 10 ka BP the lacustrine deposition (laminated clay) started and continued up to 4.5 ka BP and between 4.5 ka BP to the present the environment was generally semi-arid. In addition, variation in paleomonsoon in this region has been studied based on palynology (Bryson and Swain,1981; Swain et al,1983) which indicate sub-humid phase between 10.5–3.5 ka BP. Swain et al (1983) postulated Sambhar lake's paleolevel (based on hydrologic balance and radiation budgets) to be about 20 m above the present value during 10.5–3.5 ka BP. Furthermore, geomorphic evidences e.g. dry river beds and paleo river channels (Allchin et al, 1978; Ghose, 1964) have indications to stronger monsoon rainfall in the past compared to the present. It appears that with the onset of aridity in the region, the river tributaries were dried and some of them were buried under sand by aeolian activity. Preliminary studies on salinity of the Sambhar lake have not evidenced presence of solid evaporite deposits in the lake basin (Aggarwal,1951; Mishra,1982). In the absence of thick-evaporite deposits, the shallow hypersaline brines below the lake bed is considered to be due to paleoclimatic transition from wet to dry phases (Mishra,1982).

5.2 Present-day lake configuration

Currently salt (NaCl) is being manufactured extensively from the lake water and sub-surface brines by solar evaporation. The eastern side of the lake, occupying an area of 71 km^2 (Fig. 5.1) is at present isolated from the main reservoir by an embankment (a railway track in the figure). In this configuration, the main reservoir of the lake, therefore, is left with an effective area of 154 km^2. The isolated area (71 km^2) is utilized for salt production by pumping of waters both from the lake and shallow sub-surface brines. The sub-surface

brines which occur generally at 3 to 4 m depth below the lake bed are the principal source of salt. At some places viz. Khakarki, Sinodiya and Nawa on the periphery of lake, these brines are available even at deeper depths ranging from about 40 to 80 m mainly due to the topographic highs. On the lake bed the salt producing network consists of small to large size evaporating reservoirs, pans/kyars and areas for disposing the residual liquor of the brine i.e. the bittern [1].

Goals of the Present Study

Earlier studies on the various saline lakes in Rajasthan (Aggarwal,1951; Biswas et al,1982; Bhattacharya et al,1982; Mishra,1982; Deshmukh and Rai,1991) were mainly to evaluate their potential for commercial exploitation, though some attempts were made to speculate on the sources of salt to these lakes. In this work a detailed geochemical and isotopic study of various hydrologic systems of the Sambhar lake has been made in different seasons to obtain information on the evolution of surface and sub-surface brines and the inter-relation between them. The specific objectives of this study are:

(i) to determine the chemical and isotopic composition of the source waters, lake waters and sub-surface brines;

(ii) to simulate and model the annual evaporation cycle of the lake water and brines;

(iii) to place constraints on the possible source of salt to the lake;

(iv) to derive information on the abundances and behaviour of U–Th series nuclides in waters over wide range of salinities.

Chapter 6 describes the experimental techniques used in this study, Chapter 7 the results and discussion and Chapter 8 the summary of the present work.

[1] Bittern refers to the residual brine remaining after NaCl recovery, its major component being NaCl (~75%), Na_2CO_3 and Na_2SO_4.

Chapter 6

Experimental Techniques

The groundwaters, lake waters and sub-surface brines were sampled during different seasons (Feb 92–Oct 93) whereas water samples from the river basin were collected mainly during Oct 1993. Most of the sub-surface brine wells sampled are open wells dug in the lake bed for salt production. These wells are accessible for sampling only during Oct to June when salt production is being carried out. Also, the salt producing networks e.g. evaporating pans, kyars and bitterns were sampled. In the following sections the techniques used in field and laboratory analyses are described. The lake waters and sub-surface brine samples were analyzed (see Appendix–B, Table 1B) for oxygen isotope ratio ($^{18}O/^{16}O$) and major dissolved ions. In addition, U–Th series nuclides e.g. uranium isotopes, radium isotopes ($^{226,228}Ra$), ^{210}Po and ^{210}Pb were measured with a view to understand geochemical behaviour of these nuclides over a wide range of salinities and to use some of them as natural tracers to infer the source of salt to the lake.

6.1 Measurement of oxygen isotope ratios

The ($^{18}O/^{16}O$) ratio, expressed conventionally as $\delta^{18}O$, of water samples was measured by the CO_2 equilibration method (Epstein and Mayeda,1953). The $\delta^{18}O$ is defined as:

$$\delta^{18}O = \left[\frac{(^{18}O/^{16}O)_{Sample}}{(^{18}O/^{16}O)_{Std}} - 1\right] \times 10^3 \qquad (6.1)$$

and expressed in parts per thousand or per mil ($^0/_{00}$). The standard refers to the Standard Mean Ocean Water (SMOW) supplied by IAEA, Vienna having isotopic ratio $^{18}O/^{16}O$ of $\sim 2000\times10^{-6}$.

In brief, 2 ml of water sample was taken in a glass bottle (approximately 8 ml capacity) and treated with 1 drop of 100% orthophosphoric acid to decompose the carbonates and liberate CO_2. The acid treated samples were repeatedly frozen (three times) with liquid nitrogen and evacuated to pump out the dissolved gases. This process was carried out each time by thawing and refreezing at liquid nitrogen temperature (-196^0C). After this, high purity CO_2 gas from a tank was let into the glass bottles containing the sample to a pressure of $\sim$ 8 cm, and water and CO_2 allowed to equilibrate. In order to achieve complete isotopic equilibration between CO_2 and H_2O, the bottles were kept in a water bath at a constant temperature of 25^0C for 48 h. The isotopic exchange between CO_2 and water molecules takes place as:

$$\frac{1}{2}C^{18}O_2 + H_2^{16}O \rightleftharpoons \frac{1}{2}C^{16}O_2 + H_2^{18}O \tag{6.2}$$

Later, the CO_2 was extracted and purified for $^{18}O/^{16}O$ ratio measurement using a VG Micromass 903 mass-spectrometer. Four samples and a laboratory standard were measured in a batch. The $\delta^{18}O$ measured in fresh water replicate samples showed a precision of $\pm 0.1\ ^0/_{00}$ whereas for brines, the reproducibility was found to be $\pm\ 0.3^o/_{oo}$ (1σ). As the brines analyzed for $\delta^{18}O$ are NaCl type with trace concentrations of Ca and Mg ions, the salt-effect on the ^{18}O fractionation is assumed to be negligible (Gat,1981c). For detailed experimental procedure with PRL's set-up of CO_2 equilibration system, cross-calibration of the laboratory standard with respect to V-SMOW and correction involved in measurement of oxygen isotopic ratio ($^{18}O/^{16}O$) for water samples reference is made to Krishnamurthy (1984).

6.2 Major ion determination

The water samples were filtered using Gelman cartridge (pore size 1μm) for major ions determination, however, measurements of pH and alkalinity were done on unfiltered samples at site within a few hours of sampling. The pH was measured using a portable digital pH meter with a precision of ± 0.1 units and total alkalinity (defined as eqv. sum of HCO_3^- and CO_3^{2-} ions) by titrating the water samples with 0.02/0.2N HCl in presence of methyl orange as indicator. The precision of alkalinity measurement, based on repeated titra-

tion of the standard Na_2CO_3 and sample solution with 0.2N HCl, was found to be ±5%. The filtered water samples were analyzed for major ions (e.g. Na^+, K^+, Ca^{2+}, Mg^{2+}, Cl^-,SO_4^{2-}) by the Atomic absorption spectrophotometry (AAS) and ion chromatography. The coefficient of variation for Na and Cl ions, 2.6 and 2.2% respectively, was calculated using eqn.(2.1) (see p. 14) as a measure of precision of measurement. In a few samples, Cl estimation was done using both $AgNO_3$ titrimetry and ion-chromatography method (Table 6.1). The mean reproducibility of Cl measurement by these two independent methods was found to be better than 2%.

Table 6.1 : Reproducibility of chloride measurement by two different methods

Sample	Cl(meq/l)	
	(a)	(b)
SL #10	24.5	23.9
SL #21	19.6	18.2
SL #24	63.7	65.3
SL #44	455	445
SL #48	75.2	76.6
SL #50	23.8	22.7
SL #62	19.2	18.7
SL #77	3922	4046

(a) based on $AgNO_3$ titration, and
(b) based on ion-chromatography method

The concentration of sulphate in the brine samples was determined gravimetrically by precipitating $BaSO_4$ from the samples. Repeat measurements of SO_4 in a few samples showed reproducibility within 1%. For all groundwater samples, SO_4 was estimated by ion-chromatography with a precision of 3%.

The charge balance between Σcations and Σanions for 86 samples is 0.98±0.06. These data are shown in Fig. 6.1.

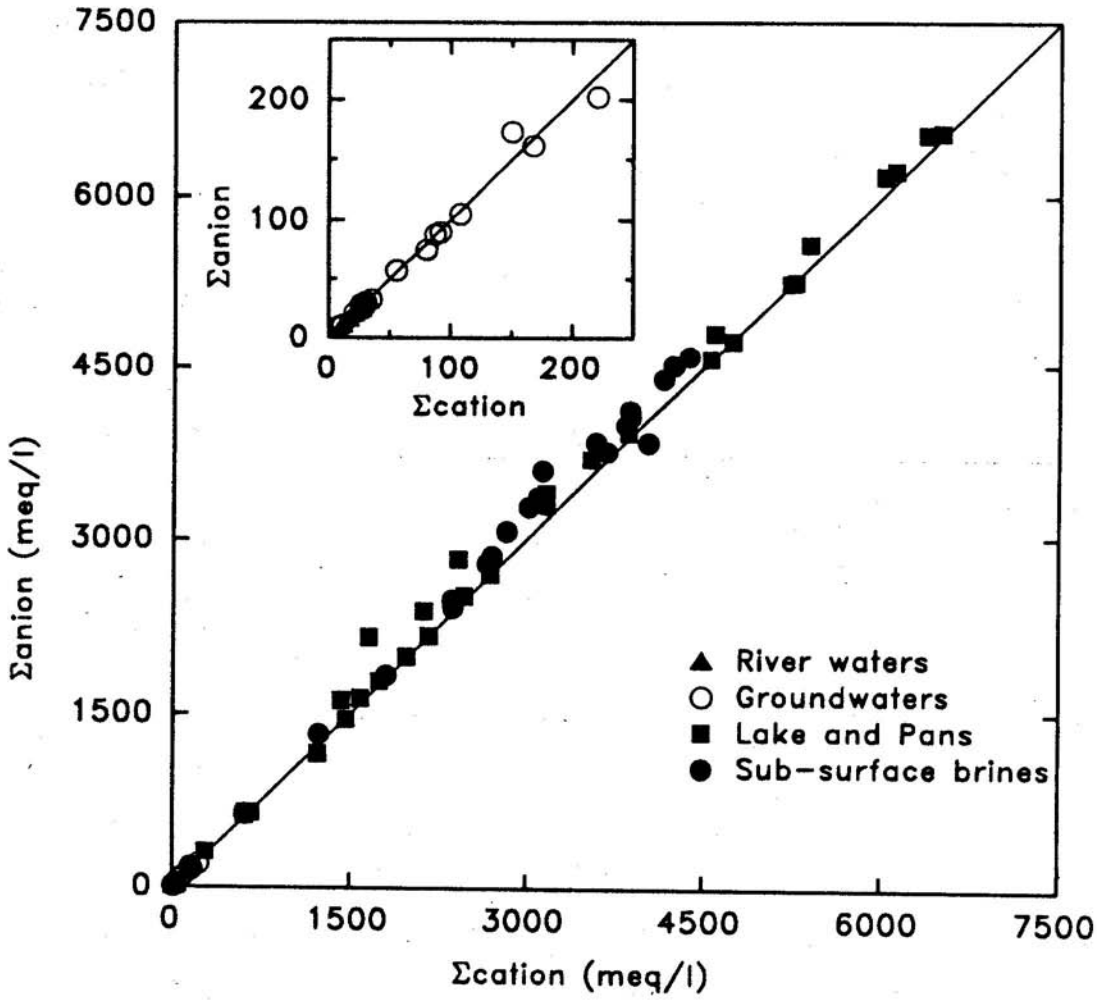

Figure 6.1: Scatter diagram of Σcations and Σanions in water samples from the various reservoirs in and around the Sambhar lake. Most of the data lie on the "equiline" indicating that the ions other than those measured in this study do not contribute significantly to the charge balance. The inset in the figure is for groundwaters and river waters.

6.3 Radionuclide measurements

For radioisotope (U, Po, Pb) measurements in groundwaters and river waters, preconcentration from $\sim 10-20\ \ell$ filtered and acidified samples was done in the field using $Fe(OH)_3$ precipitation in presence of U–Po–Pb yield tracers viz. ^{232}U, ^{209}Po and Pb-carrier (Krishnaswami et al,1982; Sarin et al,1992). The $Fe(OH)_3$ containing U, Po and Pb was dissolved in HCl and these nuclides were separated following the techniques routinely employed in our laboratory for seawater analysis (Sarin et al,1992). For brine samples, it was difficult to filter through either millipore or Whatman filter papers due to the presence of algae. Under such a condition, U, Po and Pb isotopes were determined in unfiltered smaller volume of samples (for U, 25–250 ml and for Po/Pb, $\sim 5\ \ell$) by drying and digesting with nitric acid in presence of their yield tracers. Such a scheme was followed to ensure spike equilibration with the natural isotopes in water samples. The purified U, Po and Pb (via Po) samples were α assayed to determine their concentrations. The chemical yield for uranium in groundwaters centered around 75% whereas in the brines the range was between 30–80%. For the two other radionuclides, ^{210}Po and ^{210}Pb, the chemical yield in groundwaters was observed to be around 70% and in brines the range was between 40–60 %.

The Ra isotopes ($^{226,228}Ra$) were measured by preconcentrating them on MnO_2 fibre (Moore,1976). The Mn fibre containing the Ra isotopes was brought to the laboratory, treated with 3M HCl ($\sim$ 250 ml), warmed, filtered and the acid solution transferred to a Rn flask. The ^{226}Ra was measured in the solution via ^{222}Rn (Mathieu, 1988). For this, sample solution in the Rn flask was purged with pure He gas, sealed and stored for radon to grow for about two weeks. The ^{222}Rn was purged out with He, purified and counted using scintillation counters. The efficiency of extraction and counting was ascertained using ^{226}Ra standards. The standards and blanks were periodically analyzed to check the measurement of ^{226}Ra. After the ^{226}Ra determination, $BaSO_4$ was precipitated from the sample solution, dried and sealed in a vial for γ-assay through a low background HPGe well detector coupled with multichannel analyzer. Based on the $^{228}Ra/^{226}Ra$ ratio, derived from the γ-ray spectra and concentration of ^{226}Ra determined by the radon method, the activity of ^{228}Ra was calculated.

The errors given in all the above radionuclide determinations correspond to $\pm 1\sigma$,

calculated from counting statistics and uncertainty of tracers/spikes calibrations and blank corrections.

In the following chapter, the results on the isotopic composition of oxygen, major ions and radionuclide are discussed. Major ion concentrations are reported in meq/l and those of radionuclides in (μg or dpm)/kg. All ion ratios in the following chapter refer to equivalent ratios.

Chapter 7

Results & Discussion

Chemical and isotopic analysis of the major water reservoirs in and around the Sambhar lake has been made with a view to evaluate possible relationships between them and to study the chemical evolution of the lake. The chemical and isotopic composition of continental waters is influenced by several factors such as chemical weathering of rocks, the composition of meteoric precipitation, mixing of various endmember waters, the process of evaporation and also biological activities. Groundwaters in granite and rhyolite terrains have compositions dominated by Na, HCO_3, SiO_2 and F ions whereas Ca, Mg and pH are generally low (White et al,1963). Similarly, groundwaters from sedimentary basins are characterized by low SiO_2 and high Ca, Mg and SO_4 ions. The chemistry of groundwaters is also influenced by dilution effect during recharge and dissolution of evaporite minerals formed in unsaturated zone especially in arid and semi-arid regions (Drever and Smith,1978). Using chemical data from California Sierra, Feth et al (1964) and Garrels and Mackenzie (1967) have shown that stream water chemistry is related to the chemistry of source rock and its mineral equilibria. Aquatic organisms often influence the concentration of many elements e.g. C, N, P, S, Ca, Cd etc. by metabolic uptake, transformation, storage and release (Stumm and Morgan,1981).

Among several environmental isotopes, ^{2}H, ^{18}O, ^{3}H, ^{3}He and ^{222}Rn are used widely in hydrological applications. The isotopes associated with water molecules i.e. ^{3}H, ^{2}H and ^{18}O are the ideal tracers; their spatial and temporal variabilities help to understand the origin of groundwaters on a regional scale, surface and groundwater interactions, lake water balance, leakage from water reservoirs, groundwater recharge, paleoclimates and mois-

ture circulation patterns etc. (Gat,1981a–c; Gonfiantini,1981; Fontes,1981; Payne,1981; Saxena,1987).

In this study, attempt has been made to understand the evolution of isotopic and chemical composition of the Sambhar lake waters based on the observations during annual wetting and drying cycles, mineral-aqueous equilibria, chemical weathering of surrounding rock formations and behaviour of some of the selected U-Th radionuclides in these waters over a wide range of salinity. These results are discussed in the following section.

7.1 Oxygen isotope evolution of the Sambhar lake and sub-surface waters

The oxygen isotope ratio ($^{18}O/^{16}O$) of natural waters exhibits a wide range due to isotopic fractionation processes which occur during chemical (e.g. isotopic exchange reaction) and physical processes (e.g. evaporation, condensation and gaseous diffusion). Therefore, along with the background information on environment and hydrological conditions, the variation in abundances of oxygen isotope ratio can help understand the physico-chemical processes operating in a hydrologic system. For this reason, isotopic composition of oxygen is frequently used to provide a better understanding of hydrological problems viz. identifying qualitatively and quantitatively the mixing proportion of various end-members of waters, characterization of aquifer systems and evaporation history of closed basin reservoirs.

Table 7.1: Oxygen isotope and major ion ratios in various water reservoirs in around the Sambhar lake (this study)

Reservoir	TDS range ($g.\ell^{-1}$)	$\delta^{18}O$ range ($^{o}/_{oo}$)	$\frac{Na}{Cl}$† (average)	$\frac{(Na+Cl)}{TDS}$ † (average)	$\frac{Cl}{SO_4}$† (average)	$\frac{Alk}{(Ca+Mg)}$† range
Rain water	1.6 & 2.1*	−6.4 & −3.2	1.01	–	–	–
River water	0.5–1.8	−5.4 to −3.6	2.70	0.62	3.95	1.5–15
Groundwater	0.5–12.3	−6.5 to −3.0	1.03	0.71	11.62	0.2–4
Lake water	9.0–370	−5.5 to 24	1.08	0.94	12.19	4–1100
Evaporating pan	70–392	–	1.23	0.90	7.22	150–3900
Sub-surface Brine	70–270	−1.0 to 7.4	1.17	0.90	5.78	70–3000

* TDS (total dissolved solids) in $mg.\ell^{-1}$ † equivalent ratio

7.1.1 Oxygen isotopes in atmospheric precipitation, groundwaters and river waters

The $\delta^{18}O$ of the groundwaters collected from open wells (adjacent to the lake) ranges from -6.5 to -3.0 $^{o}/_{oo}$ and the TDS content is < 12.3 g/l (Table 7.1). Similar to groundwaters, the river water samples from the Mendha and Roopangarh (with TDS <1.8 g/l) show $\delta^{18}O$ variation from -5.4 to -3.6 $^{o}/_{oo}$. These results of $\delta^{18}O$ overlap with the values of two rain water samples, $-$ 6.4 and -3.2 $^{o}/_{oo}$, collected during July 1993. This observation, though based on a limited number of rain water samples, suggests that the $\delta^{18}O$ of the groundwaters along the periphery of lake is dominated by atmospheric precipitation.

In Figs. 7.1 the $\delta^{18}O$ values of the groundwaters are plotted against TDS for the samples collected during Oct (recharge period) and Feb months. These plots have been made to discern any relation between $\delta^{18}O$ and TDS which may provide information on the mixing trend among the groundwaters. The results for the Oct and Feb months show that the $\delta^{18}O$ of groundwaters around the Sambhar lake are within the range observed for rain water from the region. The differences in salt content among the various groundwaters could be attributed to varying amount of salt derived from weathering of their local recharge zones. An alternate explanation for the trend in the Figs. 7.1 is mixing of two endmembers, one endmember with low $\delta^{18}O$ and TDS and the other with high $\delta^{18}O$ and TDS. A similar inference has been made from the distribution of uranium isotopes in these groundwaters (detail discussion follows in later section on radionuclide systematics).

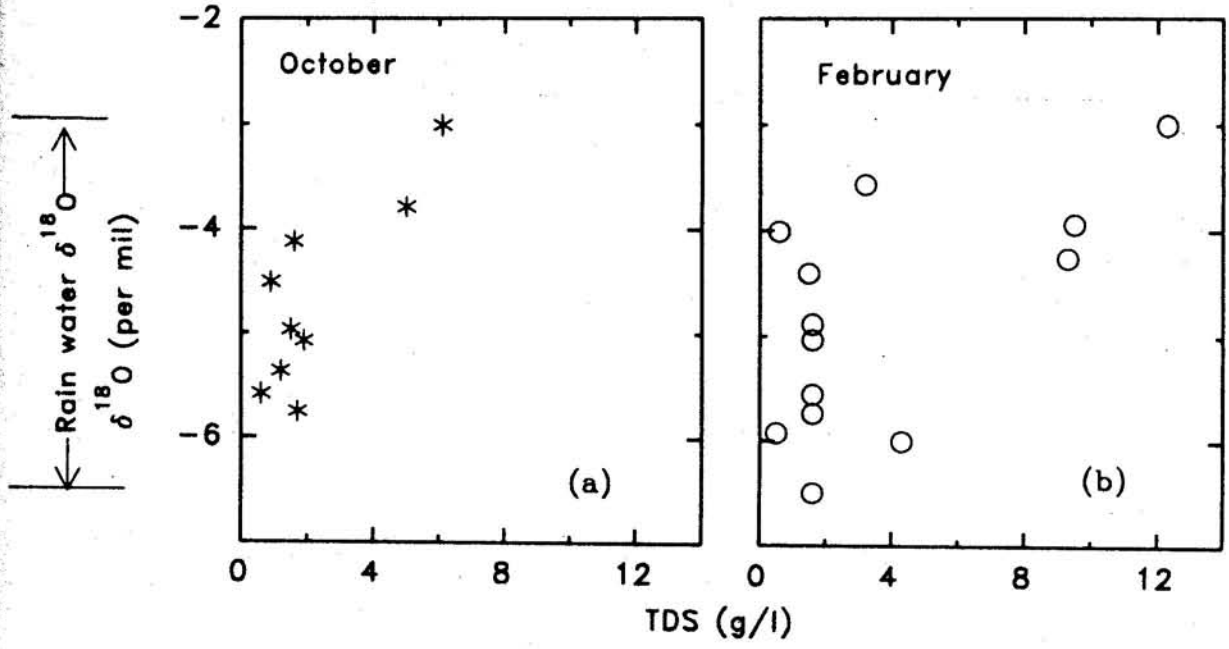

Figure 7.1: Scatter diagram of $\delta^{18}O$ vs. TDS for the Sambhar lake groundwaters collected during Oct and Feb months. The distribution of sample points collected during Oct. and Feb months essentially show two distinct group of groundwaters in terms of their salt contents. The $\delta^{18}O$ in these groundwaters are within the range of atmospheric precipitation.

The influence of evaporation on the groundwaters can be discerned through the $\delta D - \delta^{18}O$ relationship. The evaporation generally causes a shift in the slope of $\delta D - \delta^{18}O$ meteoric water line (MWL) (Dansgaard,1964). The MWL line (Craig,1961; Yurstsever and Gat,1981) defined as, δ D=(8.17±0.08) $\delta^{18}O$ + (10.56±0.64). In the present study, δD has not been measured but results of δD and $\delta^{18}O$ in groundwaters from the nearby region (Sambhar, Didwana and Kuchaman) show the following relation (Ramesh et al, 1993):

$$\delta D = 3.15 \ \delta^{18}O - 22.4 \quad (n = 26) \tag{7.1}$$

A significant deviation in the slope of $\delta D - \delta^{18}O$ line with respect to the MWL indicates the influence evaporation occurring in the groundwaters of this region.

7.1.2 Oxygen isotopes in lake, evaporating pans and sub-surface brines

With a view to understand better the chemical and isotopic relations between the lake water, the sub-surface brines which occur mostly 3–4 m below the lake bed, and the water in evaporating pans which is derived from the lake, water samples were analyzed for the measurement of major dissolved ions and oxygen isotopes in different seasons.

The lowest $\delta^{18}O$ value of -5.5 $^0/_{00}$ was measured during July 1992 when lake was recharged by precipitation. This value is within the range measured for rain and river waters (Table 7.1). The effect of evaporation is observed in subsequent months with the enrichment in both $\delta^{18}O$ and salt-content. The $\delta^{18}O$ shows a linear increasing trend up to a value of ~ 20 $^0/_{00}$ with the salt content (TDS) (Fig. 7.2a).

The $\delta^{18}O$ values and salt-content during July to April months show a strong positive correlation (r=0.91) both of them steadily increasing due to evaporation. At salinities exceeding $\sim$ 100 g/l (during May 93) there is a change in in the slope of the $\delta^{18}O$–TDS trend, the increase in $\delta^{18}O$ with TDS is much less in the salinity range 100–400 g/l, relative to that in the lower salinities, (9-100) g/l. During later stages of evaporation (TDS $>$ 200 g/l), there is scatter in $\delta^{18}O$ values, cause of which is presently unclear.

Saturation in $\delta^{18}O$ during late stages of evaporation can be understood in terms of known models (e.g. Rayleigh and Craig–Gordon models) for $\delta^{18}O$ evolution trends in the lake basin. These models take into account processes such as evaporation and isotopic exchange between liquid and atmospheric water vapour. The oxygen isotope evolution in lake water over annual cycle of evaporation (July 92–May 93) is modelled using both Rayleigh and Craig-Gorden (1965) models. The Rayleigh eqn. used in modelling is (Gonfiantini,1981):

$$\delta = \delta_0 + 10^3 \cdot (1 - \alpha)\ ln f \qquad (7.2)$$

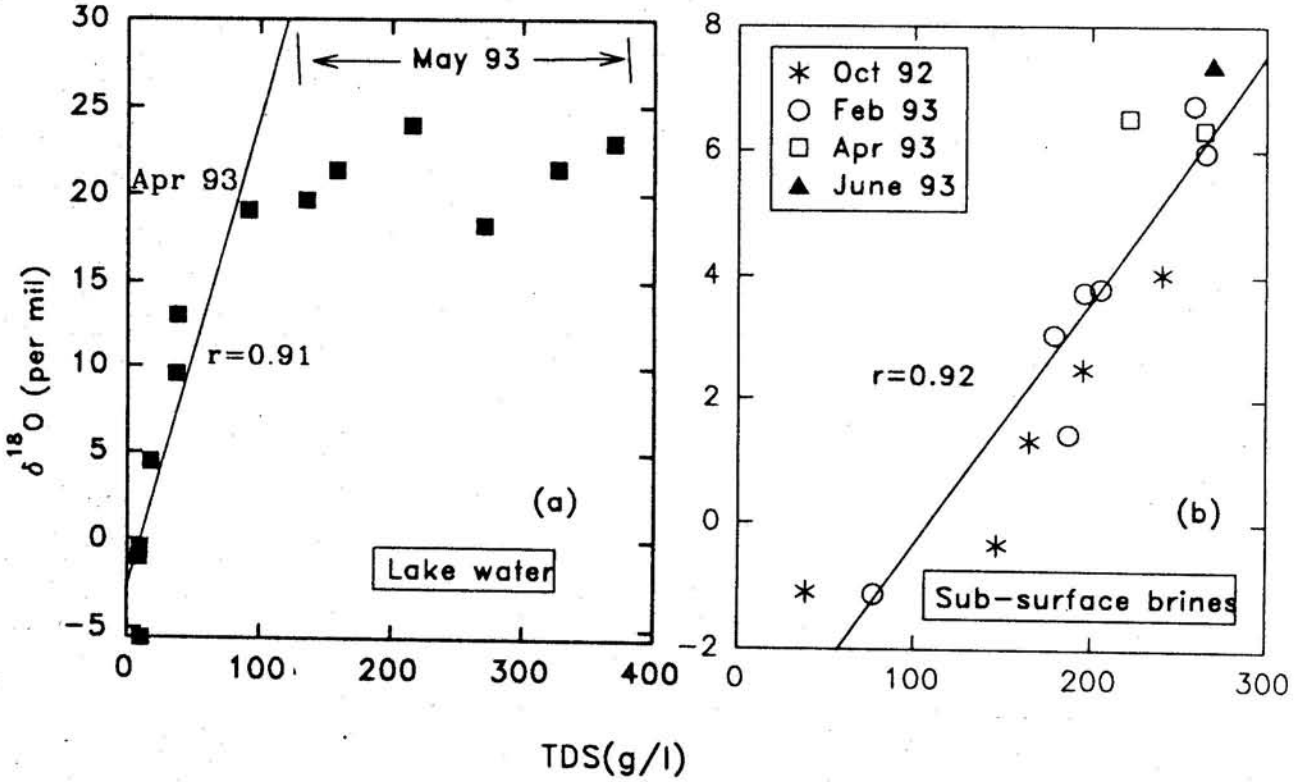

Fig. 7.2 Scatter diagram of oxygen isotopes in lake and sub-surface brines observed during the annual wetting and drying cycles (1992–1993). Fig. 7.2a shows a strong positive correlation (r=0.91) between $\delta^{18}O$ and salt content for the Sambhar lake waters during July 92–Apr 93. Such variation in $\delta^{18}O$ and TDS is explained through the process of evaporation. The $\delta^{18}O$–TDS relationship during late stage of evaporation (May 93) has a much gentler slope, resulting from the back condensation of $\delta^{18}O$ depleted atmospheric water vapour (see text for detail discussion). Fig. 7.2b also illustrates strong positive correlation (r=0.92) between $\delta^{18}O$ and salt content for the sub-surface brines. The linear trend between them is mainly attributed to a two component mixing of waters, i.e. lake/atmospheric precipitation and sub-surface brines.

where δ_0, δ are the $\delta^{18}O$ of initial water and that at any time t respectively, α the oxygen isotope fractionation factor between vapour and liquid and f is the fraction of residual lake water. In this model calculation, the fractionation factor α is considered to be constant throughout the annual evaporation period and δ of each succeeding step was calculated from the preceding δ value [eqn. (7.2)]. The residual fraction of lake water used in model calculation is estimated from concentration of uranium in the water at each evaporation step, as U is known to be a conservative tracer in an oxidising environment (see section 7.3 for detail discussion). The Rayleigh model agrees well with the measured values of $\delta^{18}O$ (assuming $\alpha = 1.0092$) in successive evaporation stages until the residual fraction of water in the lake approaches to around 10% during Apr 93 (Fig. 7.3). In later stages, model derived $\delta^{18}O$ increases sharply and does not fit the experimental data. The divergence in the $\delta^{18}O$ values calculated based on the model and those measured in later stage of evaporation could be attributed to either reduction in equilibrium fractionation factor, reduction in vapour pressure of lake water or by an increased exchange of isotopically light atmospheric water vapour.

To understand the relative importance of these factors, data were analyzed using the Craig-Gordon model where both equilibrium and kinetic fractionation factors, and the effect of changing seasonal temperature and humidity were taken into account.

The evolution of oxygen isotope as a function of time is calculated from the following relations (Gonfiantini,1986):

$$\delta = \delta_0 + \frac{d\delta}{d\ln f} \cdot \Delta \ln f \tag{7.3}$$

where,

$$\begin{aligned}
\frac{d\delta}{d\ln f} &= \frac{\frac{h}{a_\omega}(\delta - \delta_a) - (\delta + 1)(\Delta\epsilon + \frac{\alpha - 1}{\alpha})}{1 - \frac{h}{a_\omega} + \Delta\epsilon} \\
\alpha &= \exp(1137/T^2 - 0.4156/T - 0.00207) \qquad (Majoube, 1971) \\
a_\omega &= -0.000543/f^2 - 0.018521/f + 0.99931 \\
\Delta\epsilon &= 0.0142(1 - \frac{h}{a_\omega})
\end{aligned}$$

δ_a is the $\delta^{18}O$ of atmospheric water vapour, h is the fractional relative humidity, T is the temperature in ^0K and a_w is the thermodynamic activity of water.

Fig. 7.3 The annual oxygen isotopic evolution (July 92–May 93) in the Sambhar lake based on Rayleigh fractionation model. The model curve approximates the observed data points up to ~ 10 % of residal lake water. beyond which model curve diverges from observation. See text for explanation in discrepancy of the observed and modelled $\delta^{18}O$ results.

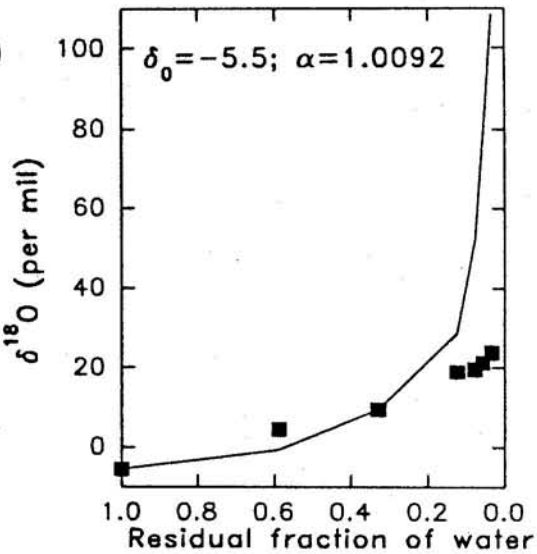

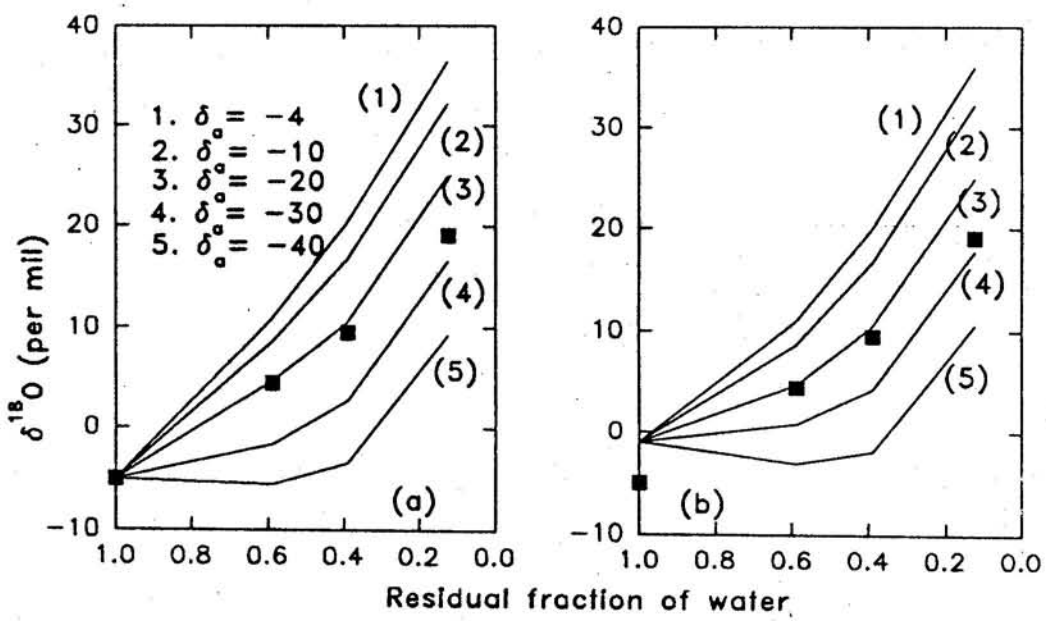

Fig. 7.4 Craig–Gordon (1965) model applied to annual isotopic evolution of oxygen (July 92–May 93) in Sambhar lake waters with initial $\delta^{18}O$ (a) −5.5 and (b) −1 per mil and different isotopic composition for atmospheric water vapour (δ_a). Comparison of Figs. (a) and (b) indicates that $\delta^{18}O$ evolution trend does not depend critically on the initial value. The model curve (3) approximates the observed data for δ_a=−20 per mil.

The Craig-Gordon model calculation was carried out until the residual fraction of lake water was 10%. Further calculations could not be made as the expression for thermodynamic activity of NaCl solution (a_w) is valid only upto the residual fraction f=0.1 (Gonfiantini,1986). The evolution of $\delta^{18}O$ as a function of residual amount of water in the lake was calculated for (i) different values of $\delta^{18}O$ in the atmospheric water vapour (Fig. 7.4) undergoing exchange with lake water and (ii) different initial values for $\delta^{18}O$ in the lake water. These results are presented in Fig. 7.4 which show that (i) the most sensitive variable affecting the $\delta^{18}O$ evolution of lake water is the isotopic composition of the atmospheric water vapour and (ii) the $\delta^{18}O$ evolution in the lake with evaporation is not critically dependent on the initial isotopic composition of either -5.5 or -1.0 $^{o}/_{oo}$. Reasonably good fit with the experimental data (Fig. 7.4) is obtained for the value of -20 $^{o}/_{oo}$ for the atmospheric water vapour. These results suggest that back condensation of isotopically light atmospheric vapour having $\delta^{18}O$ as low as -20 $^{o}/_{oo}$ plays a dominant role on the isotopic evolution of the lake water during the late stage of evaporation. A similar observation has been reported for the Owens lake, California (Phillips et al,1986). The $\delta^{18}O$ of atmospheric water vapour over the Sambhar lake has not been measured. However, a value (-20 $^{o}/_{oo}$) is reasonable for the pre and post monsoon seasons when the western disturbance brings precipitation to regions north of the Sambhar lake. Measurement of $\delta^{18}O$ in atmospheric water vapour of this region is required to confirm the model calculations.

The $\delta^{18}O$ measurements were made in two types of pan waters: different pans with varying salinity collected in a single season (Feb 92) and the same pan sampled at different times during Feb–May 92. The objective behind this study was to understand the relationship between salt content (TDS) and $\delta^{18}O$ of evaporating waters in the pans and to compare the oxygen isotopic evolution in the pan and lake waters during evaporation.

The pan waters collected during a single season (Feb 92) did not prove to be useful for studies as they were a mixture of various end members. It was learnt that water from subsurface brines were periodically mixed with the pan waters and circulated from one pan to the other during salt production. This is unlike the sample from the same pan, which was recharged with lake water only once and allowed to evaporate. The $\delta^{18}O$ evolution of this pan water, therefore, can be compared with the $\delta^{18}O$ evolution in lake waters.

In this comparative study, an assumption is made that the conditions of evaporation have remained the same over the two year periods (91−92 and 92−93) for both lake and pan waters. Fig. 7.5 shows the variation in $\delta^{18}O$ as a function of salt content. The $\delta^{18}O$ evolution shows a positive relation with TDS and does not saturate, unlike the lake waters. Also, the maximum $\delta^{18}O$ (27.5 $^{o}/_{oo}$) observed in the pan is relatively higher than that observed in lake waters (mean value, 21$^{o}/_{oo}$). Such an observation indicates difference in evolution pattern of $\delta^{18}O$ in pan compared to that of the lake. This could arise due to the high rate of evaporation in the pan for less volume of water spread over large area. Under such a condition, the process of evaporation dominates over the back condensation of atmospheric water vapour which is depleted in $\delta^{18}O$.

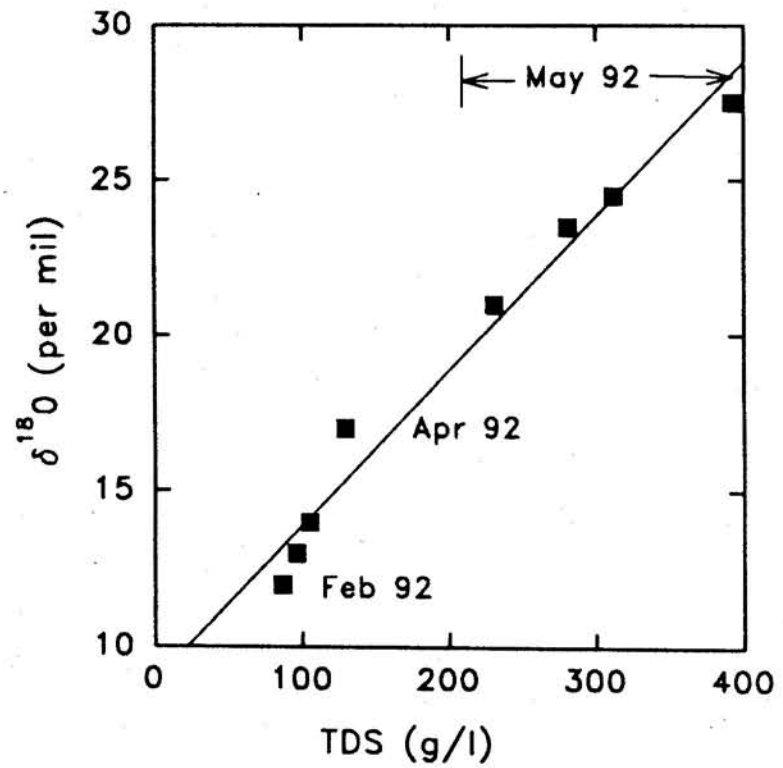

Figure 7.5: Scatter diagram of salt content (TDS) and oxygen isotope ($\delta^{18}O$) in an evaporating pan sampled during different months (Feb−May 92). The samples collected include hyper saline brines up to a stage of halite precipitation. The $\delta^{18}O$ evolution pattern in pan is different from the lake waters, see Fig. 7.2a

In contrast to the evaporating lake waters, the seasonal variations in the $\delta^{18}O$ are less pronounced in sub-surface brines. The temporal evolution of $\delta^{18}O$ in sub-surface brines has been explained in earlier studies through evaporation pattern of a "terminal lake" in

which evaporation is more or less balanced by inputs from precipitation and surface run-off during monsoon season (Ramesh et al,1993). Using a Rayleigh isotopic fractionation model for the typical temperature and humidity conditions (temp. 291^{0}K, humidity 55%) found in this region, they have shown that the saturation in $\delta^{18}O$ is about 4.8 $^o/_{oo}$ which is quite similar to that observed in most of the samples measured in this study during seasons other than the monsoon. With the onset of monsoon (July−Sept), the lake and the open dug wells are recharged by the meteoric water. As mentioned earlier, a number of open dug wells have been constructed on the lake bed for pumping out the sub-surface brines for salt production. These open wells get filled with rain water during monsoon and thus promotes recharge of sub-surface aquifers with atmospheric precipitation. However, the mixing of meteoric water with higher density sub-surface brines may be constrained, the pumping operations carried out for salt production after monsoon season may aid this mixing process. In the sub-surface brines, the mean $\delta^{18}O$ for the month of Oct 92 was lowest ($1^o/_{oo}$) and by June the value increased to 7 $^o/_{oo}$ (based on sample from one of the wells). The $\delta^{18}O$ in sub-surface brines sampled between Oct 92 to June 93 show a significant positive correlation (r=0.92) with the salt content (Fig. 7.2b). Such linear trend for sub-surface brines could be due to mixing with meteoric and/or lake waters during monsoon season and with lake waters during post monsoon seasons. The range in $\delta^{18}O$, -1 to 4 $^o/_{oo}$, of different wells in a single month (Oct 92), shows that the extent of dilution of sub-surface brines with relatively depleted $\delta^{18}O$ end-member (direct precipitation or lake water) is not uniform. A factor contributing to the different extents of mixing of two water bodies (rain or lake water and sub-surface brines) is the variable draw down of the sub-surface aquifer by pumping during salt production. In above consideration, the influence of evaporation on controlling the salinity of sub-surface brines has not been taken into account as these brines occur below the lake bed where evaporation would be resrticted and the $\delta^{18}O$ evolution trend would be unlike of the evaporating lake water.

Synthesis

The $\delta^{18}O$ of shallow groundwaters and riverwaters adjacent to the lake are similar to those in atmospheric precipitation indicating that these water bodies are recharged from

local precipitation. The $\delta^{18}O$ results for the lake and sub-surface brines suggest that these reservoirs are recharged during the monsoon season. In lake, the $\delta^{18}O$ during monsoon is very similar to that of local rain waters, whereas in sub-surface brines $\delta^{18}O$ is enriched, reaches a minimum value of $-1\ ^{o}/_{oo}$ compared to a value of $-5.5^{o}/_{oo}$. The similarity in the $\delta^{18}O$ and of the lake and rain water indicates that the lake gets recharged from atmospheric precipitation and surface run-off. The recharge to sub-surfacae brines from evaporating lake waters during the summer months (Apr–June) is limited as reflected from the large difference in $\delta^{18}O$ measured in the two reservoirs. The lake waters undergo intense evaporation showing $\delta^{18}O$ values as high as $\sim 21^{o}/_{oo}$ during the peak summer (May). In contrast, the sub-surface brines show enrichment in $\delta^{18}O$ only up to $7^{o}/_{oo}$. The $\delta^{18}O$ evolution trend in Sambhar lake is essentially of Rayleigh type, however, the exact trend can be explained through the Craig-Gordon (1965) model. The results of the Craig-Gordon model suggest that back condensation of atmospheric moisture ($\delta^{18}O \sim -20^{o}/_{oo}$) during late stage of evaporation controls the observed $\delta^{18}O$ of the lake brines. A distinct difference in $\delta^{18}O$ evolution trends between the lake and evaporating pan has been observed. The evaporation dominates over the back condensation of atmospheric water vapour even during the late stage of evaporation. Such conclusion is borne out from the linear relation between the $\delta^{18}O$ and TDS in the evaporating pan waters all through the evaporation.

7.2 Major ion composition

The major ion chemistry of various water bodies in the Sambhar lake basin forms an integral part of this thesis as this has relevance to the source of salt to the lake and evolution of brines during the annual evaporation cycle. In addition, such a study also provides a means to characterize the various water bodies in terms of their chemical composition.

The Na and Cl concentrations in the two rain water samples collected during July 93 correspond to ~ 2 mg/l NaCl (Table 7.1). The Na/Cl ratio in these two samples (0.72 and 1.12, Table 7.1) are on either side of the seawater composition (0.85). As the rain samples were collected from the Sambhar town, within a few km of the lake, part of the NaCl in

the rain could arise from its resuspension during salt production from the lake. Therefore, the content of NaCl in these rain water samples may have a local cyclic salt component, in addition to the marine component. The measured NaCl concentration in the two rain water samples, if typical of rains throughout the year, can provide an estimate of the NaCl supplied to the lake via precipitation. The estimate could be an upper limit as there could be a significant local recycling component of NaCl in rain water. The estimate is about 5000 tonnes based on NaCl concentration of 2 mg/l in the rain water, drainage area of about 5600 km^2 (Bhattacharya et al,1982) and an annual rainfall of 50 cm. This estimate when compared to the current annual salt production of 2×10^5 tons/y, suggests that the rain water is not a major contributor of salt to the lake which can sustain the current annual salt production.

An independent approach to evaluate the significance of the rain water contribution of NaCl is by comparing it with the total salt content of the lake after the monsoon. For lake area of $\sim$225 km^2, water depth of 1 m and 8.3 g/l NaCl salt, the inventory of NaCl in the lake is 18.5×10^5 tons which is many orders of magnitude higher than the atmospheric precipitation.

The river waters from the region are more saline than the rain water, with TDS ranging between 0.5–1.8 g/l (Table 7.1), with Na and Cl being the dominant components. The Na/Cl ratio in the river waters ranges between 1.9 to 3.7 with an average value of 2.7 (Table 7.1). There is an excess of sodium over chloride in these waters, which suggests that a significant part of Na is derived from the sources other than NaCl, such as weathering of silicate rocks along the river drainage basin. The TDS content of all the river water samples analyzed are significantly lower than that of the lake water sampled immediately after the monsoon season (samples: SL-46, SL-47, SL-52; Appendix–B, Table 1B). Also, the Na/Cl ratio in waters from the river basin is significantly higher than that observed in lake waters (1.08 average Na/Cl). The high TDS and the low Na/Cl ratio in the lake water compared to that in rivers results from dissolution of halite salt encrustation from the lake bed during the recharge period. These results seem to indicate that the contribution of salt from inflow river waters to the lake is significantly less compared to that recycled from within the lake basin. The average Na/Cl ratio in river waters is 2.70 (Table 7.1). If 125 meq/l of Na and Cl are added to river waters (see Appendix–B, Table 2B) then

Na/Cl ratio reduces to about the same value of lake waters. Such an addition indicates that the contribution of NaCl to the lake water by recycling of salts in the lake is about 90% and rest can be from the surface run-off. A rough estimate on the amount of NaCl recycling from the lake basin, based on NaCl content in lake water of 1 m average depth during Oct 92, is calculated to be $\sim 18.5 \times 10^5$ tons.

The TDS content of groundwaters ranges from 0.5 to 12.3 g/l but in most of the samples it centers around ~2.0 g/l with Na and Cl accounting for ~70% of the cations and anions (Table 7.1), suggesting general dominance of NaCl in the drainage basin. The Mg/Ca ratio in some of the groundwaters is > 1. This can arise due to preferential removal of Ca by mineral precipitation from these water bodies. In fact, most of the groundwaters are supersaturated with respect to calcite.

The chemical evolution of lake and pan waters was studied by analyzing samples collected during different seasons. The chemical composition of waters from these two reservoirs during their evaporation cycles is generally similar, consistent with that expected as the lake water is the dominant component of initial end-member used in the evaporating pans. The TDS content in the lake waters ranges from 9 to 370 g/l (Table 7.1), the lowest values occurring in samples collected during the period immediately following the monsoon season (Oct 1992) and highest value during the summer season just before the monsoon.

7.2.1 Chemical evolution of the Sambhar lake brine

Hardie-Eugster model

The evolution of brines in closed sedimentary basins due to evaporation of waters depends on several factors e.g. initial composition of water, mineral precipitation, selective dissolution of salt encrustation, ion exchange and sorption processes, degassing and redox reactions (Eugster and Jones,1979). Major solutes present in source water are affected differentially by these processes. Out of these, mineral precipitation is a dominant process that governs the chemical evolution of brines during evaporation (Garrels and Mackenzie,1967; Hardie and Eugster,1970; Eugster and Hardie,1978; Eugster and Jones,1979). As a consequence of evaporation, the evaporating waters follow a definite brine evolutionary path based on the concept of "Chemical Divide" (Drever,1988). The concept of chemical

divide is generalized by Hardie and Eugster (1970) for several natural water compositions. In most natural waters, calcite($CaCO_3$), is the first mineral to precipitate, followed by either gypsum ($CaSO_4.2H_2O$) or sepiolite (Mg-silicate)(Hardie and Eugster,1970). If Ca is less abundant than alkalinity (abbreviated as Alk), all the Ca would be precipitated as $CaCO_3$ and the brine would become alkaline. On the other hand, if Alk is < Ca, then (HCO_3 + CO_3) would be precipitated out and the brine would be neutral along the Cl−SO_4 path (Drever,1988). Such a brine evolution path is valid for precipitation of calcite only, however, for a combination of minerals such as calcite and sepiolite the brine evolutionary path is determined by the ratio of Alk/(Ca + Mg).

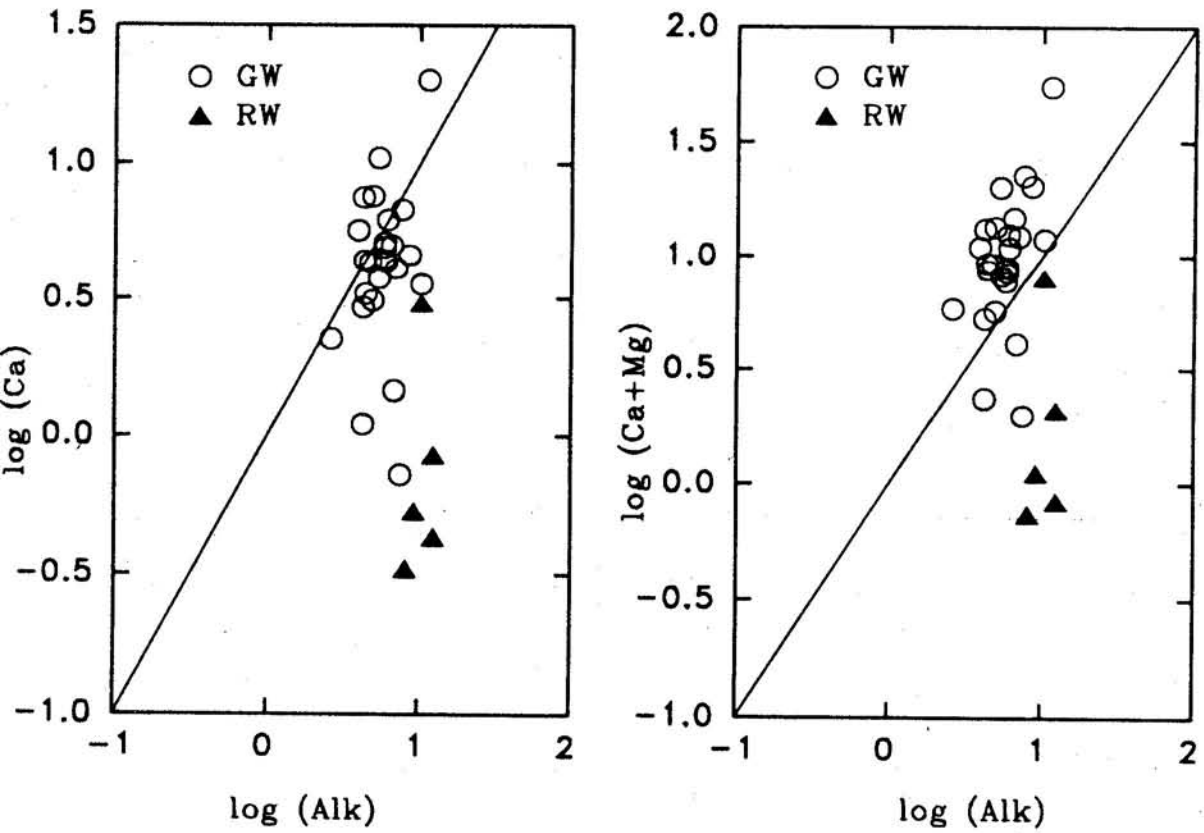

Fig.7.6(a) and (b) The relation between alkalinity (Alk) and Ca or (Ca + Mg) concentrations in ground and river waters of the Sambhar lake region. All the river waters and a few groundwater samples have Alk more than that of either Ca or sum of Ca and Mg. The evaporation of these waters would result in alkaline brines. Those having Alk less than the sum of Ca and Mg ions would produce neutral brines on evaporation (Hardie and Eugster,1970; Eugster and Hardie,1978; Eugster,1980; Drever,1988).

The effect of precipitation of sepiolite, smectite and dolomite on the alkalinity of the

brines is similar (Drever,1988); for this reason in model calculations later presents only one of the Mg-minerals such as sepiolite which is within the scope of the Hardie-Eugster model. Figs. 7.6a and 7.6b show the relation between Ca and (Ca+Mg) with Alk in groundwaters and river waters in and around the Sambhar lake. The data show that in most groundwaters alkalinity is greater than Ca concentration but it is less than the sum of the concentrations of Ca and Mg. On the other hand, all river waters have Alk greater than either Ca or sum of the concentrations of Ca and Mg. As stated earlier, following the principle of "chemical divide" evaporation of groundwaters would result in a neutral brine whereas alkaline brine would be produced by river waters if calcite and sepiolite both precipitate. As silica concentration was not measured in these waters it is assumed that the various source waters have silica concentration equal to that of amorphous silica activity (i.e. $10^{-2.7}$).

The evolution of the Sambhar lake brine has been studied following the Hardie-Eugster model (1970) (cited hereafter as H-E model). The various conditions imposed in the model calculation according to the H-E model are that the water remains in equilibrium with a CO_2 partial pressure of $10^{-3.5}$ atm., temperature remains constant at 25^0C, and pure water is continuously removed from the system. It has been further assumed that there is no interaction between solid formed and residual water during the evaporation. Also, the model calculation neglects the "ion-pairing" effects. The simulation study of evaporation was performed by increasing the concentrations of various ion species in small steps and keeping a constant track on pH, I (ionic strength), m (molality) and γ (activity coefficient) for the various pH dependent species (Hardie and Eugster,1970). The model calculation was terminated at ionic strength of 5, as beyond this ionic strength the Debye-Huckel relation used for calculating the activity coefficient of individual ion is questionable. Even for samples having ionic strength >1, the activity coefficient of ions based on Debye-Huckel relation diverges from experimental results (Garrels and Christ,1965), however, the overall evolution trend of brine can still be ascertained through the H-E model. The programming and other details of the model calculation were checked using the data from the Sierra Nevada spring water, the evaporation trend for which are reported (Garrels and Mackenzie,1967). The results show that the overall evolution trend with regard to pH, concentrations of Ca, Mg, Na, Cl, HCO_3, CO_3 and SO_4 species are similar between

those published in literature and that calculated in this study (Fig. 7.7); though there is some minor discrepancy related to the precipitation stage of calcite. This discrepancy results from different value of γ used for the Ca.

Table 7.2: Chemical composition† of source waters used for modelling the evolution of Sambhar lake brines following the Hardie–Eugster model (1970)

Reservoir	pH	Na	K	Ca	Mg	Cl	SO_4	Alk
R. Roopangarh	8.0	14.6	0.32	0.215	0.233	4.65	0.633	9.9
R. Mendha	8.2	24.1	0.365	0.972	1.525	9.75	4.15	11.35
Groundwaters	7.94	21.5	0.09	1.65	2.67	24.33	0.75	4.4
Lake water	8.4	142.6	0.31	0.665	0.185	129.28	4.165	7

† concentrations are expressed in mmol/l and charge balance of the solution is adjusted with respect to the chloride ion.

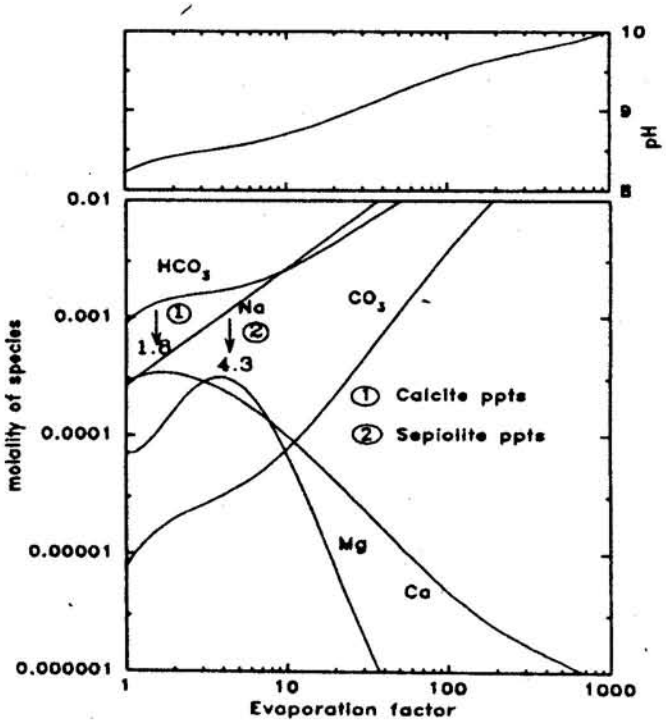

Figure 7.7: Calculated results of evaporation of Sierra Nevada spring water at constant temperature (25°C) in equilibrium with atmospheric P_{CO_2}. The chemical evolution during evaporation essentially follows the trend published by Garrels and Mackenzie (1967). This calculation was carried out to test the details of programming the H-E model.

The evolution of the Sambhar lake brine was simulated using several initial endmember water compositions e.g. the average composition of the two river waters, lake water collected just after the monsoon period and a typical groundwater (Table 7.2). The

charge balance in analytical data was achieved through Cl adjustment. The evolutionary trend obtained by evaporating the Sambhar lake water collected during Oct 92 agrees well with the experimental data in terms of increasing concentrations of Na, K, Alk and SO_4. Some of these results are shown in Fig. 7.8. The pH data for different stages of evaporation are not available to check the model results, however, the pH measurement made in one of the pan brines (SL-7, Appendix−B, Table 2B), of which the lake waters constitute a major component, showed value of about 9.5 at I=5.5. Such a value of pH agrees with the model predicted result for the lake brine (Table 7.3). A major discrepancy has been observed in the evolutionary trend for Ca and Mg ions at different stages of evaporation. The measured concentrations of Ca and Mg ions are much higher than the model predicted values (Fig. 7.8). The possible explanations could be "ion-pairing" and complex ion formation which are ignored in the model calculation. The other possibility, though very unlikely, could be the overestimation of the concentrations of Ca and Mg during measurement as the analysis was done directly in the brine.

Table 7.3 Model calculated* chemical composition of the brine

Chemical composition of brine at Ionic strength,I=5										
Reservoir	pH	Na	Ca	Mg	Alk	SO_4	Cl	Na/Cl	Na/Alk	Cl/SO_4
Lake water (1)	9.8	4.79	1.2×10^{-6}	0	0.19	0.32	4.52	1.06	25	14
Lake water (2)	-	5.0	1.0×10^{-4}	1.5×10^{-4}	0.20	0.40	4.44	1.13	25	11
R. R	10.4	3.82	0	0	2.36	0.32	1.21	3.16	1.6	3.8
R. M	10.2	3.87	2×10^{-7}	0	1.0	1.34	1.57	2.46	3.8	1.2
Groundwater	6.9	3.81	0.76	3.5×10^{-4}	1.3×10^{-4}	0.26	4.31	0.88	3×10^{4}	16.6
R.R. + salt	9.9	4.97	6×10^{-7}	0	0.32	0.044	4.62	1.08	15.5	105
R.M. + salt	9.8	4.45	2.5×10^{-7}	0	0.22	0.24	3.31	1.34	20	14

* ion concentrations in eqv./l and ion ratios in eqv.
Lake water(1) is model calculated and Lake water(2) is the observed value at I =5.2 for SL-77
R.R.and R.M. indicate the river Roopangarh and Mendha respectively.
- indicates measurement not made

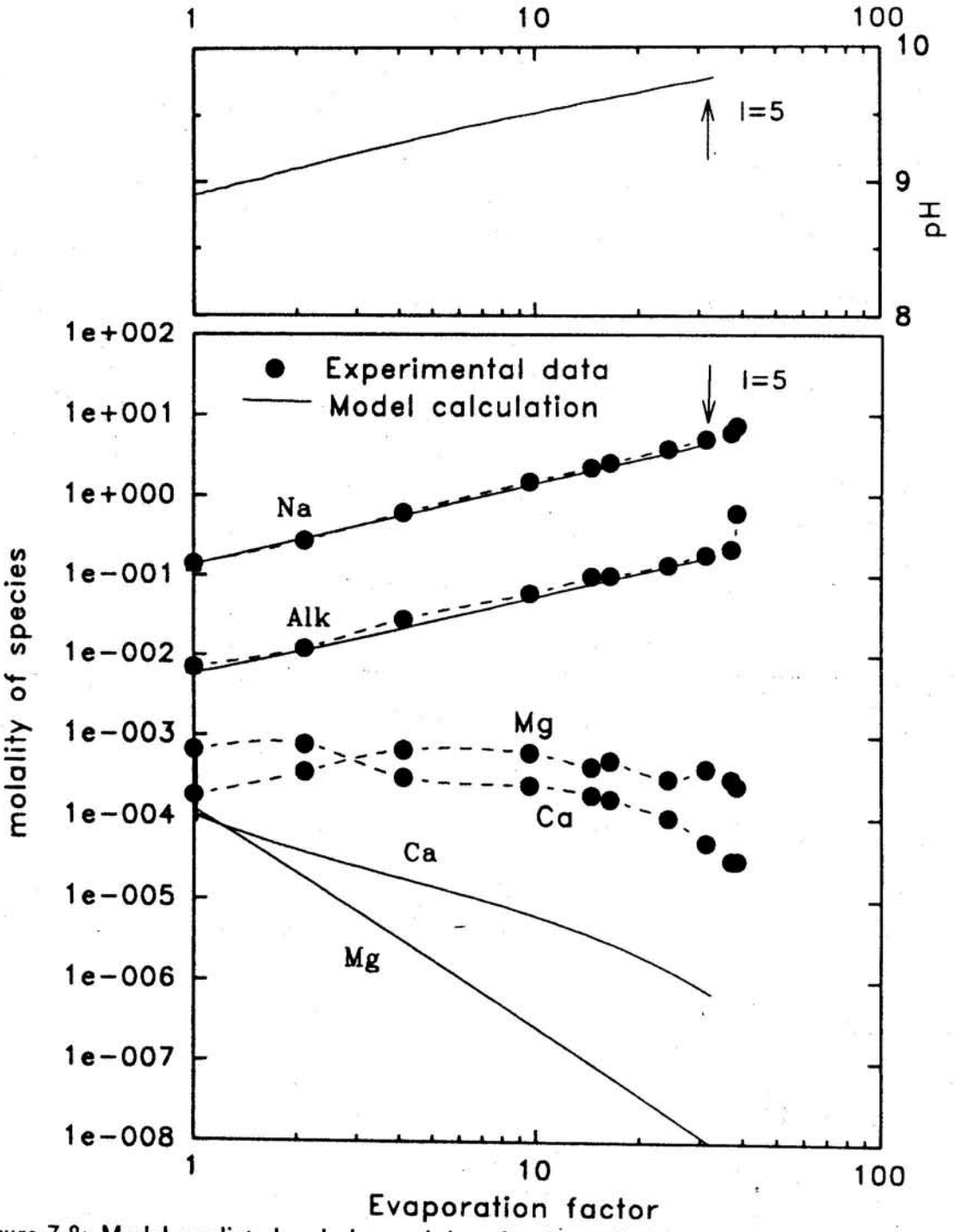

Figure 7.8: Model predicted and observed data for the evolution of the chemical composition of the Sambhar lake waters during annual evaporation. The source water used in the model calculation is the sample SL-46 collected from the lake during Oct 92 . The model calculation was terminated at ionic strength, I=5.

The model calculations were repeated using the two river waters (R. Roopangarh and R. Mendha abbreviated by R.R. and R.M.) as the initial endmembers. These waters have an average TDS value of about 1.2 g/l, significantly lower than that of the lake water endmember. Because of this low TDS, the river waters had to be evaporated much more than that was done earlier using the lake water as the initial endmember to obtain ionic strength of 5. As expected, based on the initial ratio of Alk/(Ca+Mg) greater than one, these river waters produced alkaline brine which is essentially devoid of Ca and Mg ions. The Ca and Mg concentrations decreased during successive stages of evaporation due to their removal as calcite and sepiolite minerals. The other ions such as Na, Cl, SO_4 and Alk showed a linear increase in their concentrations due to evaporative enrichment (Figs. 7.9a and 7.9b). The pH of the brine is ~10 slightly more alkaline than that measured in ione of the pan brines (sample SL-7, pH~9.5, Appendix−B, Table 2B) at I=5.5. Though the trend of the evolution of many of the major ions in Figs. 7.9a and 7.9b is similar to that of the Sambhar lake, the ratio of various ions in the brine, calculated based on the model, and those observed in the lake are distinctly different (Table 7.3).

For example, the Na/Alk and Cl/SO_4 measured in the brine is ~ 25 and ~ 11, compared to the calculated values of 1.6 and 3.8, respectively in R.R. based on the H-E model (Table 7.3). The calculated Na/Cl ratio is also quite different from the observed result. Similar results were obtained when the calculation was repeated for the river Mendha water as the initial endmember (Table 7.3). Based on these ratios, it seems that evaporation of pure R.R. and R.M. endmembers cannot produce the chemical composition of the brine observed in the Sambhar lake. Such a discrepancy can be explained in terms of the chemical composition of the endmembers. The lake water is mainly of Na−Cl type whereas in river waters Na, Cl and HCO_3 constitute the dominant components of the total dissolved salts. One approach to obtain better agreement between the calculated and observed chemical composition is to enrich the initial endmember with NaCl, a process which is very likely to occur during the wetting cycle of the lake when halite crust from the lake bed could dissolve. As a test case, Na and Cl contents were increased in the R.R. and R.M. waters by 125 and 120 mmol/l respectively to match the Na and Cl content of lake water initial endmember.

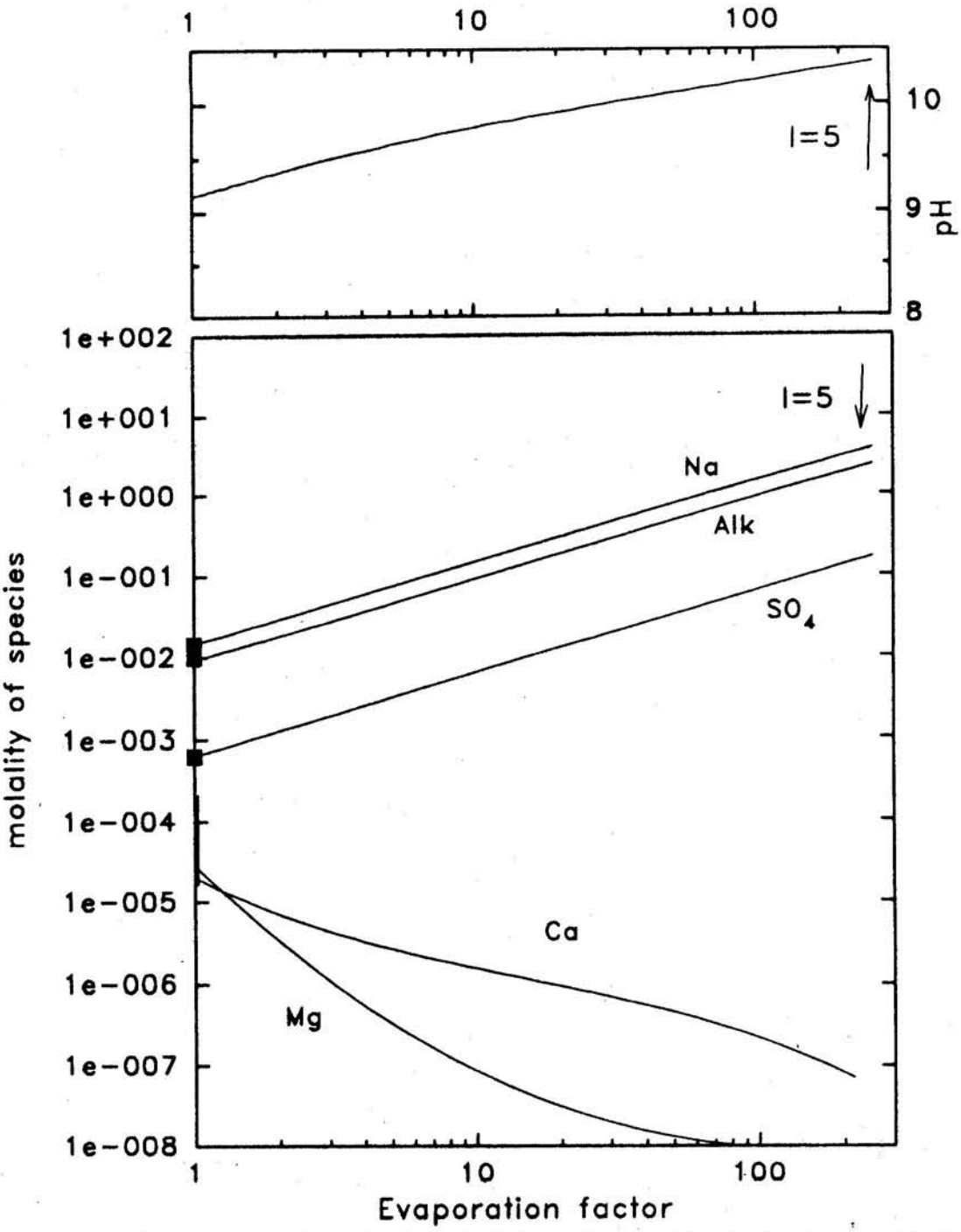

Figure 7.9a The evolution of brine calculated using the Hardie-Eugster model of evaporation for the Roopangarh river water as the initial endmember. The evolution trends of pH, Na, Ca, Mg, Alk and SO_4 is found to be similar with the Sambhar lake water (Fig. 7.8), however, the ion ratios in the calculated brine differ from the lake waters. The model calculation was terminated at ionic strength, I=5.

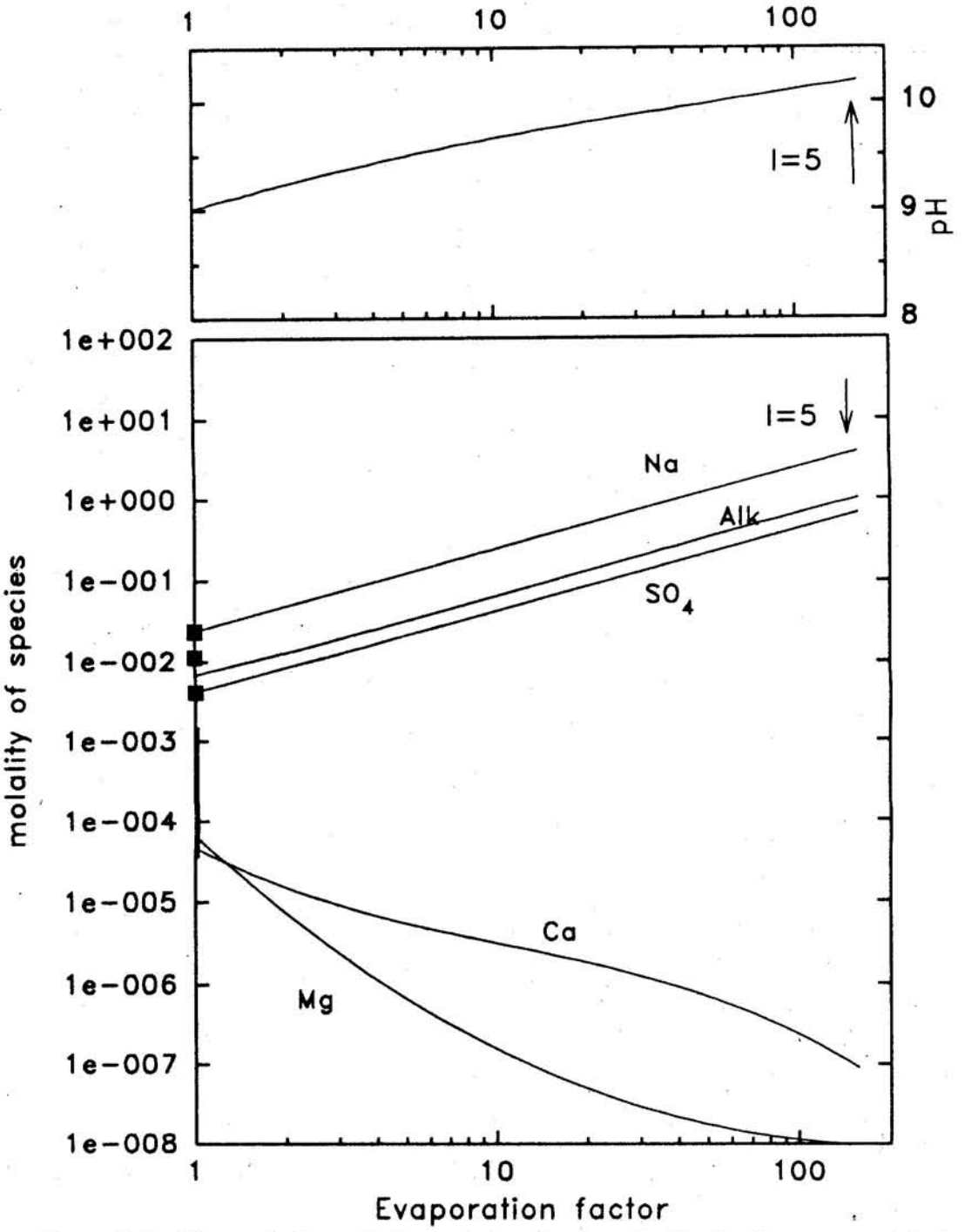

Figure 7.9b The evolution of brine calculated using the Hardie-Eugster model of evaporation for the Mendha river water as the initial endmember. The evolution trends of pH, Na, Ca, Mg, Alk and SO_4 is found to be similar with the Sambhar lake water (Fig. 7.8), however, the ion ratios in the calculated brine differ from the lake waters. The model calculation was terminated at ionic strength, I=5.

Evaporation of these modified river waters resulted in Na-Cl type and alkaline brines (pH of the brine at I=5 found to be 9.9 and 9.8 respectively for R.R. and R.M. waters). The ratios of Na/Alk and Cl/SO_4 in the brines at I=5 are 15.5 and 105 for R.R. and 20 and 14 for R.M. waters. These values are in better agreement with the measured values of the Sambhar lake brine compared to those obtained by evaporating pure R.R. and R.M. waters as the initial endmembers.

The H-E model calculation using a typical groundwater as initial endmember was also done to follow its chemical evolution during evaporation and compare the results with the lake brine. The groundwater chosen for this purpose has Alk/(Ca+Mg) ratio < 1, typical of most of the groundwaters adjacent to the lake (Fig.7.6b). As expected, the calculated brine composition is Na-Cl type but neutral (pH $\sim$7) in character. Based on this result, it appears that evaporation of such groundwaters cannot account for the type of brine available in the lake basin. However, mixing of river and groundwaters (e.g. 80% R.R. + 20% groundwater, Table 7.2) can produce a resultant water with Alk/(Ca + Mg) >1, which can produce an alkaline brine on evaporation. Such a brine also differs from the observed lake brine in terms of Na/Cl, Na/Alk and Cl/SO_4 ratios.

The above calculations, therefore, suggest that it is difficult to account for the observed chemical composition and ion ratios by evaporating pure initial river and groundwater endmembers for the region. Important processes governing the Sambhar lake brine evolution is the recycling of salt during the recharge period from the salt encrustation in the lake bed followed by the mineral precipitation such as the calcite and sepiolite or dolomite during evaporation. The recycling of salt from lake basin during recharge period is also evidenced from the low Na/Cl ratio (as discussed earlier) and low U/TDS ratio which will be discussed in the next section.

Another approach to identify the freshwater endmember for evolution of Sambhar lake brine can be made by studying the behaviour of major solutes (i.e Na and Cl) after halite saturation. The major ion Na shows a significant increase in its concentration with respect to the Cl both in lake and pan waters after halite saturation (Figs. 7.10a and 7.10b). Such an increase in Na over Cl provides a clue to the brines parent water composition with Na/Cl ratio > 1 based on the concept of "Chemical divide" (Drever, 1988).

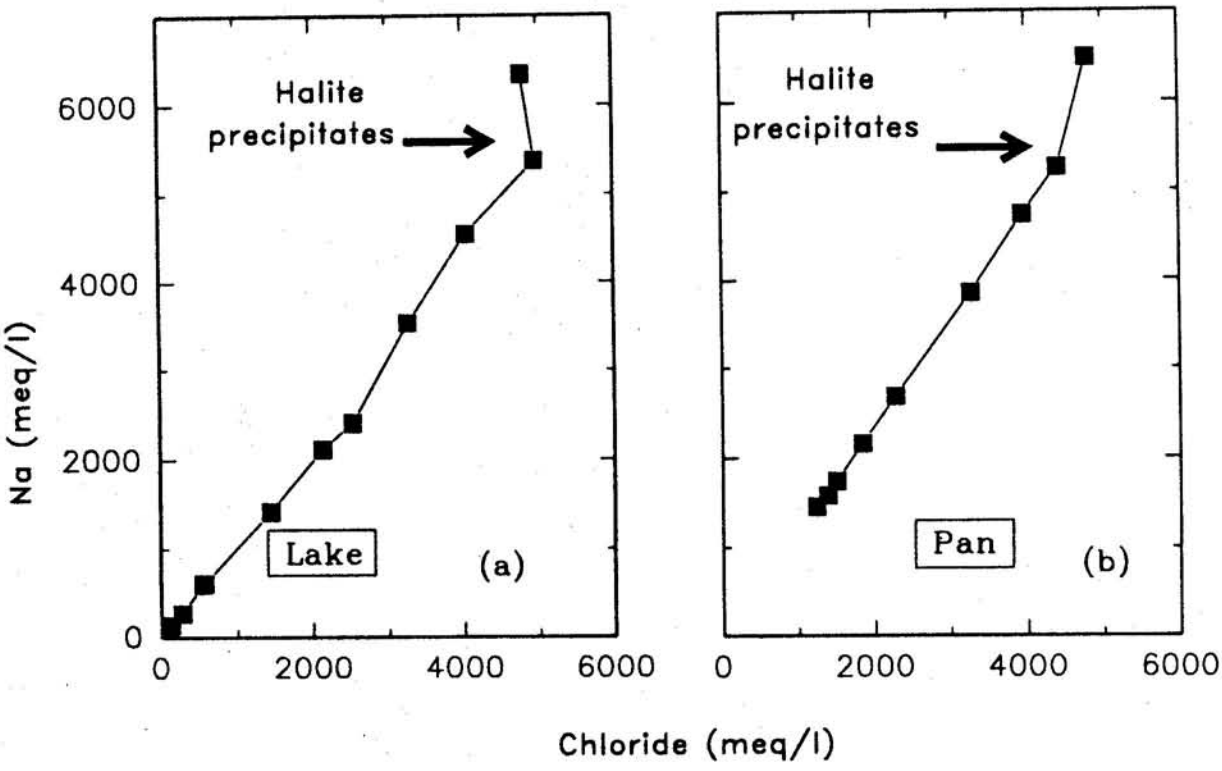

Figures 7.10a and 7.10b: Variation in the abundances of Na as a function of chloride during evaporation of the lake and pan waters, a major change in trend is seen beyond halite crystallization stage.

According to the chemical divide concept, Na concentration should increase relatively with respect to chloride after halite saturation for the initial water composition having Na/Cl ratio >1. In fact, Na concentration should increase followed by a decrease in Cl concentration after the the halite crystallization so that ion activity product of NaCl remains constant. Such an indication is seen only with the lake waters (Fig. 7.10a). In pan waters, decrease in Cl concentration after halite saturation is not observed which could be due to limited data. In order to observe the above trend, more number of samples are required to be analyzed after the halite crystallization. It was observed that the lake waters immediately after monsoon season had an average Na/Cl ratio of 1.08 (Table 7.1). Considering average Na/Cl ratio in all freshwater endmembers, it is found that only river waters do have Na/Cl ratio >1 and groundwaters have this ratio $\sim$ 1 (Table 7.1). Therefore, groundwaters alone cannot be considered as the initial endmember for the evolution of Sambhar lake brine. With these results, it is apparent that a multiple

component of waters viz. river waters, groundwaters and rainwaters can be considered for the Sambhar lake brine evolution.

The TDS content of the sub-surface brines over an annual evaporation cycle ranges between 40–270 g/l (Table 7.1). A range of TDS, 40 to 240 g/l, observed in sub-surface brines during Oct 92 (soon after monsoon) could be attributed to non-uniform mixing of meteoric waters. This observation is consistent with the $\delta^{18}O$ results observed during the same season. Similar to lake waters, both Na and Cl are the major ions, accounts for nearly 90% of the TDS and average Na/Cl ratio is 1.2 (Table 7.1). Among the sub-surface brines a striking difference in Alk and (Ca,Mg) concentrations has been observed in few samples collected from Khakarki along the periphery of lake. The Alk in these samples is lower and (Ca,Mg) concentrations are higher by about one and three orders of magnitude respectively compared to that from the lake bed. In addition to the major ion differences, the $\delta^{18}O$ is also unusually -1.12 and $1.45\ ^{o}/_{oo}$ in these two samples which were collected during winter season (Feb 93). The relatively depleted $\delta^{18}O$ in these samples reflect possibly influence of mixing of the adjacent groundwaters with the sub-surface brines. The above results, therefore, indicate that some of the sub-surface brines are chemically and isotopically different from those mainly available at salt producing sites.

7.2.2 Aqueous mineral equilibria

As discussed earlier, mineral precipitation in evaporating waters governs the brines evolutionary path. The identification of authigenic minerals in solid phase such as the lake's sediment would provide information about the minerals controlling the brines evolution. However, among the Mg-minerals e.g. dolomite, smectite and sepiolite all have similar effects on alkalinity of the evolving brine from evaporation of freshwater endmember (Drever,1988). The minerals precipitating from waters to solid phase can be judged from their positive saturation indices (SI) in waters and their actual presence in the solid phase. The calculation of SI for the common minerals and their identification in solid phase such as the sediments and bitteren crust have been made in this study, as mentioned below.

The saturation state of various minerals present in all water types analyzed in this study is calculated based on ion activity product of the individual ions. In this context, the SI of the mineral is defined by log(IAP/K), where IAP is the ion activity product

and K is the equilibrium constant of the mineral concerned. The Debye–Huckel relation was used for all freshwater samples (river waters and groundwaters) and a computer program PHRQPITZ (Plummer et al,1988) especially designed for brines calculation was used for all saline water samples (TDS > 70 g/l). The PHRQPITZ has incorporated thermodynamic data base of Harvie and Weare (1980) and Harvie et al (1984), and takes care of the effects of ion pairing and complex ion formations. All the water types viz. river waters, groundwaters, lake waters and sub-surface brines are found to be supersaturated with respect to calcite and dolomite minerals but undersaturated with gypsum (Table 7.4).

Table 7.4 Saturation index (SI) of a few common minerals in various water reservoirs in and around the Sambhar lake

Water type	SI(Calcite)	SI(dolomite)	SI(gypsum)
River water	0.89–1.89	2.29–4.39	-(3.33–1.69)
Groundwater	0.74–2.29	1.94–6.82	-(2.77–0.86)
Lake water	0.54–1.04	0.70–2.73	-(3.47–2.05)
Sub-surface brine	0.02–1.04	0.70–2.73	-(3.47–2.05)

X-ray diffraction (XRD) analysis was done on the sediment sample from the lake bed and the bittern crust to substantiate some of the minerals crystallizing from evaporating lake water. The XRD results for sediments confirm the presence of calcite and dolomite minerals, however, there is no indication of these minerals in bittern crust. Such an observation indicates that Ca-Mg minerals are precipitated out from the lake waters during early stage of evaporation and hence they cannot be identified in the last stage of brine i.e. the bittern crust. The bittern crust sample showed the presence of carbonate and sulphate minerals besides halite such as trona ($Na_2CO_3 \cdot NaHCO_3 \cdot 2H_2O$), thenardite ($Na_2SO_4$) and burkeite ($2\ Na_2SO_4 \cdot Na_2CO_3$). Except halite none of these minerals have been found to be saturated in the brine (Table 7.5). It could be possible that these minerals precipitate from the brines during much later evaporation stage. A conclusion can be made based on aqueous mineral equilibria that since all water bodies in and around the Sambhar lake are supersaturated with respect to calcite and dolomite minerals, it implies essentially similar

weathering environment.

Table: 7.5 Saturation states of minerals in a Sambhar lake brine sample

SL-3 pH=9.48 Ion strength= 7.66	
	SI†
Aragonite ($CaCO_3$)	0.35
Burkeite ($2\ Na_2\ SO_4 \cdot Na_2CO_3$)	−0.84
Calcite ($CaCO_3$)	0.54
Dolomite ($CaCO_3 \cdot MgCO_3$)	1.97
Gaylussite ($Na_2CO_3 \cdot CaCO_3 \cdot 5\ H_2O$)	0.22
Gypsum ($CaSO_4 \cdot 2\ H_2O$)	−3.32
Halite ($NaCl$)	0.01
Magnesite $MgCO_3$)	0.59
Mirabilite ($Na_2\ SO_4 \cdot 10\ H_2O$)	−0.54
Nahcolite ($NaHCO_3$)	−0.25
Pirssonite ($Na_2CO_3 \cdot CaCO_3 \cdot 2\ H_2O$)	0.42
Trona ($Na_2CO_3 \cdot NaHCO_3 \cdot 2\ H_2O$)	−0.55

†SI is the saturation index of minerals

Synthesis

In this study an attempt has been made to assess the importance of various sources of salt to the present-day Sambhar lake and also model the evolution of the lake brine based on the evaporation of inflow river and groundwaters. Analysis of rainwater from the region shows that the atmospheric precipitation is only a minor contributor of salt to the lake basin, it only accounts for $\sim$ 3% of the current industrial salt production and less than 1% of the standing crop in the lake following recharge. The chemical analysis of river

and groundwaters from the region are quite saline indicating the general preponderance of evaporite minerals like halite in the area. The evolution of the chemical composition of the Sambhar lake brine during annual cycle of wetting and drying was studied by model simulation using the Hardie-Eugster model. Towards this, several initial endmember waters were evaporated based on the model and their chemical composition compared with those measured in the lake during different seasons. The results show that the evaporative enrichment of lake water collected immediately after the monsoon by and large agrees with the observed chemistry through the annual cycle. The evaporative enrichment of the river and groundwaters though yield brines, their chemical composition and ion ratios differ significantly from the measured values. This suggests that evaporation of pure river and groundwater endmembers cannot produce the observed chemistry of the Sambhar lake brines. Mixing of the river and groundwaters with NaCl (a process likely to occur during wetting cycle of the lake in which salt encrustation would dissolve from the lake bed in the recharging water) and evaporating the mixture water, yields brines whose chemical compositions are in better agreement with those measured. During evaporation of the initial endmember of lake waters viz. river and groundwaters showed saturation with calcite and sepiolite minerals. The presence of some of these minerals such as calcite and dolomite have been identified in the lake sediments. This reaffirms the brine alkaline evolutioary path for the Sambhar lake brine evolution which is consistent the model predicted results.

7.3 Uranium isotopes

Isotopes of uranium (^{238}U, ^{238}U) were measured in the various reservoirs of the Sambhar lake region with a view to understand their geochemical behaviour over a wide range of salinities and also to use uranium as a tracer to infer on the source of salt to the lake. It has been well documented that in oxidizing surface and sub-surface waters ^{238}U is a ubiquitous trace constituent, its mobility being governed primarily by its tendency to form soluble complex ions such as $[UO_2(CO_3)_3]^{4-}$ (Osmond and Cowart,1976). Also, during chemical weathering ^{234}U is fractionated from its parent ^{238}U due to α-recoil effects. This is reflected in the $^{234}U/^{238}U$ activity ratio greater than unity in surface and sub-surface

waters.

The Sambhar lake, its adjacent groundwaters and river waters can be characterized based on ^{238}U abundance in much the same way as was done based on the major ion composition. Both ^{238}U content and $^{234}U/^{238}U$ ratio in the river waters (from Mendha and Roopangarh) and groundwaters exhibit a wide range. The concentration of U and the $^{234}U/^{238}U$ activity ratio in groundwaters range from 3.6 to 71.6 ppb and 1.15 to 1.98, respectively (Table 7.6). The uranium concentration in groundwaters is similar to those reported by Baskaran et al (1986) from the same region.

Table 7.6: U, Ra abundances and $^{234}U/^{238}U$, $^{228}Ra/^{226}Ra$ and $^{210}Po/^{210}Pb$ activity ratios

Water Type	^{238}U Range (ppb)	$^{234}U/^{238}U$ AR@	U/TDS $\mu g\ g^{-1}$	^{226}Ra† $dpm.g^{-1}$	$^{228}Ra/^{226}Ra$ AR	$^{210}Po/^{210}Pb$ AR
River water	12–103	(1.33–2.26)	14–69	(0.11–0.54)	(1–6)	-
Groundwater	3–72	(1.15–1.98)	3–11	(0.11–1.8)	(0.6–2.6)	(0.08–0.73)
Lake water	8–1117	1.64*	0.7–4	$(1.8–6.2)\times10^{-3}$	(2–3)	(1.2–3.0)
Pan water	200–1200	1.62*	3–6	$(1.5–6)\times10^{-3}$	(1.6–2)	2
Sub-surface brine	10–600	1.62**	.05–5	$(4–9.5)\times10^{-3}$	(2–3)	(0.50–0.90)

@ AR is the activity ratio
† concentration normalized to TDS
* average over the annual cycle
** average of several brines

The ^{238}U concentration as a function of TDS for the groundwaters sampled during Feb 92 and Oct 93 is plotted in Fig. 7.11a. The results show a linear trend between U abundance and TDS. Such a trend can be interpreted in terms of a two component mixing - one endmember having low U and low salt content and the other having high U concentration and high TDS. This mixing trend is also evident from the plot of reciprocal concentration of U and $^{234}U/^{238}U$ activity ratio (Fig. 7.11b). A similar mixing trend is observed, though not conclusive, based on the $\delta^{18}O$ and salt content of the groundwaters.

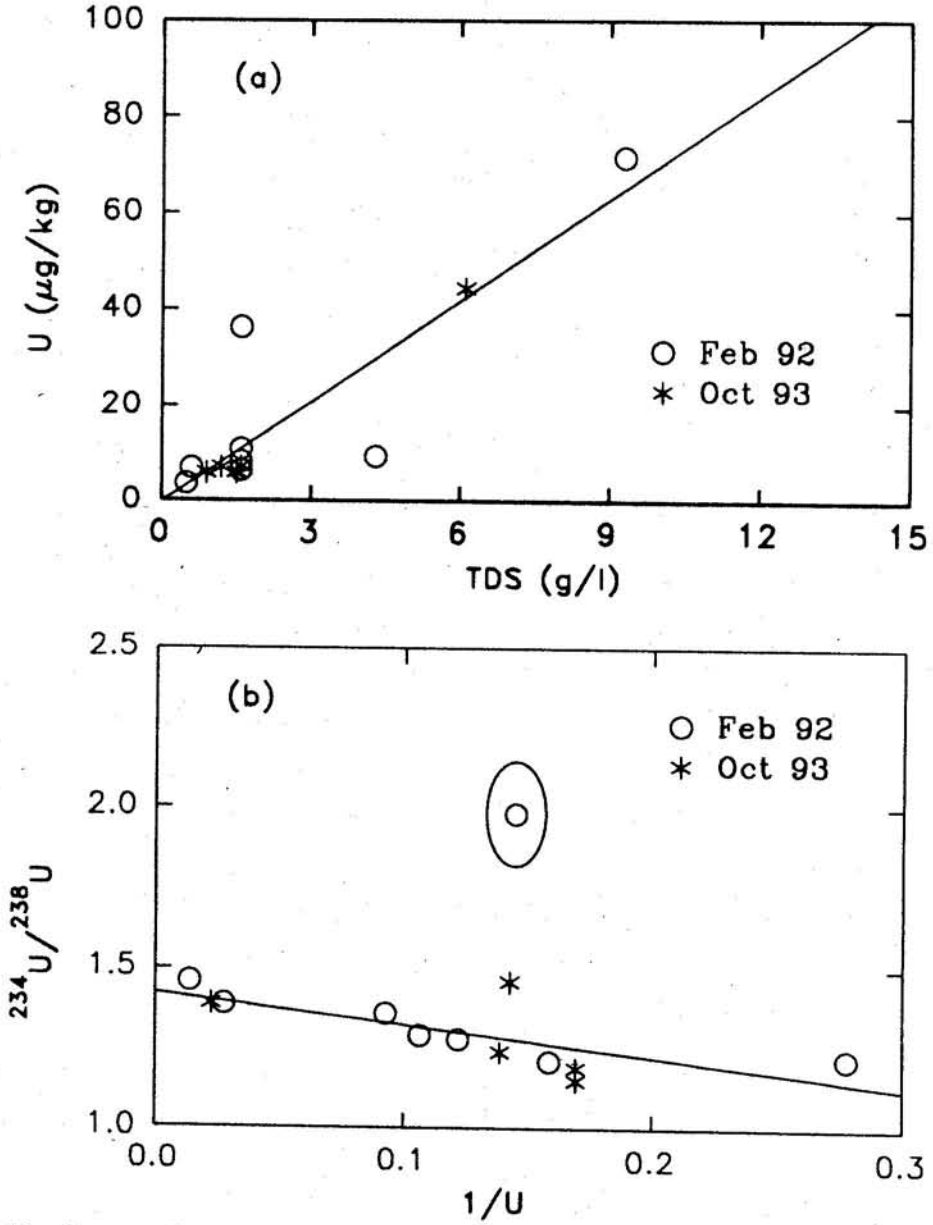

Fig. 7.11a Scatter diagram of uranium concentration and salt content (TDS) in groundwater samples collected during Feb 92 and Oct 93. A linear trend between them is evident. Such relationship can be interpreted in terms of a two component mixing. This inference is also attested by the linear trend between $^{234}U/^{238}U$ and 1/U in Fig. 7.11b., The plot in Fig. 7.11b has been drawn according to Osmond et al,1974, and Osmond and Cowart,1976. The regression line in Fig. 7.11b excludes one encircled data point.

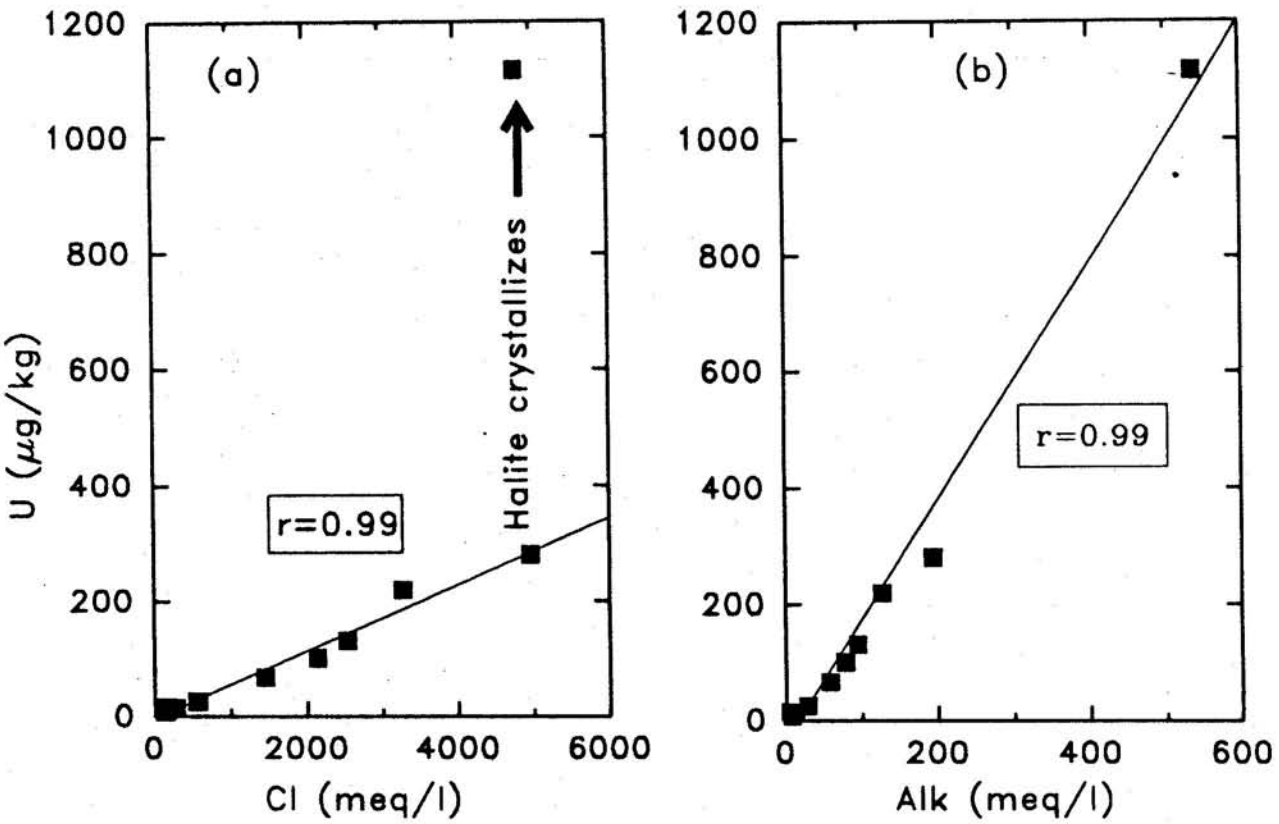

Figures 7.12a and 7.12b: Scatter diagrams of U vs. Cl and U vs. Alk in the Sambhar lake. In Figure 7.12a best fit line has been drawn excluding the data point which corresponds to halite crystallization stage. A strong positive correlation between U and Cl, Alk indicates that U behaves conservative in the lake upto a stage just before the halite crystallization.

In contrast to the groundwaters and river waters, the Sambhar lake waters are characterized by a uniform $^{234}U/^{238}U$ activity ratio, centering around 1.64 (Table 7.6), though the abundance of uranium varies over nearly two orders of magnitude (9−1117 ppb) over the annual cycle. The lowest uranium concentration was measured in samples collected during Oct 92 just after the monsoon season and highest concentration in sample taken during the summer months (May 93). A nearly uniform activity ratio of $^{234}U/^{238}U$ with the large variation in concentration of uranium suggests that behaviour of uranium in lake is influenced by dilution and evaporation processes. This inference is further supported by variation in uranium concentration with Cl and Alk over the annual cycle of evaporation (Fig. 7.12). Both Cl and Alk show a strong positive correlation with the U abundance in the lake basin indicating that their increasing trend is mainly controlled by a common

process of evaporation. In Fig. 7.12a, it is noteworthy that when lake waters reach halite saturation, the U/Cl ratio increases sharply. The information on halite saturation is obtained through the NaCl crystals observed during the brine sampling. The high uranium concentration in residual brine after halite crystallization indicates that U is preferentially retained in the aqueous phase and its concentration rises due to evaporative enrichment.

A unique feature of the Sambhar lake water and sub-surface brine is that both are characterized by the uniform $^{234}U/^{238}U$ activity ratio of 1.62±0.02. This activity ratio is intermediate between the values for the river and groundwater samples (Table 7.6). Such an observation, therefore, suggests that U in the lake basin is derived from the local drainage area and then being recycled within the lake basin. An attempt to derive information on mixing of lake waters with the sub-surface brines using the U isotopes could not be successful because of the constant $^{234}U/^{238}U$ activity ratio (as mentioned above) unlike the inference drawn from the oxygen isotopes.

7.3.1 U–TDS relation: Implication of source of salt to the lake basin

The U concentration in the lake immediately after monsoon is 9 ppb which steadily increases to a value of 1117 ppb during summer. A linear relation exists between U concentration and TDS in the lake (U/TDS ratio ~1.0 μg/g) until the latter reaches a value of 327 g/l after which at TDS of about 360 g/l NaCl begins to precipitate (Fig. 7.13). These results suggest that U concentration and TDS in lake water are intimately coupled and modified only at and beyond halite saturation. It is to be noted that the U/TDS ratio of ~1 μg/g has been observed in lake waters and many sub-surface brine samples which constitute a major source for the current salt production from the lake basin. The U–TDS relation in lake waters has an important bearing on the source of salt to the Sambhar lake. It has been suggested that atmospheric transport and salt deposition from the Rann of Kutch is a source of salt to the lake basin (Holland and Christie, 1909). Results obtained on the U–TDS relation and constancy of the uranium activity ratio during the evaporation cycle suggest that marine aerosols are not an important source of U (and hence salt) to the Sambhar lake.

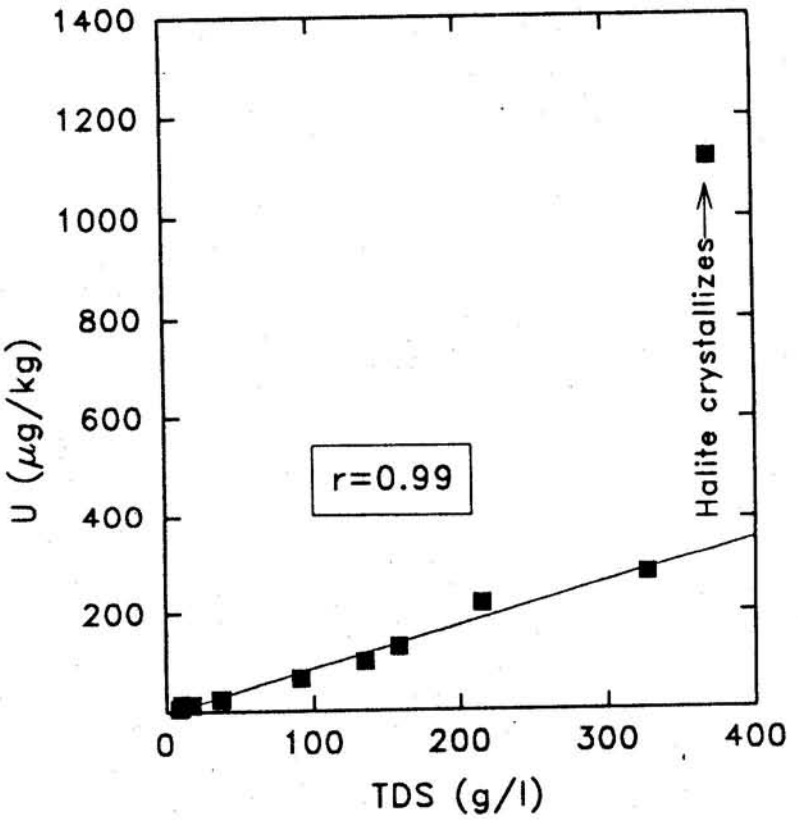

Fig. 7.13 Concentration of uranium in lake waters as a function of salt content (TDS) (i.e. temporal evolution). A strong positive correlation between concentration of uranium and TDS is observed throughout, except during the final stage when halite precipitation occurs. The correlation coefficient (r=0.99) shown is for all the sample points except the one which refers to halite precipitation stage.

If the marine aerosols are not fractionated between uranium and salt, then this result would imply that marine aerosols are not a major source of salt to the Sambhar lake. This is because seawater is characterized by a U/TDS ratio ($\sim$0.1 μg/g) and $^{234}U/^{238}U$ activity ratio of 1.14$\pm$0.02 (Ku et al,1977; Chen et al,1986), which are distinctly lower than the U/TDS of $\sim$1 and $^{234}U/^{238}U$ of 1.64 in the Sambhar lake. Therefore, if seasalt is a major contributor of U to the lake, it would have reduced U/TDS and $^{234}U/^{238}U$ ratio of the lake water. As this is not observed, it is concluded that the marine aerosols from the Gulf of Kutch are not a major source of U and hence salt to the Sambhar lake. The uranium is probably derived from the weathering of Aravalli granites and schists. The $^{234}U/^{238}U$ activity ratio in Sabarmati river basin which drains through Aravalli is 1.59$\pm$0.01 (Borole et al,1979), very similar to that of the Sambhar lake brines.

7.3.2 Fate of uranium in the Sambhar lake

In order to study the fate of uranium in the lake basin, it is essential to know its geochemical behaviour in Sambhar lake waters during evaporation and its association with the end product of the brine i.e. the liquid bittern. It has been discussed above that U in Sambhar lake waters is conservative and its distribution is governed predominantly by dilution/evaporation processes during annual wetting and drying cycle. The high U concentration in lake/pan brines during late stage of evaporation (Figs. 7.12 and 7.13) suggests that U is retained in the aqueous phase. The uranium concentration in bittern (residual brine after halite recovery) is observed to be $\sim$ 3000 μg/l (see Appendix–B, Table 2B) which is about two orders of magnitude higher than the initial lake water value. In an earlier study, Baskaran et al (1986) reported trace concentration of uranium ($\sim$ 0.04 ppb) in the sambhar lake NaCl samples which further supports preferential retention of U in liquid phase of the brine. These results, therefore, indicate that U is not being removed from the lake waters. during the salt production. The concentration of uranium in lake waters was found to be 8.8 μg/l when lake had water depth of 1 meter. Assuming the lake area of about 225 km^2 and 1 m water depth, the amount of uranium recycling in the lake basin is estimated to be 1.98 tons which is consistent with that reported by Baskaran et al (1986).

The present day U/TDS ratio (in μg/g) of lake waters during most of the seasons is $\sim$ 1, which is significantly lower than those measured in the river waters and groundwaters, typically $\sim$ 20 and $\sim$ 5 respectively (Table 7.6). This observation suggests that the U/TDS ratio in the lake is mainly dominated by recycling of the salt from the lake bed during recharge period. Considering the dilution effect on U/TDS ratio due to recycling of the salt, it can be estimated that nearly 95% of the salt is to be added from lake itself in order to bring down the ratio from about 20 (observed in river water) to 1. Such an estimate is consistent with that calculated for the low Na/Cl ratio in lake water compared to the high value in river waters.

7.4 Ra, ^{210}Po and ^{210}Pb nuclides

Studies on the geochemical behaviour of natural radionuclides in sub-surface medium have direct relevance to the management and storage of nuclear wastes. The daughter nuclides of the U-Th series provide useful information of their residence times and retardation characteristics of the aquifer medium. Because of different geochemical properties and varying half lives, the daughter nuclides of the U-Th series serve as in-situ indicators of chemical behaviours for other fission product nuclides injected into the medium. The measurement of Ra, Po and Pb in freshwater and brines from the Sambhar lake region provides opportunity to study their behaviours over wide range of salinities. The concentration of ^{226}Ra in the freshwaters viz. river and groundwaters range between 0.10 to 1.32 dpm/kg which are within the range reported for potable waters from other regions (Hussain,1983). The ^{226}Ra concentration in the pan brines centers around a value of about 0.5 dpm/kg and is nearly independent of salinity in the range $\sim$ 100–400 g/l.

The concentration of ^{226}Ra (normalized to TDS) in groundwaters and river waters ranges from 0.1 to 1.8 dpm/g (Table 7.6), which is about two orders of magnitude higher than that observed in the lake, evaporating pans and sub-surface brines. A possible cause for the low Ra/TDS ratio in the lake and associated brines is that Ra is removed in early stage of brine evolution through co-precipitation with Ca-Mg minerals and during subsequent evaporation (as seen in pan waters) it saturates probably due to equilibration with clay minerals (Fig. 7.14a). The near constancy of Ra concentration over wide range of TDS for the pan waters differ from the trend reported in earlier studies where it showed general increase in concentration with TDS (Kraemer and Reid,1984; Krishnaswami et al,1991). Therefore, in view of the present results, it is suggested that radium may not necessarily show a linear relation with the salt content in chloride brines. The fate of radium in the brine probably depends on the presence of Ca and Mg ions which are controlled by mineral precipitation as discussed in the previous section. The other controlling factor of Ra in solution is the ion-exchange process between the dissolved ions and the clay minerals (Kraemer and Reid,1984). Since all waters in and around the Sambhar lake are saturated with respect to calcite and dolomite minerals, it could be possible that Ra nuclides got removed in the early stage of brine evolution along with the Ca-Mg minerals.

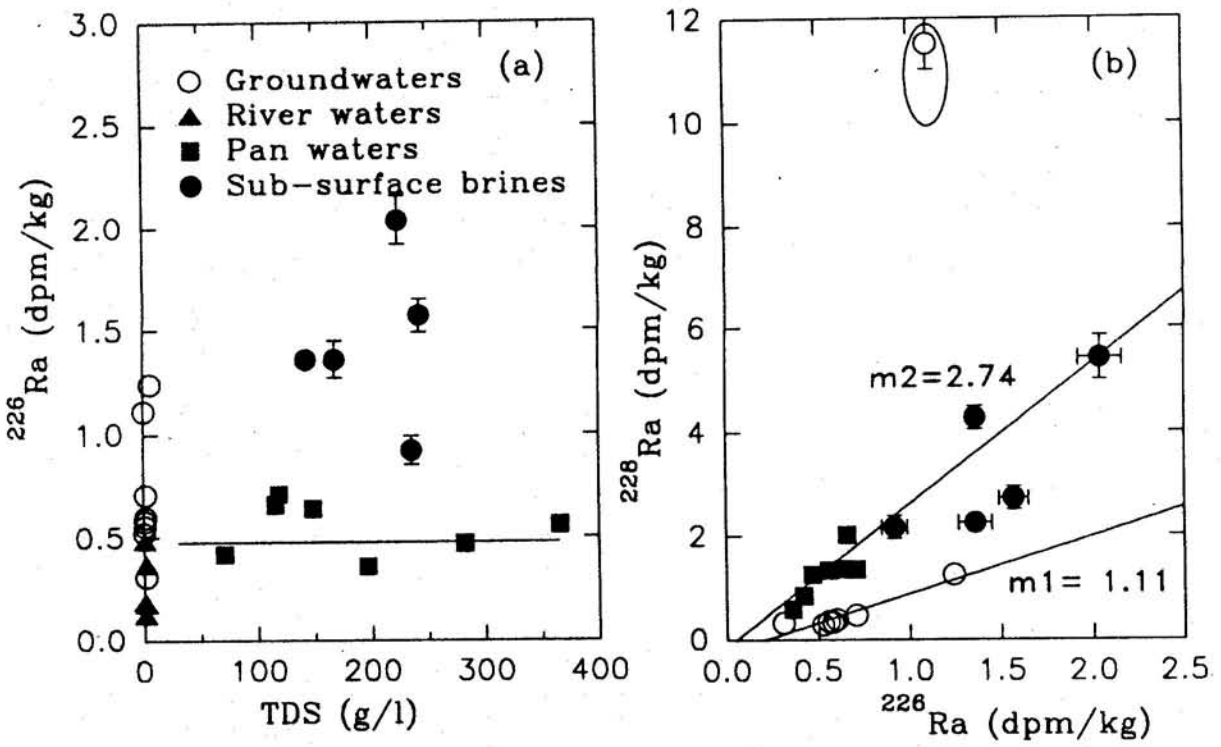

Fig. 7.14a shows relation between radium isotope and the salt content. Despite increase in salt content the radium concentration saturates as shown by an 'eye fit' line implying that the latter possibly equilibrates with the clay minerals. Fig.7.14b indicates a significant positive relation between two radium isotopes although they are supported by different parent nuclides. The slope of the best fit lines through groundwaters (m1) and brines (m2) provides the $^{228}Ra/^{226}Ra$ activity ratio 1.11 and 2.74 respectively.

Since Ra (^{226,228}Ra) is brought into solution by chemical weathering of rocks and α-recoil effects during radioactive decay of their respective parents. A good correlation ($r\sim 0.9$) between ^{226}Ra and ^{228}Ra isotopes has been found (although they are radiogenically supported by different parent nuclides) in both brines and groundwater samples (Fig. 7.14b). The slope of the best fit line for the brine is 2.74 whereas for the groundwaters the slope is 1.11. This indicates that the $^{228}Ra/^{226}Ra$ ratio in these two systems are controlled by different mechanisms. The $^{228}Ra/^{226}Ra$ based on the Th/U weight ratio in soil cores from the region centers around 1.5 (Baskaran et al,1986). Comparing this ratio with that obtained for the brines and groundwaters, it is evident that the Ra isotopes in groundwa-

ters are simply controlled by leaching of the aquifer grains whereas in brines abundance of ^{228}Ra is more than the expected value which could be due to its preferential leaching in high alkaline condition or due to increased α recoil effects. Further study is required to understand the exact mechanism for the high $^{228}Ra/^{226}Ra$ ratio in the brine. As ^{224}Ra is not measured in various waters, it is difficult to determine the adsorption-desorption characteristics of the nuclides in the aquifer medium (Krishnaswami et al,1982,1991). It is interesting to note that in the Sambhar lake brines, ^{226}Ra abundance is very low which is attributed to removal through mineral precipitation in early stage of brine evolution. If these minerals be identified and separated out from the sediments, then it may be possible to use ^{226}Ra as a chronometer tracer.

The $^{210}Po/^{210}Pb$ activity ratio in groundwaters from open wells is far less than 1 (observed range is: 0.08–0.73, Table 7.6) indicating preferential removal of ^{210}Po on to particulates. Such an observation is typical of the ^{210}Po and ^{210}Pb systematics in groundwater regimes (Krishnaswami et al,1982; Simpson et al,1982; Dickson and Herczeg,1992). However, in the lake and evaporating pan waters, the $^{210}Po/^{210}Pb$ ratio is greater than 1 (ranges from 1.2 to 3.0, Table 7.6) which is unlike of the most of the natural waters. This can result from preferential complexation and retention of ^{210}Po in lake/pan waters by algae, being abundant in these waters. In order to understand the role played by algae in complexing ^{210}Po and ^{210}Pb nuclides in these waters, their temporal variations in concentrations of particulate and dissolved phases are required to be known. The sub-surface brines have $^{210}Po/^{210}Pb$ activity ratio close to equilibrium value which suggest that the reactivity of both the nuclides are similar in this environment.

Synthesis

Studies on U($^{238,234}U$), Ra ($^{226,228}Ra$), ^{210}Po and ^{210}Pb show that U is generally conservative in lake waters over the annual cycle of evaporation; low concentration of Ra/TDS (by about two orders of magnitude) in brines compared to the groundwaters and river waters suggests that Ra isotopes are being removed along with the Ca-Mg minerals in early stage of evaporation and in later stage they saturate probably due to exchange with the clay minerals. The U/TDS ratio in lake waters ($\sim$ 1 μg/g) remains almost constant during the annual cycle of evaporation. Such an observation suggests that U and salt

in the lake are are intimately coupled. It has an important implication to the source of salt in the lake basin. The hypothesis that source of salt to the lake by aeolian transport of marine aerosol particles from the Gulf of Kutch can be ruled out since seawater is characterized by U/TDS ratio $\sim$ 0.1. This is further substantiated if $^{234}U/^{238}U$ activity ratio in lake waters (1.64) is compared with the seawater (1.14$\pm$0.02). The source of salt to the lake by aeolian transport of marine aerosol particles requires that the U/TDS and $^{234}U/^{238}U$ activity ratio in lake waters should reduce to lower side over the annual evaporation period. Furthermore, both these ratios indicate that U and salt in lake basin is continentally derived. When comparison is made for U/TDS ratio (μg/g) among lake waters, adjacent groundwaters (range: 3 to 11) and inflow river waters (range: 14 to 69) it is clear that neither salt nor U is added significantly to the lake either from surface run-off or from the groundwater discharge. This demonstrates that U and salt in the lake basin are self-sustained in the present-day hydrologic set-up.

The distribution of ^{210}Po and ^{210}Pb in various water reservoirs of the lake area indicates their differential behaviours in terms of the particle reactivity. In groundwaters, the $^{210}Po/^{210}Pb$ activity ratio is far less than one which is typical of the groundwater regimes. This indicates that ^{210}Po is removed preferentially onto particulates or on the aquifer grains. However, in sub-surface brines their particle reactivity seems to be equal as they are characterized by $^{210}Po/^{210}$ activity ratio nearly one. However, in lake and evaporating pans the ^{210}Po is retained preferentially over the ^{210}Pb by algae showing $^{210}Po/^{210}Pb$ activity ratio > 1.

Chapter 8

Summary and Conclusions

Summary

This study evaluates relationship among various water reservoirs of the Sambhar lake in terms of their chemical and isotopic composition. In addition, the evolution of brine from evaporation of various initial endmembers of the lake has been studied following the concept of Hardie-Eugster model. The results on $\delta^{18}O$, major ions and radionuclides in lake, atmospheric precipitation, river waters, groundwaters and sub-surface brines are summarized below:

(i) The $\delta^{18}O$ content of the lake and groundwaters sampled during the recharge period overlaps with that of local precipitation (-6.4 to -3.2 $^{o}/_{oo}$) suggesting that oxygen isotopic composition of these reservoirs is dominated by atmospheric precipitation. The annual oxygen isotopic evolution in lake waters is of Rayleigh type and model calculations suggest that isotopically light atmospheric water vapour with $\delta^{18}O$ of about -20 $^{o}/_{oo}$ controls the evolution trend through back condensation during pre and post monsoon months. The $\delta^{18}O$ in sub-surface brines shows a linear increasing trend with TDS which is interpreted in terms of a two component mixing.

(ii) The chemical composition of the Sambhar lake brines and adjacent groundwaters is of Na–Cl type as they constitute more than 70% of the TDS (total dissolved solids). The general dominance of NaCl in the various water reservoirs of the region points to the presence of halite minerals in the drainage basin. Based on NaCl concentration in local rain water, an estimate of the upper limit of salt depositing over whole of the catchment area ($\sim$5600 km^2) of the lake through atmospheric precipitation, is $\sim$5000

tons. This estimated amount of salt is less than 1% of the salt inventory present the lake ($\sim 10^6$ tons). Furthermore, study of uranium isotopes in the lake at different stages of annual evaporation suggests that U/TDS (1 μg/g) and $^{234}U/^{238}U$ (1.65±0.03) ratios remain almost constant indicating that neither U nor salt is added significantly to the system by atmospheric transport of salt-laden marine aerosols. (Otherwise, U/TDS and $^{234}U/^{238}U$ ratios would have been reduced since seawater is characterized by U/TDS and $^{234}U/^{238}U$ ratios of 0.1 μg/g and 1.15±0.02 respectively). These results, therefore, discard the hypothesis for the source of salt to the lake through atmospheric transport by the marine aerosols from the Gulf of Kutch.

(iii) Studies on the evolution of the chemical composition of the Sambhar lake brine based on the Hardie-Eugster model and using dilute lake water as the initial endmember, yields brines with composition similar to that measured in the lake in terms of its alkalinity and major ions. The evaporation of pure river water endmember does not produce brine similar to that of the lake brine. The difference lies with the Na/Cl, Na/Alk and Cl/SO_4 ratios. However, one common observation is that the use of dilute lake water and river waters as initial endmembers produce brines which follow an alkaline path (pH increases increases from 8 to about 10). The difference in ion ratios observed in the lake brine and in the calculated brine from the river water evaporation is attributed to recycling of salt from the lake basin during recharge period. The chemical composition of most of the groundwaters in terms of their concentrations for Ca, Mg and alkalinity favours the neutral path of brine evolution following the Hardie-Eugster model. Such brines are neutral contrary to that of the major pool of alkaline brine found in the Sambhar lake. Thus, groundwaters alone cannot account for the chemistry of brines observed in the lake.

(iv) All Sambhar lake water systems viz. river waters, groundwaters, lake waters and sub-surface brines are supersaturated with respect to calcite and dolomite minerals. XRD results showed the presence of calcite and dolomite minerals in the lake sediments which is consistent with the calculated saturation index for these minerals.

(v) The Na/Cl and U/TDS ratios of the river waters differ from those of lake waters. Both these ratios are higher in the river waters compared to the lake. The river waters show an average value of Na/Cl ratio $\sim$ 2.7 and typical U/TDS ratio of $\sim$ 20 μg/g compared to the values of 1.08 and $\sim$1μg/g respectively in the lake. Low Na/Cl and low

U/TDS ratios in the lake compared to the river waters are interpreted in terms of the dilution effect by salt present in the lake basin. An estimate of about 95% of the salt is required to be added from recycling of the salt in the lake basin which can account for the reduction in both Na/Cl and U/TDS ratios of the river waters in the lake. Such an estimate on recycling of the salt is also consistent with that based on the salt input through surface run-off and the total salt inventory of the lake.

(vi) Studies on uranium, radium isotopes, ^{210}Po and ^{210}Pb show that U behaves generally conservative in the lake over the annual cycle of evaporation. Major increase in U/TDS ratio occurs during the late stage of the brine evolution after the halite saturation is reached in the month of May, the peak summer season. Increase in U/TDS ratio beyond halite saturation indicates preferential retention of U in aqueous phase. This aqueous phase gets completely dried up during the summer leaving uranium on the lake bed as a part of salt encrustation. The salt and the uranium becomes available for redissolution during the subsequent wetting period, the monsoon season. Low Ra/TDS ratio (lower by two to three orders of magnitude) in the Sambhar lake brines compared to the groundwaters and river waters suggests that Ra isotopes have been removed since the early stage of brine evolution. Low concentration of Ra is consistent with the low concentrations of Ca and Mg ions in the brine. This indicates removal of radium isotopes probably along with the Ca-Mg minerals. The concentration of ^{226}Ra shows saturation in pan waters in the salinity range of 100 to 370 g/l which is interpreted in terms of equilibration with the clay minerals. Results on ^{210}Po and ^{210}Pb have shown that the former is more efficiently scavenged (onto particulate or aquifer grains) than the latter in groundwaters leading to ^{210}Po/^{210}Pb activity ratio far less than 1. In case of sub-surface brines, these two radionuclides are more or less present in equal activity levels indicating that their reactivities are similar. On the contrary, lake and evaporating pans exhibit ^{210}Po/^{210}Pb activity ratio greater than 1 unlike of many natural waters which has happened due to preferential complexation and retention of ^{210}Po in lake/pan waters by algae.

Conclusions

In the present day hydrologic set-up of the Sambhar lake, the source of water is atmospheric and surface run-off via two major rivers namely Roopangarh and Mendha. The δ^{18}O content of the lake waters during monsoon period (month of July) resembles

very closely to that of the local atmospheric precipitation and groundwaters. Assuming an average depth of 1 m for the lake and average rainfall of 50 cm falling on the lake, the water budget of the lake suggests that one-half of the total lake volume ($\sim 225\times10^9$ ℓ) is contributed by direct precipitation and remaining half by the surface run-off. Based on the NaCl concentration (equivalent of 142 meq/l Cl), the total amount of salt in the lake during Oct 92 is estimated to be $\sim 18.5\times10^5$ tons. Of this, nearly 6% of the salt is transported via river and groundwater sources (based on the geometric mean of Cl concentration 15.8 meq/l for 18 samples). The amount of salt transported through atmospheric precipitation is also relatively insignificant compared to the standing crop of the lake. This illustrates the importance of recycling of salt taking place in the lake basin during recharge period which amounts to nearly 95% of the total salt in the lake. Similar conclusion is also borne out from the low U/TDS ratio measured in the lake water compared to that observed in the river and groundwaters. It is noteworthy that the brine evolution from evaporation of river and groundwater endmembers cannot account for the observed chemical composition of the brine in the lake. Assuming no fractionation between seasalt and uranium, the observed U/TDS and $^{234}U/^{238}U$ activity ratios in the lake brine are significantly different from the seawater values, and hence uranium and salt in the lake basin cannot be coupled to the marine aerosol particles. Thus, the source of salt in the lake via atmospheric transport is limited. Based on these considerations it can, therefore, be concluded that the lake in present day condition is self-sustained and is not influenced significantly by input of salt via atmospheric sources and surface run-off. However, it is quite possible that salt in the lake basin would have formed due to evaporation of a multiple component of source waters viz. river waters, groundwaters and atmospheric precipititaion in the geological past which may explain the resources of salt present in the lake.

Scope of future work

In the present study, water samples from the lake and sub-surface brines were chemically analyzed to arrive at conclusion on their inter-relationships (an indirect method). However, concentration gradients of major ion constituents and isotopic signature of oxygen in interstitial waters of sediment core from the lake during monsoon season may

provide better information of the solute transport and/or water recharge to sub-surface brines. Some of the indirect conclusions e.g. marine vs. nonmarine origin of salt made in the present study can also be verified by the measurement of element B and $\delta^{11}B$ in the lake sediments, lake waters and sub-surface brines (Venghosh et al,1991 and 1992). The distinction between marine and non-marine evaporite deposits in terms of $\delta^{11}B$ lies with its enrichment in marine sediments and seawater relative to the continental crust (boron concentrates in seawater/marine sediments due to isotopic fractionation during its adsorption onto clays). It has been reported that marine evaporite borates are enriched with ^{11}B ($\delta^{11}B$=18 to 31 $^{o}/_{oo}$) relative to non-marine evaporite borates ($\delta^{11}B$=$-$22 to 0 $^{o}/_{oo}$) (Swihart et al,1986). Thus, the issue of marine and non-marine origin of salt in the lake basin can be resolved through the boron isotope measurements.

References

Aggarwal S C (1951) The Sambhar lake salt source, Govt. of India Press, Delhi, pp 365.

Allchin B, Goudie A and Hegde K T M (1978) *The prehistory and paleogeography of the Great Indian desert*, Academic Press, London, pp 370.

Anderson R F, Bacon M P and Brewer P G (1982) Elevated concentrations of actinides in Mono Lake, *Science*, **216**, 514–516.

Baskaran M, Krishnaswami S and Bhandari N (1986) The geochemistry of uranium and thorium isotopes in the salt lakes and adjacent groundwaters of Rajasthan, *J. Geol. Soc. India*, **27**, 90–101.

Bhattacharya B N, Gupta S K, Rishi B P, Mitra A K, and Kashyap V K (1982) Seasonal variation in the composition of Sambhar lake brine and possible origin of its salinity on the salinity problems of the inland lakes of Rajasthan, *Proc. of the workshop on the problems of the deserts in India*, Geol. Surv. of India, Misc. Pub. No. **49**, 80–91.

Biswas R K, Chattopadhyay G S and Sinha Subrata (1982) Some observations on the salinity problems of the inland lakes of Rajasthan, *Proc. of the workshop on the problems of the deserts in India*, Geol. Surv. of India, Misc. Pub. No. **49**, 68–79.

Borole D V, Gupta S K and Krishnaswami S (1979) Uranium isotopic investigations and radiocarbon measurements of river-groundwater systems, Sabarmati basin, Gujarat, India. In: *Isotope Hydrology*, **1**, IAEA.

Bryson R A and Swain A M (1981) Holocene variations of monsoon rainfall in Rajasthan, *Quat. Res.*, **16**, 135–145.

Chen J H, Edward R L and Wasserburg G J (1986) ^{238}U, ^{234}U and ^{232}Th in seawater, *Earth Planet. Sci. Lett.*, **80**, 241–251.

Craig H (1961) Isotopic variations in meteoric waters, *Science*, **133**, 1702.

Craig H and Gordon L I (1965) Deuterium and oxygen-18 variations in the ocean and the marine atmosphere, pp 9–130. In: *Stable isotopes in oceanographic studies and paleotemperatures*, Tongiorgi E (ed.), Consiglio di Geologia Nucleare, Pisa.

Dansgaard W (1964) Stable isotopes in precipitation, *Tellus*, **16**, 436.

Deshmukh G P and Rai V (1991) Some observations on the origin of saline lakes/ranns of Rajasthan, India, *Proc. Quat. landscape of Indian sub-continent*, M S U Baroda (Geology Dept.), 41–47.

Dickson B L and Herczeg A L (1992) Naturally-occurring radionuclides in acid-saline groundwaters around lake Tyrrell, Victoria, *Chem. Geol.*, **96**, 95–114.

Drever J I (1988) Evaporation and Saline waters, pp 232–260. In: *The geochemistry of natural waters*, Printice Hall, Inc., Englewood Cliffs, New Jeresy.

Drever J I and Smith C L (1978) Cyclic wetting and drying of the soil zone as an influence on the chemistry of Groundwater in arid terrains, *Am. J. Sci.*, **278**, 1448–1454.

Epstein S and Mayeda T (1953) Variation of O^{18} content of waters from natural sources, *Geochim. Cosmochim. Acta*, **4**, 213.

Eugster H P (1980) Geochemistry of evaporitic lacustrine deposits, *Ann. Rev. Earth Planet. Sci.*, **8**, 35–63.

Eugster H P and Hardie L A (1978) Saline lakes, pp 237–293. In: *Lakes: Chemistry, Geology, Physics*, A. Lerman(ed.), Springer-Verlag, New York.

Eugster H P and Jones B F (1979) Behaviour of major solutes during closed-basin brine evolution, *Am. J. Sci.*, **279**, 609–631.

Feth J H, Roberon C E, Polzer W L (1964) U S Geological Survey Water Supply Papers, No. 1535I, Washington D C.

Fontes J Ch (1981) Paleowaters. In:*Stable Isotope Hydrology, Deuterium and oxygen-18 in the water cycle*, Gat J R and Gonfiantini R (eds.) IAEA Tech. Rep. Ser. No.**210**, Vienna, pp 273–298.

Garrels R M and Christ C L (1965) *Solutions, Minerals and Equilibria*, Harper and Row, New York, p 450.

Garrels R M and Mackenzie F T (1967) Origin of the chemical composition of some springs and lakes. In: *Equilibrium Concepts in Natural Water Systems, Am. Chem. Soc. Adv. Chem.*, **67**, 222–242.

Gat J R (1981a) Lakes, pp 203–219. In:*Stable Isotope Hydrology, Deuterium and oxygen-18 in the water cycle*, Gat J R and Gonfiantini R (eds.), IAEA Tech. Rep. Ser. No.**210**, Vienna.

Gat J R (1981b) Groundwater, pp 223–238. In:*Stable Isotope Hydrology, Deuterium and oxygen-18 in the water cycle*, Gat J R and Gonfiantini R (eds.), IAEA Tech. Rep. Ser. No.**210**, Vienna.

Gat J R (1981c) Properties of the isotopic species of water: the "isotope effect", pp 7–19. In:*Stable Isotope Hydrology, Deuterium and oxygen-18 in the water cycle*, Gat J R and Gonfiantini R (eds.), IAEA Tech. Rep. Ser. No.**210**, Vienna.

Ghose B (1964) Geomorphological aspects of the formation of salt basins in western Rajasthan, *Proc. UNESCO Symp. on problems of Indian arid zone, Jodhpur*, 79–83.

Godbole N N (1952) The salinity of Sambhar lake, *Proc. Symp. Rajputana Desert, Bull. Nat. Inst. Sci. India*, **1** 89–93.

Gonfiantini R (1981) The δ-notation and the mass-spectrometric measurement techniques, pp 35–84. In: *Stable Isotope Hydrology, Deuterium and oxygen-18 in the water cycle*, Gat J R and Gonfiantini R (eds.), IAEA Tech. Rep. Ser. No. **210**, Vienna.

Gonfiantini R (1986) Environmental isotopes in lake studies, pp 113–163. In: *Handbook of Environmental Isotope geochemistry*, Fritz P and Fontes J Ch (eds.), **2**, the terrestrial envronment, B, Elsevier, New York, NY.

Hardie L A and Eugster H P (1970) The evolution of closed-basin brines, *Mineral. Soc. Amer. Spec. Pap.*, **3**, 273–290.

Harvie C E and Weare J H (1980) The prediction of mineral solubilities in natural waters: The Na-K-Mg-Ca-Cl-SO_4-H_2O systems from zero to high concentration at 25°C, *Geochim. Cosmochim. Acta*, **44**, 981–997.

Harvie C E, Moller Nancy and Weare J H (1984) The prediction of mineral solubilities in natural waters: The Na-K-Mg-Ca-H-Cl-SO_4-OH- HCO_3-CO_3-CO_2-H_2O system to high ionic strengths at 25°C, *Geochim. Cosmochim. Acta*, **48**, 723-751.

Herczeg A L, Simpson H J, Anderson R F, Trier R M, Mathieu G G and Deck B L (1988) Uranium and radium mobility in groundwaters and brines within the Delaware basin, Southeastern New Mexico, U S A, *Chem. Geol. (Isot. Geosci.)*, **72**, 181–196.

Holland T H and Christie W A K (1909) The origin of the salt deposits of Rajputana, *Rec. Geol. Surv. India*, **38(2)**, 154–186.

Hussain N (1983) Behaviour of uranium-thorium series radionuclides in groundwaters : application to study aqifer processes, *PhD thesis*, Guj. Univ., India, pp. 207.

Kraemer T F and Ried D F (1984) The occurrence and behavior of radium in saline formation water of the U. S. Gulf coast region, *Isotope Geoscience*, **2**, 153–174.

Krishnamurthy R V (1984) Stable isotope studies on sedimentary deposits and groundwaters and their climatic implications, *PhD thesis*, pp 127.

Krishnaswami S, Graustein W C, Turekian K K and Dowd J F (1982) Radium, Thorium and Radioactive Lead Isotopes in Groundwaters: Application to the in situ determination of Adsorption–Desorption Rate Constants and retardation factors, *Water Resour. Res.*, **18**(6), 1633–1675.

Krishnaswami S, Bhushan R and Baskaran M (1991) Radium isotopes and ^{222}Rn in shallow brines, Kharaghoda (India), Chemical Geology (Isot. Geosci.), **87**, 125–136.

Ku T L, Knauss K G and Mathieu G G (1977) Uranium in open ocean : Concentration and isotopic composition, *Deep-Sea Res.*, **24**, 1005–1017.

Langmuir D and Riese A C (1985) The thermodynamic properties of radium, *Geochim. Cosmochim. Acta*, **49**, 1593–1601.

Majoube M (1971) Fractionnement en oxygen-18 et en deuterium entre l'eau et sa vapour, *J. Chem. Phys.*, **197**, 1423–1436.

Mathieu G G (1988) Systems for measurement of ^{222}Rn at low levels in natural waters. Health Phys., **55**, 989–992.

Mishra S P (1982) Geochemical evolution of Sambhar salt lake, Jaipur and Nagaur districts, Rajasthan, *Proc. of the workshop on the problems of the deserts in India*, Geol. Surv. of India, Misc. Pub. No. **49**, 92–98.

Moore W S (1976) Sampling Ra-228 in the deep ocean, Deep-Sea Res., **23**, 647–651.

Osmond J K, Kaufman M I and Cowart J B (1974) Mixing volume calculations, sources and aging trends of Floridan aquifer water by uranium isotopic methods, *Geochim. Cosmochim. Acta*, **38**, 1083–1100.

Osmond J K and Cowart J B (1976) The theory and uses of natural uranium isotopic variations in hydrology, Atomic energy review, **144**, 621–679.

Payne B R (1981) Practical applications of stable isotopes to hydrological problems, pp 303–332. In:*Stable Isotope Hydrology, Deuterium and oxygen-18 in the water cycle*, Gat J R and Gonfiantini R (eds.), IAEA Tech. Rep. Ser. No.**210**, Vienna.

Phillips F M, Person M A, and Muller A B (1986) A numerical lumped-parameter model for simulating the isotopic evolution of closed basin lakes, *J. Hydrology*, **85**, 73–86.

Plummer N L, Parkhurst D L, Fleming G W, and Dunkle S A (1988) A computer program incorporating Pitzer's equations for calculation of geochemical reaction in brines, *U. S. Geol. Surv. Water Res. Invest. Rep.* 88-4153.

Ramesh R, Jani R A Bhushan R (1993) Stable isotopic evidence for the origin of salt lakes in the Thar desert, J. Arid Environ, **25**, 117-123.

Sareen J L (1952) Stratigraphic and radiocarbon evidence for the age and development of three salt-lake deposits in Rajasthan, India, *Quat. Res.*, **2(4)**, 496–505.

Sarin M M, Bhushan R, Rengarajan R and Yadav D N (1992) Simultaneous determination of ^{238}U series nuclides in waters of Arabian sea and Bay of Bengal, Indian J. Mar. Sci., **21**, 121-127.

Saxena R K (1987) Oxygen-18 fractionation in nature and estimation of groundwater recharge,*PhD thesis*, Uppsala Univ, pp 152.

Simpson H J, Trier R M, Toggweiler J R, Mathieu G, Deck B L, Olsen C R, Hammond D E, Fuller C and Ku T L (1982) Radionuclides in Mono lake, California, *Science*, **216**, 512– 514.

Singh G, Joshi R D and Singh A B (1972) Stratigraphic and radiocarbon evidence for the age and development of three salt lake deposits in Rajasthan, India, *Quat. Res.*, **2**, 496-505.

Stumm W and Morgan J J (1981) Aquatic Chemistry : An introduction emphasizing chemical equilibria in natural waters, John Wiley and Sons, New York, pp. 780.

Swain A M, Kutzbach J E and Hastenrath S (1983) Estimates of holocene precipitaion for Rajasthan, India, based on pollen and lake-level data, *Quat. Res.*, **19** , 1-17.

Swihart G H, Moore P B and Callis E L (1986) Boron isotopic composition of marine and non-marine evaporite borates, *Geochim. Cosmochim. Acta*, **50**, 1297-1301.

Vengosh A, Chivas A R, McCulloch M T, Starinsky A and Kolodny Y (1991) Boron isotope geochemistry of Australian salt lakes, *Geochim. Cosmochim. Acta*, **55**, 2591-2606.

Vengosh A, Starinsky A, Kolodny Y, Chivas A R, Raab M (1992) Boron isotope variations during fractional evaporation of seawater: New constraints on the marine vs. nonmarine debate, *Geology*, **20**, 799–802.

Yurtsever Y and Gat J R (1981) Atmospheric waters, pp 103–139. In:*Stable Isotope Hydrology, Deuterium and oxygen-18 in the water cycle*, Gat J R and Gonfiantini R (eds.), IAEA Tech. Rep. Ser. No.**210**, Vienna.

Wasson R J, Smith G I and Agrawal D P (1984) Late quaternary sediments, minerals and inferred geochemical history of Didwana lake, Thar desert, India, *Paleogeog., Paleocli., Paleoeco*, **46**, 345–372.

White D E, Hem J D and Waring G A (1963) Chapter F. Chemical Composition of Subsurface waters. In: *Data of Geochemistry*, U S G S Prof. Pap. 440–F, Washington D C.

Appendix–A

Table 1A: Major and trace element concentrations† in upper slope sediments

Depth (cm)	Al (%)	Fe (%)	Ca (%)	Mn (ppm)	Ni (ppm)	Cu (ppm)	Zn (ppm)	Pb (ppm)
L-8								
(0-1)	3.48	2.31	15.4	198.4	89.9	39.4	93.8	55.2
(1-2)	3.16	2.05	17.9	179.6	83.1	59.4	61.7	64.4
(2-3)	2.94	1.88	20.0	163.3	76.8	55.3	56.5	63.6
(3-4)	3.04	1.96	19.2	165.8	83.7	59.1	91.4	58.3
(3-4)R	2.99	1.92	19.7	168.9	79.9	58.6	88.6	50.3
(4-5)	3.07	2.08	18.2	177.5	89.5	63.8	64.6	54.4
(5-6)	3.19	2.18	18.2	182.7	89.7	63.8	67.6	54.4
(6-7)	3.03	2.03	18.8	172.6	87.1	59.9	61.4	44.3
(8-10)	2.70	1.78	18.7	158.9	75.4	53.3	55.5	42.8
(10-14)	2.62	1.72	19.8	162.2	76.7	52.7	54.0	41.7
(18-20)	2.27	1.74	21.9	149.2	75.3	49.2	53.0	40.9
J-7								
(0-2)	1.68	1.22	29.1	107.5	55.8	28.1	34.8	45.8
(2-3)	1.77	1.29	29.2	117.6	54.5	28.6	38.4	44.9
(3-4)	1.59	1.18	26.0	99.2	59.1	28.5	37.6	44.6
(4-5)	1.57	1.09	30.3	103.0	52.1	27.7	35.1	45.0
(5-6)	1.60	1.12	30.5	101.8	52.4	27.1	33.5	44.2
(6-7)	1.79	1.29	29.2	114.3	56.3	30.1	38.4	45.6
(9-10)	1.54	1.13	30.3	101.4	53.7	28.2	34.9	44.3
(9-10)R	1.61	1.17	31.2	102.7	54.4	28.6	34.2	44.9
(10-12)	2.17	1.61	26.8	130.4	65.9	39.5	44.9	41.3
(14-16)	1.95	1.45	26.4	124.3	61.3	37.2	41.1	39.9
(18-20)	1.62	1.17	29.1	107.8	54.5	31.2	33.1	40.4
(20-22)	1.78	1.34	27.6	117.1	58.2	36.8	37.1	43.1
I-5								
(0-2)	1.02	1.84	32.5	71.1	54.2	25.7	39.4	42.0
(2-4)	1.00	1.88	65.8	65.8	55.8	26.6	39.9	40.2
(4-6)	1.42	2.63	29.1	77.4	61.8	31.3	45.7	40.5
(4-6)R	1.37	2.39	30.0	72.6	60.5	30.4	44.1	42.9
(6-8)	1.44	2.29	30.3	82.4	62.7	31.2	52.6	42.5

† concentration expressed on bulk sediment basis

R denotes repeat measurement

Table 2A: Major and trace elements concentrations† in lower slope sediments

Depth (cm)	Al (%)	Fe (%)	Ni (ppm)	Cu (ppm)	Zn (ppm)
K-11					
(0-1)	3.75	2.52	71.3	57.5	70.8
(1-2)	3.74	2.49	74.8	58.9	73.3
(2-3)	3.75	2.88	74.3	56.7	72.3
(3-4)	3.75	2.42	90.4	59.4	74.8
(4-5)	3.65	2.38	79.3	57.8	74.8
(5-6)	3.62	2.33	64.5	58.7	77.9
(6-7)	3.54	2.33	64.1	57.4	70.6
(7-8)	3.35	2.20	49.6	54.0	66.2
(7-8)R	3.32	2.29	57.8	56.9	65.7
(8-9)	3.24	2.19	55.3	55.9	64.7
(9-10)	3.26	2.21	49.7	54.2	62.8
(10-12)	3.33	2.29	47.5	56.1	66.8
(12-14)	3.27	2.25	38.9	55.1	63.8
(12-14)R	3.32	2.34	45.3	53.4	60.9
(14-16)	3.21	2.37	42.7	58.0	60.2
(16-18)	3.48	2.31	44.6	56.3	62.8
(18-20)	3.07	2.26	39.2	47.8	53.6
(20-22)	3.04	2.24	38.9	55.0	52.3
(22-24)	3.00	2.12	46.1	52.4	61.3

Depth (cm)	Al (%)	Fe (%)	Ni (ppm)	Cu (ppm)	Zn (ppm)
M-12					
(0-1)	6.24	4.46	103.4	57.4	108.8
(1-2)	6.15	4.26	87.2	56.5	94.6
(2-3)	6.02	4.00	63.8	51.6	86.9
(3-4)	5.96	3.86	63.2	50.2	87.3
(4-5)	5.44	3.85	64.2	50.0	85.5
(4-5)R	5.64	3.91	65.5	56.2	88.5
(5-6)	5.07	3.81	63.3	58.7	91.0
(6-7)	4.94	3.49	59.1	57.8	89.8
(7-8)	4.77	3.53	70.2	65.6	90.6
(8-9)	4.59	3.52	70.7	59.6	86.9
(9-10)	4.49	3.59	78.1	62.8	86.8
(10-12)	4.52	3.53	73.5	59.2	89.8
(12-14)	4.55	3.44	80.5	63.2	89.5
(14-16)	4.62	3.29	78.9	59.2	90.7
(16-18)	4.44	3.09	72.3	58.2	86.6
(18-20)	4.29	3.06	73.4	57.3	83.0
(20-25)	4.37	3.03	71.9	56.9	82.9

† concentration expressed on bulk sediment basis
R denotes repeat measurement

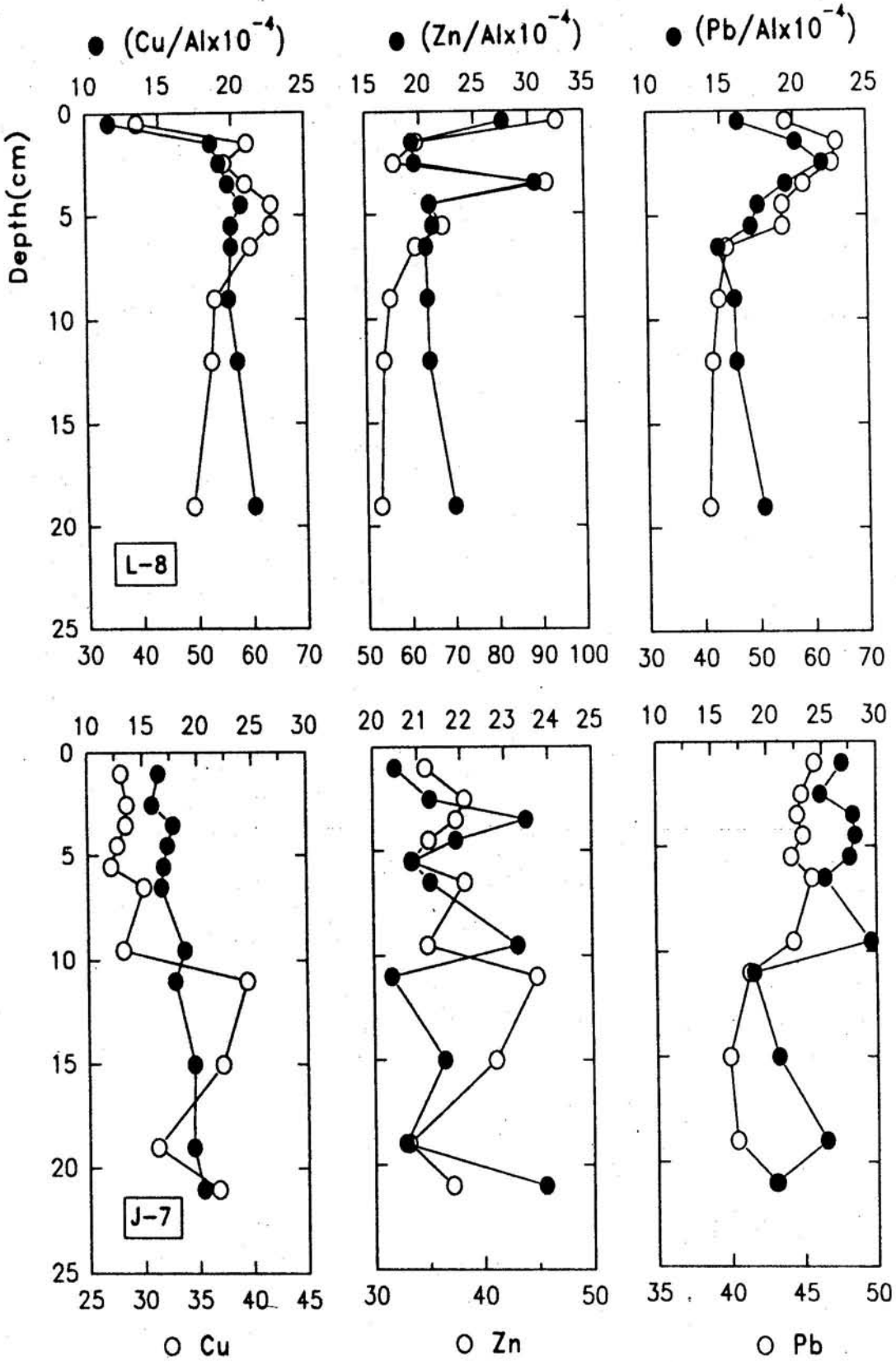

Fig. 1A: The depth profile of metal and metal/Al weight ratios in upper slope sediment cores L-8 and J-7. As there is no uniform increase in either metal or metal/Al ratios for Cu, Zn and Pb from bottom section of the cores, the influence of anthropogenic inputs is not clearly discernible in these sediments.

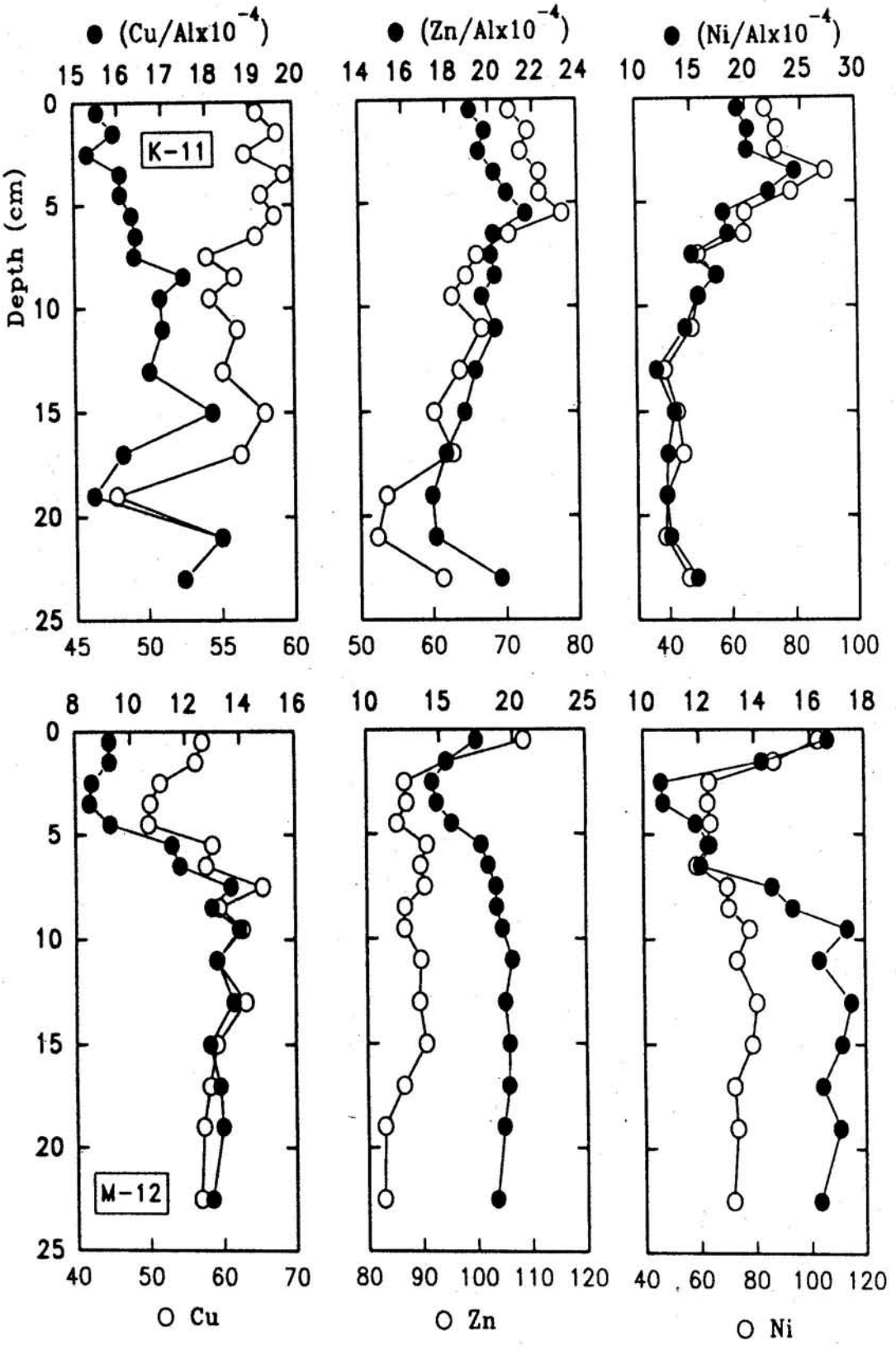

Fig. 2A: The depth profile of metal and metal/Al weight ratios for K-11 and M-12 sediment cores from the lower slope region. The sedimentary record does not illustrate unequivocal indication of recent anthropogenic inputs of these metals.

Appendix–B

Density of saline waters

The density of saline waters in the Sambhar lake study was calculated based on the TDS–density relationship, assuming that chemical composition of solution remains same over the wide range of salinity. Such relation was obtained for about 12 samples with TDS (determined by summing all major ions) rannging from 9 to 370 g/l and density was determined by weighing the known volume of sample. The TDS–density relationship obtained is given by:

$$\boxed{\text{Density (g/cm}^3\text{)} = 0.0007 \cdot \text{TDS (g/l)} + 0.9874}$$

Table 1B: Details of samples collected from the Sambhar lake area

Sample code/Collection period	Location	Sample description
Rain Waters		
Smb1,Smb2 (July 93)	Sambhar town	Two samples over a week interval were collected using clean polyethylene funnel in bottles during July 93
River Waters		
SL #82 (Oct 93)	Sinodiya	~4 km upstream of the lake, open well in river bed of Roopangarh, depth ~3 m
SL #83 (Oct 93)	Bhadun	~ 10 km upstream of the lake, open well in river bed of Roopangarh, depth ~4 m
SL #84 (Oct 93)	Roopangarh	~ 22 km upstream of the lake, open well in river bed of Roopangarh, depth ~19 m
SL #86 (Oct 93)	Dabsi	~6 km upstream of the lake, open well in river bed of Mendha, depth ~2 m
SL #85 (Oct 93)	Naulasia	~16 km upstream of the lake, open well in river bed of Mendha, depth ~3 m
Ground Waters		
SL #10 (Feb 92), #41 (July 92), #54 (Oct 92), #90 (Oct 93)	Gudha Railway Station -do-	closed Tube well, potable water
SL #21 (Feb 92), #39 (July 92), #50 (Oct 92), #62 (Feb 93), #91 (Oct 93)	Sambhar town -do-	open well, potable water, depth ~ 10m

Table 1B: Details of samples collected from the Sambhar lake area (CONTINUED)

Sample code/Collection period	Location	Sample description
Ground Waters		
SL #22 (Feb 92), #40 (July 92), #51 (Oct 92), #61 (Feb 93), #92 (Oct 93)	Sambhar town (Pipe Factory) -do-	Tube well, potable water, depth ~ 11m
SL #17 (Feb 92), #38 (July 92), #48 (Oct 92), #68 (Feb 93), #88 (Oct 93)	Sambhar town (Madarsa School) -do-	open well, brackish water,depth~ 4m
SL #23 (Feb 92), #87 (Oct 93)	Sambhar town (Guest House)	Tube well, potable water
SL #24 (Feb 92)	Sambhar town (Guest House)	Tube well
SL #18 (Feb 92)	Jhapok village	open well, potable water, depth ~10 m
SL #20 (Feb 92)	Korshina village	open well, potable water, depth ~10 m
SL #65 (Feb 93)	Jhag village	Open well, brackish water, depth ~6 m
SL #66 (Feb 93)	Jajota village	Open well, potable water, depth ~8 m

Table 1B: Details of samples collected from the Sambhar lake area (CONTINUED)

Sample code/Collection period	Location	Sample description
Lake Waters		
SL #8 (Feb 92), #28 (July 92), #46 (Oct 92)	Jhapok	Surface water
SL #47 (Oct 92)	Gudha	-do-
SL #52 (Oct 92)	Mata pahar	-do-
SL #55 (Feb 93), #69 (Apr 93), #72 (Apr 93)	Jhapok	-do-
SL #73 (Apr 93), #74 (May 93), #75 (May 93)	Jhapok	-do-
SL #76 (May 93), #77 (May 93), #78 (May 93)	Jhapok	-do-
SL #79 (May 93), #89 (Oct 93)	Jhapok	-do-
Evaporating Pans		
SL #1 (Feb 92), #2 (Feb 92), #3 (Feb 92)	Jhapok	-
SL #4 (Feb 92), #5 (Feb 92), #6 (Feb 92)	-do-	-
SL #7 (Feb 92), #27 (Feb 92)	-do-	-
SL #29 (Mar 92), #30 (Mar 92), #31 (Apr 92)	-do-	Collected from same pan at different times

Table 1B: Details of samples collected from the Sambhar lake area (CONTINUED)

Sample code/Collection period	Location	Sample description
Evaporating Pans		
#32 (Apr 92), #33 (May 92), #34 (May 92)	Jhapok	same pan at different times
#35 (May 92), #36 (May 92), #37 (May 92)	-do-	-do-
Sub-surface brines		
SL #9 (Feb 92), #11 (Feb 92),	Gudha kyar	open wells, depth ~ 3 m
#12† (Feb 92), #13 (Feb 92)	-do-	
SL #14 (Feb 92), #44 (Oct 92)	Deodani	open wells, depth ~ 3 m
SL #15 (Feb 92), #42 (Oct 92), #58 (Feb 93)	-do-	-do-
SL #16 (Feb 92), #43 (Oct 92), #59 (Feb 93)	-do-	-do-
SL #45 (Oct 92), #60 (Feb 93)	-do-	-do-
SL #49 (Oct 92), #57 (Feb 93)	Main Line Pan work	open wells, depth ~ 5 m
SL #56 (Feb 93), #70 (Apr 93) #80 (June 93)	-do-	Bore well, depth ~ 30 m
SL #63 (Feb 93)	Khakarki	Tube well, depth ~ 50 m
SL #64 (Feb 93)	-do-	Tube well, depth ~ 40 m
SL #71 (Apr 93)	Nawa	Tube well, depth ~ 30 m

† A seeping brine collected from the well SL #9

Table 2B: Major ions, oxygen and uranium isotopes in Sambhar lake water systems

Code	pH	Na $meq.\ell^{-1}$	K $meq.\ell^{-1}$	Ca $meq.\ell^{-1}$	Mg $meq.\ell^{-1}$	Cl $meq.\ell^{-1}$	SO_4 $meq.\ell^{-1}$	Alk $meq.\ell^{-1}$	$\delta^{18}O$ $^{o}/_{oo}$	^{238}U $\mu g.kg^{-1}$	$^{234}U/^{238}U$ AR	TDS $g.\ell^{-1}$
Rain waters												
Smb1	*	14†	*	*	*	15†	*	*	− 3.2	*	*	0.8†
Smb2	*	37†	*	*	*	34†	*	*	− 6.4	*	*	2.0†
River waters												
SL #82	8.10	19.0	0.09	0.5	0.6	9.9	2.4	9.2	− 4.4	25.6	1.99	1.2
SL #83	8.00	14.8	0.47	0.4	0.4	3.6	0.8	12.4	− 5.0	13.0	2.26	0.9
SL #84	8.00	10.0	0.40	0.3	0.4	2.8	0.6	8.1	− 5.4	11.9	1.88	0.6
SL #85	7.80	24.4	0.29	3.04	4.9	18.0	4.6	10.3	− 4.2	40.8	1.39	1.9
SL #86	8.60	23.7	0.44	0.9	1.2	9.5	3.7	12.4	− 3.6	103.4	1.33	1.5
Groundwaters												
SL #10	7.94	21.5	0.09	3.30	5.34	24.5	1.5	4.4	− 6.5	8.2	1.28	1.8
SL #41	*	3.2	0.09	2.9	2.3	4.1	0.5	4.2	*	*	*	0.6
SL #54	7.40	5.3	0.14	2.3	3.5	7.0	0.6	2.6	− 5.6	*	*	0.6
SL #90	8.00	13.2	0.16	3.8	4.3	14.9	1.1	5.4	− 5.4	7.0	1.26	1.2
SL #17	7.51	144	0.48	6.8	15.9	142	11.7	7.6	− 4.3	71.6	1.46	9.6
SL #38	*	79.2	0.28	4.3	8.1	78.0	7.0	6.0	*	*	*	5.5
SL #48	7.86	75.0	0.30	4.1	8.2	75	5.6	7.0	− 3.8	*	*	5.0
SL #68	*	129.6	0.50	4.6	15.8	152	13.2	8.5	− 3.9	*	*	9.5
SL #88	7.80	92.6	0.34	5.00	9.8	92	7.0	6.5	− 3.0	44.4	1.39	6.1

† Na and Cl concentration in $\mu eq.\ell^{-1}$ and TDS (NaCl) in $mg.\ell^{-1}$. ‡ density calculated based on TDS−Density relationship (see p. 129).
* measurements not made.

Table 2B: Major ions, oxygen and uranium isotopes in Sambhar lake water systems

Code	pH	Na $meq.\ell^{-1}$	K $meq.\ell^{-1}$	Ca $meq.\ell^{-1}$	Mg $meq.\ell^{-1}$	Cl $meq.\ell^{-1}$	SO_4 $meq.\ell^{-1}$	Alk $meq.\ell^{-1}$	$\delta^{18}O$ $^{o}/_{oo}$	^{238}U $\mu g.kg^{-1}$	$^{234}U/^{238}U$ AR	TDS $g.\ell^{-1}$
Groundwaters												
SL #18	7.91	25.2	0.07	1.5	2.6	19.6	1.6	6.8	– 5.0	36.2	1.39	1.8
SL #20	7.85	8.4	0.96	0.72	1.3	2.6	1.4	7.5	– 4.0	6.9	1.98	0.9
SL #21	7.29	21.5	0.44	4.4	3.2	19.6	2.1	5.8	– 5.6	6.3	1.21	1.8
SL #39	*	20.8	0.44	5.12	3.6	19.4	2.2	5.8	– 5.6	*	*	1.8
SL #50	6.65	23.2	0.65	6.2	4.7	23.8	2.6	6.1	– 5.1	*	*	1.9
SL #62	*	19.7	0.44	5.14	3.8	19.2	2.3	5.9	– 4.9	*	*	1.6
SL #91	7.50	19.6	0.52	4.9	3.4	17	2.3	5.9	– 4.9	5.9	1.19	1.5
SL #24	7.15	59.6	0.18	10.5	9.7	64	6.1	5.3	– 5.9	9.4	1.29	4.6
SL #22	7.21	17.6	0.12	5.70	5.3	24.5	1.4	3.9	– 5.7	10.8	1.36	1.8
SL #40	*	16.8	0.10	4.34	4.9	22	1.5	4.7	– 5.4	*	*	1.7
SL #51	5.86	17.5	0.16	7.5	5.7	24.2	1.5	4.2	– 5.8	*	*	1.7
SL #61	*	16.7	0.13	4.4	4.9	21.3	1.7	4.3	– 4.4	*	*	1.5
SL #92	7.40	17.5	0.12	7.6	5.8	22.2	1.8	4.9	– 4.1	7.2	1.24	1.6
SL #23	7.19	6.2	0.04	1.1	1.3	4.9	0.6	4.2	– 5.9	3.6	1.22	0.6
SL #87	8.40	10.3	0.05	3.1	2.5	10.4	0.9	4.9	– 4.5	5.9	1.22	0.9
SL #65	*	141.0	25.0	20.2	35	178	13.3	11.3	– 3.0	57.2	1.78	12.3
SL #66	*	44.0	0.17	3.58	8.4	44	2.6	10.3	– 3.6	21.3	1.67	3.2

† Na and Cl concentration in $\mu eq.\ell^{-1}$ and TDS (NaCl) in $mg.\ell^{-1}$. ‡ density calculated based on TDS–Density relationship (see p.129).
* measurements not made.

Table 2B: Major ions, oxygen and uranium isotopes in Sabhar lake water systems (CONTINUED)

Code	pH	Na $meq.\ell^{-1}$	K $meq.\ell^{-1}$	Ca $meq.\ell^{-1}$	Mg $meq.\ell^{-1}$	Cl $meq.\ell^{-1}$	SO_4 $meq.\ell^{-1}$	Alk $meq.\ell^{-1}$	$\delta^{18}O$ $^{o}/_{oo}$	^{238}U $\mu g.kg^{-1}$	$^{234}U/^{238}U$ AR	TDS $g.\ell^{-1}$	Density‡ $g.cm^{-3}$
Lake waters													
SL #8	9.61	3160	2.86	0.13	0.16	2942	308	139	18	662	1.68	196	1.125
SL #28	*	158	0.36	0.98	0.48	142	11	5	− 5.5	15.9	1.51	10.4	0.995
SL #46	8.50	138	0.31	1.27	0.35	130	6	7	− 1.4	9.0	1.66	8.6	0.993
SL #47	8.50	139	0.31	1.26	0.35	122.6	9	7	− 1.0	8.1	1.67	8.8	0.994
SL #52	8.18	151	0.31	1.47	0.40	146	10	7	− 0.5	9.4	1.71	9.3	0.994
SL #55	*	273	0.49	1.54	0.72	273	23	12	4.5	14.8	1.63	17.5	0.999
SL #69	*	603	1.16	0.59	1.32	551	50	28	9.6	25.6	1.61	36.7	1.013
SL #72	*	615	1.75	0.66	1.36	570	52	28	13.0	25.6	1.63	37.7	1.014
SL #73	*	1420	2.19	0.48	1.20	1445	117	58	19.1	67.4	1.68	91.3	1.051
SL #74	*	2120	3.20	0.37	0.79	2135	171	78	19.7	101	1.62	135	1.082
SL #75	*	2410	3.76	0.32	0.94	2530	204	94	21.4	131	1.66	158	1.098
SL #76	*	3540	5.15	0.19	0.59	3268	292	127	24.0	220	1.65	215	1.138
SL #77	*	4550	5.72	0.09	0.69	4042	365	166	18.3	*	*	270	1.176
SL #78	*	5380	14.54	0.06	0.51	4958	438	194	21.5	281	1.65	327	1.216
SL #79	*	6346	23.16	0.06	0.43	4789	896	537	23.0	1117	1.66	376	1.251
SL #89	10.3	658	0.98	0.38	0.05	581	46	22	5.6	51	1.66	39	1.015
Sub-surface brines													
SL #9	8.78	2360	6.79	0.52	0.96	2037	278	100	3.5	398	1.53	143	1.087
SL #11	9.11	3670	12.30	0.03	0.07	2942	562	250	5.1	645	1.59	223	1.143
SL #12	8.78	1800	4.27	0.09	0.36	1546	204	85	3.9	515	1.64	109	1.064
SL #13	9.12	3830	11.47	0.03	0.06	3187	524	272	4.4	339	1.60	235	1.152

* measurements not made. ‡ density calculated based on TDS−Density relationship (see p. 129).

Table 2B: Major ions, oxygen and uranium isotopes in Sabhar lake water systems (CONTINUED)

Code	pH	Na $meq.\ell^{-1}$	K $meq.\ell^{-1}$	Ca $meq.\ell^{-1}$	Mg $meq.\ell^{-1}$	Cl $meq.\ell^{-1}$	SO_4 $meq.\ell^{-1}$	Alk $meq.\ell^{-1}$	$\delta^{18}O$ $^{o}/_{oo}$	^{238}U $\mu g.kg^{-1}$	$^{234}U/^{238}U$ AR	TDS $g.\ell^{-1}$	Density‡ $g.cm^{-3}$
Sub-surface brines													
SL #14	9.42	2690	10.82	0.04	0.09	2206	462	184	3.2	198	1.61	168	1.105
SL #44	10.15	604	2.0	0.15	0.06	455	160	24	− 1.1	*	*	39	1.015
SL #15	9.14	3860	15.64	0.04	0.07	3187	663	261	5.1	248	1.62	242	1.157
SL #42	9.48	3140	13.62	0.03	0.11	2594	528	179	2.5	174	1.66	195	1.124
SL #58	*	3080	13.91	0.02	0.09	2570	578	211	3.8	253	1.61	196	1.125
SL #16	9.08	4020	13.79	0.06	0.09	2942	643	244	5.1	195	1.60	235	1.152
SL #43	9.73	2360	5.46	0.04	0.07	1964	409	101	− 0.3	85	1.65	147	1.09
SL #59	*	3120	9.76	0.02	0.08	2861	558	172	3.8	156	1.57	205	1.131
SL #45	9.52	2650	10.1	0.04	0.08	2206	433	152	1.3	114	1.67	165	1.103
SL #60	*	2820	10.88	0.09	0.08	2425	483	160	3.1	213	1.62	179	1.113
SL #49	8.25	3860	17.56	0.05	0.31	3395	574	82	4.0	22	1.63	240	1.155
SL #57	*	4220	19.35	0.08	0.84	3831	604	78	6.0	10	1.66	265	1.173
SL #56	*	4140	22.13	0.02	0.20	3540	601	255	6.7	104	1.50	258	1.168
SL #70	*	4220	23.90	0.02	0.21	3637	613	260	6.3	118	1.61	264	1.172
SL #80	*	4350	26.24	0.02	0.29	3803	521	272	7.4	*	*	269	1.176
SL #63	*	1140	2.99	20.96	71.92	1103	210	10	− 1.1	192	1.65	77	1.041
SL #64	*	2820	3.41	42.16	151	2958	309	7	1.5	149	2.56	187	1.118
SL #71	*	3580	7.19	0.12	0.05	3152	375	305	6.5	438	1.77	221	1.142

* measurements not made. ‡ density calculated based on TDS–Density relationship (see p. 129).

Table 2B: Major ions, oxygen and uranium isotopes in Sabhar lake water systems (CONTINUED)

Code	pH	Na $meq.\ell^{-1}$	K $meq.\ell^{-1}$	Ca $meq.\ell^{-1}$	Mg $meq.\ell^{-1}$	Cl $meq.\ell^{-1}$	SO_4 $meq.\ell^{-1}$	Alk $meq.\ell^{-1}$	$\delta^{18}O$ $^{o}/_{oo}$	^{238}U $\mu g.kg^{-1}$	$^{234}U/^{238}U$ AR	TDS $g.\ell^{-1}$	Density‡ $g.cm^{-3}$
Evaporating Pans													
SL #1	9.82	1220	2.30	0.26	0.18	981	114	65	10.6	200	1.59	70	1.036
SL #2	9.52	1650	5.73	0.02	0.03	1226	318	618	12.5	536	1.62	115.3	1.068
SL #25	*	4400	26.18	0.09	0.11	*	*	*	*	1415	1.59	325[a]	1.215
SL #3	9.48	6010	19.34	0.04	0.09	4903	819	456	14.0	1198	1.65	365	1.243
SL #26	*	4400	23.04	0.10	0.12	*	*	*	*	1186	1.63	325[a]	1.215
SL #4	9.62	1970	5.92	0.12	0.07	1552	267	178	12.0	569	1.65	119	1.071
SL #5	9.45	2460	5.27	0.34	0.29	2109	257	144	14.1	395	1.64	148	1.091
SL #6[aa]	9.54	6557	31.94	0.10	0.11	4243	1469	819	12.0	2342	1.63	398	1.266
SL #7	9.47	4580	12.58	0.12	0.09	3879	588	334	13.5	925	1.62	281	1.184
SL #27	*	5218	13.76	0.06	0.08	4290	632	328	13.8	1022	1.61	313	1.206
SL #29	*	1460	3.05	0.15	0.21	1237	136	82	11.9	228	1.58	86	1.048
SL #30	*	1580	3.42	0.18	0.23	1382	158	98	12.8	228	1.73	96	1.055
SL #31	*	1740	3.88	0.16	0.25	1503	171	109	13.9	*	*	105	1.061
SL #32	*	2160	4.90	0.15	0.24	1843	207	125	16.7	*	*	129	1.077
SL #33	*	2680	6.19	0.14	0.28	2279	256	166	*	448	1.64	160	1.099
SL #34	*	3850	9.16	0.13	0.29	3273	389	250	21.0	644	1.59	231	1.149
SL #35	*	4730	11.19	0.15	0.38	3952	476	304	23.5	763	1.59	281	1.184
SL #36	*	5260	12.30	0.09	0.43	4413	526	318	24.6	*	*	312	1.206
SL #37	*	6480	23.05	0.09	0.54	4800	1090	658	27.5	1804	1.61	392	1.262

[a] TDS estimated based on Σcation measurements. ‡ density calculated based on TDS–Density relationship (see p. 129).
* measurements not made. [aa] a bittern sample collected from one of the evaporating pans.

Table 3B: Ra, ^{210}Po and ^{210}Pb radionuclides in Sambhar lake water systems

Code	^{226}Ra (dpm.kg^{-1})	^{228}Ra/^{226}Ra (Activity Ratio)	^{210}Po (dpm.kg^{-1})	^{210}Pb (dpm.kg^{-1})	^{210}Po/^{210}Pb (Activity Ratio)
Groundwaters					
SL #10	.21 ±.01	2.14 ± 0.19	.009±.001	.031±.003	.290±.043
SL #90	.36 ±.01	1.59 ± 0.09	.011±.001	.032±.002	.339±.035
SL #17	1.32 ±.08	1.59 ± .05	.027±.002	.037±.002	.729±.067
SL #88	1.05 ±.03	1.18 ± .04	.013±.001	.065±.003	.205±.013
SL #18	.31±.03	1.04 ±.10	.011±.002	.075±.003	.147±.027
SL #20	1.11 ±.04	10.37 ±.24	.033±.003	.216±.006	.153±.015
SL #21	.71 ±.04	.65 ± .05	.019±.002	.089±.005	.213±.025
SL #91	.58 ±.01	.57 ± .04	.011±.001	.097±.004	.108±.008
SL #22	.60 ±.02	.63 ± .05	.019±.002	.049±.003	.388±.047
SL #92	.56 ±.01	.63 ± .04	.003±.001	.126±.004	.231±.004
SL #23	.31 ±.02	–	.004±.001	.028±.002	.143±.037
SL #87	.52 ±.02	.57 ±.04	.003±.0004	.036±.002	.085±.001
SL #24	.48 ±.01	2.59 ±0.10	.011±.002	.022±.002	.500±.102
River waters					
SL #82	.13 ±.01	1.08 ± .23	–	–	–
SL #83	.49 ±.01	5.76 ± .19	–	–	–
SL #84	.19 ±.01	6.16 ± .38	–	–	–
SL #85	.37 ±.01	1.51 ± .09	–	–	–
SL #86	.18 ±.01	1.59 ± .14	–	–	–

- indicates measurement not made

Table 3B: Ra, ^{210}Po and ^{210}Pb radionuclides in lake waters (CONTINUED)

Code	^{226}Ra (dpm.kg^{-1})	^{228}Ra/^{226}Ra (Activity Ratio)	^{210}Po (dpm.kg^{-1})	^{210}Pb (dpm.kg^{-1})	^{210}Po/^{210}Pb (Activity Ratio)
Lake and evaporating pans					
SL #1	.40 ±.02	2.06 ± .13	–	–	–
SL #2	.62 ±.03	3.27 ± .20	–	–	–
SL #3	.45 ±.01	2.99 ± .20	–	–	–
SL #4	.66 ±.01	2.04 ± .10	–	–	–
SL #5	.59 ±.03	2.34 ± .11	–	–	–
SL #7	.39 ±.04	3.14 ± .21	–	–	–
SL #8	.32 ±.03	1.87 ± .12	–	–	–
SL #89	.23±.01	1.61 ± .12	1.21 ± .21	.61±.02	1.99±.07
SL #25	–	–	8.16 ± .22	2.68±.06	3.04±.11
SL #26	–	–	7.58 ± .24	2.86±.07	2.64±.10
SL #27	–	–	8.94 ± .29	7.34±.15	1.22±.05
Sub-surface brines					
SL #9	1.25 ±0.05	3.41 ± .10	.26±.01	.12±.01	2.19 ± .26
SL #11	1.78 ±.12	3.04 ± .10	.48±.02	.55±.02	.87±.05
SL #13	1.67 ±.07	–	.16 ±.01	.16 ± .01	.97 ± .07
SL #14	1.28 ±.09	1.75 ± .10	.29±.02	.56±.01	.51±.04
SL #15	1.36 ±.08	2.00 ±.10	.06±.01	.10±.01	.61±.02
SL #16	.80 ±0.06	2.71 ± .13	.05±.01	.06±.01	.85±.09

- indicates measurement not made